

WELLS, BRIAN DAVID. Filament Winding Multifunctional Carbon Nanotube Composites of Various Dimensionality. (Under the direction of Dr. Philip Bradford and Dr. Yuntian Zhu).

Carbon nanotubes (CNT) have been long considered an optimal material for composites due to their high strength, high modulus, and electrical/thermal conductivity. These composite materials have the potential to be used in the aerospace, computer, automotive, medical industry as well as many others. The nano dimensions of these structures make controlled alignment and distribution difficult using many production techniques. An area that shows promise for controlled alignment is the formation of CNT yarns. Different approaches have been used to create yarns with various winding angles and diameters. CNTs resemble traditional textile fiber structures due to their one-dimensional dimensions, axial strength and radial flexibility. One difference is, depending on the length, CNTs can have aspect ratios that far exceed those of traditional textile fibers. This can complicate processing techniques and cause agglomeration which prevents optimal structures from being created. However, with specific aspect ratios and spatial distributions a specific type of CNT, vertically aligned spinnable carbon nanotubes (VASCNTs), have interesting properties that allow carbon nanotubes to be drawn from an array in a continuous aligned web.

This dissertation examines the feasibility of combining VASCNTs with another textile manufacturing process, filament winding, to create structures with various levels of dimensionality. While yarn formation with CNTs has been largely studied, there has not been significant work studying the use of VASCNTs to create composite materials. The studies that have been produced revolve around mixing CNTs into epoxy or creating uni-directional wound structures. In this dissertation VASCNTs are used to create filament wound materials with various

degrees of alignment. These structures include 1 dimensional coatings applied to non-conductive polymer monofilaments, two dimensional multifunctional adhesive films, and three dimensional hybrid-nano composites. The angle of alignment between the individual CNTs relative to the overall structure was used to affect the electrical properties in all of these structures and the mechanical properties of the adhesive films and hybrid-nano composites. Varying the concentration of CNT was also found to have a significant effect on the electrical and mechanical properties. The variable properties that can be created with these production techniques allow users to engineer the structure to match the desired property.

Filament Winding Multifunctional Carbon Nanotube Composites of Various Dimensionality

by

Brian David Wells

A dissertation submitted to the Graduate Faculty of
North Carolina State University
in partial fulfillment of the
requirements for the Degree of
Doctor of Philosophy

Materials Science and Engineering
Fiber and Polymer Science

Raleigh, North Carolina

2017

APPROVED BY:

Philip Bradford
Co-Chair of Advisory Committee

Yuntian Zhu
Co-Chair of Advisory Committee

Kara Peters

Lewis Reynolds

DEDICATION

To my parents: Gary & Elise; my sister, brother in-law, and nephew: Ann, Ben, and David; and to my girlfriend Marilyn.

BIOGRAPHY

Brian David Wells was born in Raleigh, North Carolina and grew up in Garner, North Carolina. He attended Aversboro Elementary for grades K-2, Timber Drive Elementary for grades 3-5, West Lake Middle for grades 6-8, Middle Creek High for grades 9-12. He attended North Carolina State University for his undergraduate education as a Centennial Scholar and graduated Suma Cum Laude with double major in Textile Engineering and Materials Science & Engineering in May of 2013. During summers of his undergraduate career he worked at the Analytical Instrumentation Facility, Institut für Textiltechnik at the Rheinisch-Westfälische Technische Hochschule in Aachen, Germany, and National Aeronautics and Space Administration, Langley Research Center in Hampton, Virginia. Upon completing the internship at NASA he began the journey to complete a lifelong goal of earning a PhD as Co-major in Materials Science & Engineering and Fiber & Polymer Science in August of 2013. His PhD was focused on merging vertically aligned spinnable carbon nanotubes with filament winding technology to create structures of various dimensionality while examining structure property relationships and the effect of processing parameters on these properties.

ACKNOWLEDGEMENTS

I would like to thank many of my teachers and professors that have had a significant impact on my academic career. My 7th grade math and science teacher Dr. Knox was my favorite teacher in middle school and really instilled a love for science in his classes. My AP chemistry teacher, the late Ms. Ozoma, who let me explore the world of the chemistry classroom in my own way and provided the basis of my advanced chemistry education that I would grow throughout the rest of my college career. Dr. Zhu for first introducing me to the exciting field of carbon nanotube research. Dr. Bradford for accepting me into his research group and the constant mentoring over the past three years. Dr. Reynolds for exposing me to a mind set and approach to research that I have truly valued and utilized that focuses on understanding fundamental properties to explain different phenomena. Dr. Peters for providing a mechanical engineering perspective on the various aspects of my dissertation that has allowed me to apply textile and materials knowledge toward solving these problems And to Dr. Bolotnov for being willing to serve on my committee on last minute notice as my graduate school representative. I am sure there are people I have not mentioned that have played a significant role in educational background, but I would not be where I am today without the support I have received.

I would also like to acknowledge the Summer Textile Exploration Program with the College of Textiles and North Carolina State University and the North Carolina State University Engineering Summer Camp for Materials Science and Engineering. I attended these camps when I was a rising senior in high school and they played a pivotal role on my selection of undergraduate and graduate programs. I would also like to thank the North Carolina Textile Foundation for their support of the College of Textiles and its students. I was very honored to have been selected as a Centennial Scholar and would have likely not participated in the UROP program at the RWTH in Aachen, Germany had I not. That summer provided me with a tremendous amount of personal growth, amazing experiences, and lifelong friends. The following summer my internship with NASA provided me a fantastic research experience at I have applied in my PhD research and hope to continue working on in my professional career. Finally, I would also like to thank all of my past and present group members and fellow classmates.

TABLE OF CONTENTS

	Page
List of Figures	viii
List of Tables	xii
1. Introduction	1
2. Literature Review	2
2.1 Composites Overview	2
2.2 CNT Overview	3
2.2.1 Types of CNTS	3
2.2.2 Growth Techniques.....	6
2.2.3 Chemical Vapor Deposition and Floating Catalyst Chemical Vapor Deposition.....	6
2.3 Overview of CNT Properties.....	8
2.3.1 Mechanical Properties.....	8
2.3.2 Electrical Properties.....	10
2.3.3 Thermal Properties	11
2.4 Linear Assemblies.....	11
2.4.1 Production.....	12
2.4.2 Electrical Properties.....	15
2.4.3 EMI Shielding.....	18
2.5 Electrical Properties	19
2.5.1 Individual CNTs.....	19
2.5.2 Assemblies.....	23
2.5.3 Transport Mechanisms of Individual CNTs.....	25
2.5.4 Transport Mechanism of CNT Assemblies.....	25
2.6 High Volume Fraction CNT Films.....	27
2.6.1 Conductive CNT Films.....	27
2.6.2 Electrically Conductive Adhesives.....	31
2.6.3 Thermally Conductive Adhesives.....	32

2.7 Fiber Reinforced Composites with Nanomaterial Additives.....	34
2.7.1 Mechanical Properties of Composites with CNT Additions.....	35
2.7.2 Mechanical Properties of Composites with Non-CNT Nanomaterial Additions.....	39
2.7.3 Properties of Multifunctional Fiber Reinforced Composites...	41
2.8 Critical Summary.....	44
3. Tunable Electrically Conductive Carbon Nanotube Coatings for Monofilaments Applied via Filament Winding.....	46
3.1 Abstract.....	46
3.2 Introduction.....	47
3.3 Materials and Methods.....	49
3.4 Results and Discussion.....	54
3.4.1 Resistance Versus Thickness Coating.....	54
3.4.2 Resistance Versus Winding Angle.....	61
3.5 Conclusions.....	64
4. Highly Anisotropic Magneto-transport and Aharonov-Bohm Oscillations in Carbon Nanotube/Epoxy Composites	66
4.1 Abstract.....	66
4.2 Introduction.....	67
4.3 Experimental	69
4.4 Results and Discussion.....	70
4.4.1 Electrical Transport	70
4.4.2 Magnetotransport Measurements.....	73
4.5 Conclusions.....	78
5. Filament Wound Multifunctional Carbon Nanotube Adhesives.....	79
5.1 Abstract.....	79
5.2 Introduction.....	80
5.2.1 Thermally Conductive Adhesives.....	81
5.2.2 Mechanical Properties and Synthesis.....	83
5.3 Experimental Methods.....	84
5.3.1 Sample Production.....	84

5.3.2 Measurements.....	86
5.4 Results and Discussion.....	86
5.5 Conclusion.....	95
6. Filament Winding Vertically Aligned Spinnable Carbon Nanotubes and E-Glass to Create Hybrid-Nano Composites.....	97
6.1 Abstract.....	97
6.2 Introduction.....	98
6.3 Experimental Methods.....	103
6.3.1 Materials and Fabrication.....	103
6.3.2 Measurements.....	108
6.4 Results and Discussion.....	109
6.5 Conclusion.....	122
7. Summary and Future Work.....	124
7.1 Summary.....	124
7.2 Future Work.....	126
7.2.1 Chapter 3 Future Work.....	127
7.2.2 Chapter 4 Future Work.....	127
7.2.3 Chapter 5 Future Work.....	129
7.2.4 Chapter 6 Future Work.....	129
8. References.....	131

LIST OF FIGURES

Figure 2.1: A) Spinnable vertically aligned carbon nanotubes being drawn from an array and twisted. B) Magnified image of the sheet being twisted into a yarn like structure..... 5

Figure 2.2: Transmission electron microscope image of two carbon nanotubes side by side. Measurements show that the outer walls labeled A and are wider than the adjacent walls where the CNTs have deformed..... 9

Figure 2.3: a) Schematic of continuous CNT yarn production. b) Image of the CNTs before consolidation occurs. c) CNT assembly before and after consolidation. d) Consolidated CNT exiting the water bath. e) CNT fiber wound onto the take up spool..... 13

Figure 2.4: Scanning electron microscope images of A) a single CNT yarn, B) two-ply CNT yarn, and C) a four-ply CNT yarn..... 14

Figure 2.5: Electrical properties versus the yarn porosity, which was manipulated by changing the surface twist..... 16

Figure 2.6: Electrical conductivity normalized by density versus the yarn porosity, which was manipulated by changing the surface twist..... 17

Figure 2.7: Example of the convention used to relate folded graphene to the curvature of CNTs..... 20

Figure 2.8: Examples of carbon nanotube folding with zig-zag (12,0), armchair (6,6) and chiral (6,4) structures..... 20

Figure 2.9: (a) Zone folding theory of allowed states in the Brillouin zone. (b) Allowed states overlaid onto the band gap diagram for graphene in the Brillouin zone..... 22

Figure 2.10: The formation of a pseudo band gap occurs when an isolated CNT (a) is surrounded by other CNTs (b) and mirror symmetry is destroyed..... 24

Figure 2.11: Distribution of particles with various sizes and shapes all with 0.1% volume in 1 cubic millimeter. A) Spherical alumina particles, B) carbon fiber, C) graphite nanoparticles, and D CNTs..... 27

Figure 2.12: Schematic of the microcombing process (a) angled view (b) profile view... 29

Figure 2.13: Thermal diffusivity and conductivity properties of CNTs with various amounts of prestraining..... 30

Figure 2.14: (a) Scanning electron image of bare carbon fiber and (b) carbon nanotubes grown on carbon fiber..... 35

Figure 2.15: A) Schematic of the printing transfer process used to apply CNTs to a prepreg ply. B) Prepreg after transfer of CNTs. C) Scanning electron microscope of the CNT prepreg interface. D) Magnified image of the transferred CNTs showing the retained alignment... 38

Figure 2.16: Representation of aligned CNTs in a laminated composites A) during mode 1 delamination and B) before delamination..... 39

Figure 2.17: Various deformation stages: Stage 1, resistance stable near R_0 levels; Stage 2-4, increasing resistances with various slopes; and Stage 5, stable resistance at value much higher than R_0	43
Figure 3.1: Modified X-winder for use with polymer filament mandrels. Timing belts allow for synchronized rotation of fiber chucks which grip the filaments.....	50
Figure 3.2: SEM images of a CNT coated filaments with CNTs oriented a, b) 45° c) 60° and d) 75° to the fiber axis. All images were taken at the same magnification, note the different in diameter between the two 45° samples a, b). The coating in image a) is approximately 11 layers thick while the coating in image b) is approximately 88 layers thick.....	51
Figure 3.3: a) CNT array attached to the mandrel before winding commences, b) CNT array at the end of the winding process showing the decrease diameter along the leading edge, c-g) schematic representation of winding process, as the array traverses sequential layers are deposited as characterized by the darker sections applied to the fiber.....	53
Figure 3.4: Resistance versus probe spacing for 45° -degree samples with various number of layers applied to the mandrel.....	55
Figure 3.5: Resistance versus the number of layer for various spacings between electrodes for samples with 45° -degree winding.....	56
Figure 3.6: Resistivity versus the number of layers for 45° -degree samples for various spacings between electrodes.....	57
Figure 3.7: The effect of winding speed versus the resistivity on samples with 45° -degree winding angle and 22 layers.....	59
Figure 3.8 The effect of consolidation on the resistance of filament coatings.....	60
Figure 3.9 Resistance versus probe spacing for samples with various winding angles and approximately 83 layers applied to the mandrel.....	62
Figure 3.10 Resistance versus winding angle for various spacings between electrodes for different samples with approximately 83 layers applied.....	63
Figure 3.11 Resistivity versus Winding Angle.....	64
Figure 4.1 Temperature dependence of resistance with the current flowing (a) perpendicular and (b) parallel to the CNT axis. The inset shows the ratio of resistance perpendicular to that parallel to the CNT axis.....	71
Figure 4.2 Approximately linear relationship between the $\ln(\sigma T^{1/2})$ versus $T^{-1/4}$ indicating charge carriers undergo hopping conduction from 5 to 300K.....	72
Figure 4.3 (a) MR with current flowing along the CNT axis and the applied out-of-plane field is normal to the current and CNT axis, (b) MR with current flowing perpendicular the CNT axis and the applied out-of-plane field is normal to the current and CNT axis.....	74
Figure 4.4 (a) In-plane MR with current flowing perpendicular to the CNT axis and the applied in-plane field is normal to the current and parallel to the CNT axis, (b) In-plane MR with current	

flowing along the CNT axis and the applied in-plane field is normal to the current direction and the CNT axis. (c) MR with current flowing perpendicular to the CNT axis and the applied in-plane field is parallel to the current direction and normal to the CNT axis and (d) MR with current flowing along the CNT axis and the applied in-plane field is along the current direction and the CNT axis..... 76

Figure 5.1: a.) Picture of the modified X-winder filament winding apparatus and epoxy dropper set up used to create the 0-90 orientation CNT epoxy films. b.) Optical image of the CNT coatings applied at 45-degree angles..... 84

Figure 5.2: Lap shear strength of CNT epoxy adhesives and reference neat epoxy..... 90

Figure 5.3: Images of the failure surface after shearing showing the cohesive failure. The two samples on the left had the CNTs oriented in the direction perpendicular to the strain and the two samples on the right had the CNTs oriented in the direction of strain..... 91

Figure 5.4: Load vs Extension with extension normalized to exclude non-representative data. a.) high volume fraction CNT sample, b.) low volume fraction CNT sample, c.) silver reference sample..... 92

Figure 5.5: Image of a +/- 45° cross ply CNT coating applied to the glass mandrel with the CD and RD directions labeled. The areas outside of the red dashed lines represent the transition points during the winding and were discarded since their alignment doesn't represent the programmed alignment..... 94

Figure 6.1 a.) Filament wound CNTs applied to a mandrel at a 45° orientation prior to b.) glass fiber filament winding. In c.) a co-wound structure is shown where the CNTs are wound throughout the thickness of the tub and consolidated through a small knitting eyelet. In d.) the offset co-winding composite tube structure with the CNTs in an unconsolidated state.... 105

Figure 6.2 a.) Filament wound composites with various winding angles. Left to right 30°, 45°, 60° winding orientations. b.) Filament wound composite tubes with various CNT locations and distributions. c.) Filament wound composite tubes cut down for compression testing..... 110

Figure 6.3 Composite tubes on the MTS between platens at various degrees of strain and failure for axial and radial compression..... 112

Figure 6.4 Stress strain curves for axial compression of the NS and OS samples..... 112

Figure 6.5 Stress strain curves for radial compression of the NS and OS samples..... 113

Figure 6.6 Yield strength of the composite tubes under axial compression..... 114

Figure 6.7 Max loads of the composite tubes under radial compression applied tangentially by flat platens..... 116

Figure 6.8 Stress-strain curves with real time resistance measurements for axial compression of the four-layered composite structure. Resistance measurements represent the interior CNT pathway a.) the full strain measured b.) strain values just past strains that correspond to the yield stress..... 120

Figure 6.9 Stress-strain curves with real time resistance measurements for radial compression of the four-layered composite structure. Resistance measurements represent the interior CNT pathway..... 121

Figure 6.10 CNT epoxy tubes creating using filament winding techniques. Fracture occurred during the removal from the mandrels along 45 degrees..... 122

LIST OF TABLES

Table 3.1:	Summary of the processing parameters and characteristics for each sample. *Note sample 5 and 7 are the same sample but listed separately because of different parameter investigated.....	52
Table 5.1:	Mass fraction of filler material for CNT epoxies and commercial silver filled epoxy. *The electrical resistivity of the silver epoxy varies as a function of the temperature profile used during the curing schedule.....	88
Table 5.2:	The ratio of the sheet resistance of a single layer of CNTs in orthogonal directions.....	95
Table 6.1:	Summary of the orientation and distribution of glass fiber and CNTs for the composites created. *4XS had 4 time the number of CNTs as the other structures by pre-winding 4 full layers prior to the application of the glass fiber....	106
Table 6.2:	Electrical properties of filament wound composite tubes.....	111
Table 6.3:	Summary of axial yield strength and radial max load of the composite tubes and the percent change compared to the neat sample without CNTs.....	117

1. Introduction

Carbon nanotubes have outstanding mechanical, electrical, and thermal properties that make them an ideal choice to be used in composite materials. The physical dimensions can range from a few angstroms to tens of nanometers in diameter and nanometers long to a few millimeters in length. This equates to an aspect ratio of approximately 1,000,000:1 and very high surface area to volume ratios. These properties in combination with their nano-scale dimensions can make carbon nanotubes difficult to process into usable composite structures. To obtain composites with high volume fractions, advanced processing techniques must to be employed. The discovery of spinnable carbon nanotubes, those which can be drawn from an array into a continuous web, has allowed for the creation of aligned high volume fraction composites. However, most of the structures that have been created have 90-0 degree orientations. The subsequent chapters cover a literature review, and research focused on combining filament winding techniques with spinnable carbon nanotubes. These studies create assemblies with carbon nanotubes aligned over a range of angles. The assemblies will also have different levels of dimensionality: one dimensional, linear fiber coatings; two dimensional, planar films; and three dimensional, hybrid composite tubes. There is a particular focus on the electrical properties of these assemblies and how they're affected by processing parameters.

2. Literature Review

The following is a literature brief review covering the benefits of composite materials, types of carbon nanotubes (CNTs), growth methods, and CNT properties. There is an in-depth review of linear assemblies made from CNTs, the electrical properties and conduction mechanisms of carbon nanotubes, two dimensional electrically and thermally conductive materials, and the properties of fiber reinforced composites modified with nanomaterial additions. Each of these topics will focus on materials that incorporate CNTs with high volume fraction and controlled alignment of nanotubes.

2.1 Composites Overview

A composite material can be generally defined as a material composed of two phases of matter. While that description fits the materials that are discussed in this literature review, it is too generic for our purposes. In [1] a composite material is defined as an artificially made material with multiple phases. This more rigorous definition will be used for the review. Under this definition, naturally occurring multiphase materials such as seashells, wood, and pearlitic iron are excluded. Composite materials have multiple phases and therefore their properties are a blend of their constituent materials. Insulating materials can be made conductive, flexible materials can become rigid, and strong brittle materials can transform into strong, ductile objects. Composites can be group into subcategories based on the dimensions of their reinforcement phase. “Zero” dimensional particle reinforced composites, one dimensional fiber reinforced composites, and two dimensional laminar composites. In laminar composites, it is common for fibers to be used as the reinforcement material. The planar dimensionality comes from directional properties achieved from layer by layer processing with layers oriented differently. This review will focus on fiber reinforced composites and laminar composites as they’re most closely related to the structures

created in this research. There are many different methods for creating fiber reinforced composite materials, each with subcategories. Some of these broad categories are layup methods, molding techniques, and pultrusion approaches.

The materials created throughout this research project were created using filament winding principles. Filament wound composites are traditionally used to create tubular materials with various cross-sectional shapes. This method can also create planar composites by cutting the tube before it cures and flattening the material out. Filament wound composites are known to have tunable mechanical properties that depend upon the winding angle [2], [3]. This is true for both static loads and cyclic fatigue enabled failure [4]. When multiple layers with various winding angles are used, the properties depend upon the order the layers and applied [5]. Their properties also change with respect to the wall thickness [3]. While these production parameters affect the performance of filament wound composites, the properties of the constituent materials are just as important. The following sections provide an overview of carbon nanotubes, which are used as the reinforcement material for the composites in this research.

2.2 CNT Overview

2.2.1 Types of CNTs

The simplest of carbon nanotubes is the single wall carbon nanotube (SWCNT) and can be thought of as a sheet of graphene that has been rolled into a cylinder. These structures have very small diameters on the range of 1 nanometer or smaller as first reported in 1993 [6]. The next level of complexity is the double walled carbon nanotube (DWCNT), which has similar radial dimensions to SWCNTs but is composed of two concentric nanotubes [7]. The first carbon nanotube to be discovered has the most complex structure and is the multiwalled carbon nanotube

(MWCNT) [8]. Like the DWCNT, multiwalled carbon nanotubes consist of concentric tubes, but have significantly more walls and can have diameters one to two orders of magnitude larger. Another category of carbon nanotubes is vertically aligned carbon nanotubes (VACNTs). While the previous categories related to the structure of the nanotubes, VACNTs refer to the orientation relative to one another [9]. An important subsection of VACNTs are those that are spinnable vertically aligned carbon nanotubes (SVACNTs), which can be drawn into a continuous sheet of nanotubes [10]. Figure 2.1 shows SVACNTs being drawn from an array and the sheet being twisted together.

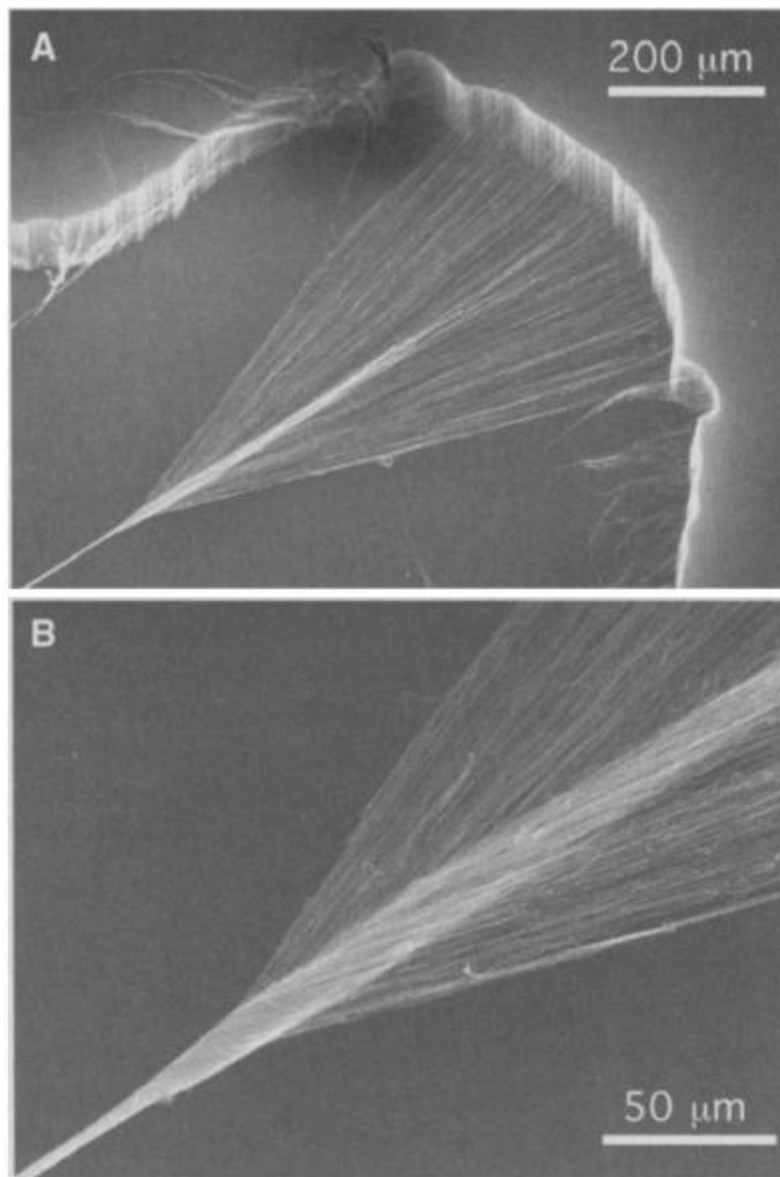


Figure 2.1: A) Spinnable vertically aligned carbon nanotubes being drawn from an array and twisted. B) Magnified image of the sheet being twisted into a yarn like structure. [11]

Spinnable vertically aligned carbon nanotubes provide unique processing opportunities because of their high degree of alignment and ability to form continuous sheets. SVACNTs are used for the experiments and research conducted by the author in subsequent sections.

2.2.2 Growth Techniques

There are many different growth techniques to create carbon nanotubes and can be classified as one step procedures or two step. In a single step procedure, the catalyst is inherently combined with the carbon source such as metallo-organics [12]. While in a double step method the catalyst is applied to a substrate in a controlled manner [12]. Thermal pyrolysis, flame synthesis, physical vapor deposition, solution based catalyst precursors, catalyst, chemical vapor deposition (CVD) and super growth are discussed in [12], which provides a good overview of the benefits and mechanism for these different techniques. This review will focus primarily on CVD and the subset floating catalyst chemical vapor deposition (FCCVD), because these techniques are commonly used to create spinnable carbon nanotubes.

2.2.3 Chemical Vapor Deposition and Floating Catalyst Chemical Vapor Deposition

As the name suggests chemical vapor deposition involves reactive gases flowing through a heated chamber and depositing a new material onto a substrate. In the growth of CNTs via CVD it is common for the substrate to be a silicon wafer or high purity alumina substrate. This is because the reactions occur at high temperatures and the substrate must have a melting temperature that can handle this environment. Before the growth process starts, the substrate is coated with a thin film of catalyst. In [13] the researchers used a 0.5-1.0 nm thick film of iron deposited via electron beam evaporation. A draw back to coating substrates and inserting them into a furnace for CVD is that it is a batch technique and therefore has trouble scaling up to industrial levels. To help address these problems, researchers produced spinnable carbon nanotube forests grown on thin, flexible stainless steel substrates [14]. While this research was still done in a batch process, the ability to grow upon a cheap flexible material shows promise of continuous processing were stainless steel

films could function as the substrate and catalyst, moving as a conveyor belt through the growth chamber [14].

The carbon is provided by the chemical reduction of a gaseous hydrocarbon, commonly methane, ethylene, or acetylene. Hydrogen gas has traditionally been used as a reducing agent and an inert gas such as argon is commonly used to dilute the spatial concentration of the reactants without changing the pressure or participating in the reaction. The reduction of carbon into carbon nanotubes is not a perfect process and often leaves amorphous carbon on the surface of the nanotubes [9]. This buildup of amorphous carbon, depletes catalyst life and activity, which results in shorter nanotubes. It was found that the effect can be mitigated by the addition of controlled amounts of water vapor into the growth reaction zone [9]. Another way to help address the inactivation of catalyst is to provide a continuous supply of catalyst like can be done in FCCVD.

In floating catalyst chemical vapor deposition, instead of having a catalyst deposited onto the surface of the substrate, the catalyst flows through the reaction chamber with the gases. This growth technique is affected by the temperature at which the reaction takes place. [13] showed that there was an increase in growth height from 690 C degrees up to a plateau at 750 C followed by a substantial drop off at 780 C degrees. The temperature was not the only factor shown to affect growth rate. Varying the flow rate of the acetylene and hydrogen gas independently of one another influenced the growth height. In this experiment, there was a maximum growth height of 630 microns at a time of 10 minutes, after which the growth was relatively constant. The limit to this growth is likely due to the inactivation of the catalyst. The addition of chlorine gas in [15] helped grow longer nanotubes likely due to the catalyst remaining active for a longer period of time. In [15] there was also evidence that the pressure the reaction occurs at will affect the growth rate and maximum growth height. These studies show that there are many different factors interacting with

one another affecting the growth of high quality, long, spinnable vertically aligned carbon nanotubes. While the studies have provided insight into the growth process and mechanisms, a universal method or overarching formula has not been developed. Despite the growth problems associated with current methods, the outstanding properties of carbon nanotubes have kept these nanomaterials in the forefront of research.

2.3 Overview of CNT Properties

2.3.1 Mechanical Properties

Single wall carbon nanotubes have the highest theoretical modulus, 1000 GPa, and tensile strength, 300 GPa, of any known material [16]. While MWNTs have lower theoretical values, their measured properties provide much promise for incorporation into structural composites. In [16] individual MWNTs were measured and found to have a modulus between 270 and 950 GPa and a tensile strength between 11 and 63 GPa. It is important to note that this is in the axial direction of the CNT. In the perpendicular or radial direction, it has been shown that the nanotubes are very easily strained. Additionally, a near order of magnitude change in the modulus of SWCNTs occurs, 57 to 9 GPa, when the diameter increases from 0.92 nm to 1.91 nm [17]. However, in MWCNTs it was found that an increase in diameter will reduce the radial modulus until a minimum value of approximately 30 +/-10 GPa is reached [18]. Even van der Waals forces can deform the cross section enough to affect the properties in the axial direction [19].

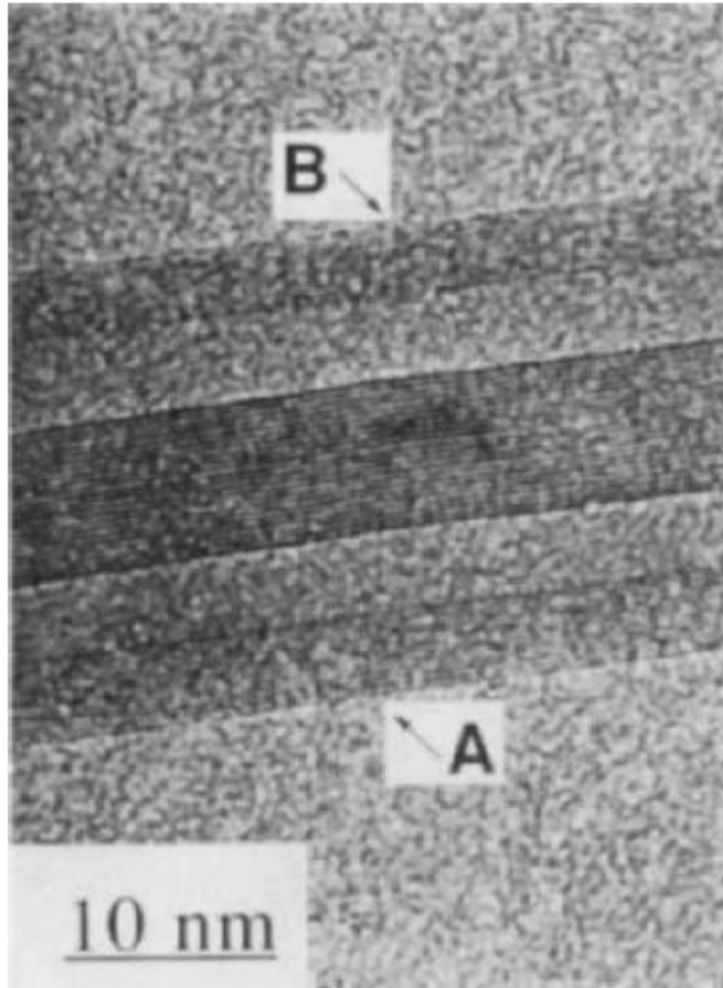


Figure 2.2: Transmission electron microscope image of two carbon nanotubes side by side. Measurements show that the outer walls labeled A and are wider than the adjacent walls where the CNTs have deformed. [19]

While the modulus in the radial direction is low, they can undergo significant compressive strain, 60%, and return to their original position [20]. The tubes can even flatten out completely, but this requires a nonlinear application of force and plastic deformation in the tubes [20]. Even when nanotubes are bent axially they can exhibit up to 40% compressive strain in the radial direction. These high strain values are not limited to compression of the tube radially. The bending strain of the axial direction allows the tube to be bent back upon itself without failure; however, there will

be plastic deformation that occurs [21]. Even in the axial direction there are some unique strain properties. At high axial strain, reversible bonding defects can form to accommodate large deformation [22]. Interestingly, these defects do not significantly change the modulus of the tube, but do affect the strength [22]. This differs from traditional crystalline defect theory where dislocations lower moduli and defects that pin dislocations increase moduli. While the theoretical axial modulus and axial tensile strength are highly desirable properties for composites, their electrical properties are just as intriguing.

2.3.2 Electrical Properties

The electrical properties of carbon nanotubes far exceed the properties of even the highest performing metals. CNTs could revolutionize electrical wiring, field effect transistors, and electrically conductive composites. One of the reasons these optimal properties have not translated into commercial applications is that carbon nanotubes have variable properties. A more in-depth discussion will be given in subsequent sections about why this is the case. This section will serve as an overview to the most promising properties of carbon nanotubes. The current density in carbon nanotubes can reach $4 \times 10^9 \text{ Acm}^{-2}$ compared to 10^6 A/cm^{-2} for typical metals [23], [24]. The mobility of charge carriers in nanotubes have been found to be greater than $100,000 \text{ cm}^2/\text{Vs}$ compared to $1,400 \text{ cm}^2/\text{Vs}$ in silicon [23], [25]. The conductivity of nanotubes has been reported to reach super conducting levels [26]–[29]. Other reports describe nanotubes as being semi-ballistic conductors with near-quantum conductance [30]–[33]. While the nanotubes themselves have variable properties, additional variation is added when tube-tube interactions occur [34], [35]. A massive overview of the properties of carbon nanotubes and their structures can be found in [34], [36], [37]. The impressive electrical conductivity of carbon nanotubes provides CNTs with high thermal conductivity as the two are inherently related.

2.3.3 Thermal Properties

The transport of thermal energy through a material is governed by the electronic contribution and the phononic contribution. As discussed earlier, CNTs have outstanding electrical conductivity and in combination with the very high modulus of CNTs the thermal conductivity of a SWCNT is $3500 \text{ Wm}^{-1}\text{K}^{-1}$ [38]. For comparison, the thermal conductivity of copper and silver is 386 and $407 \text{ Wm}^{-1}\text{K}^{-1}$ respectively. The thermal conductivity of multiwall carbon nanotubes is lower than that of its single wall counter parts but very high values of $3000 \text{ Wm}^{-1}\text{K}^{-1}$ have been reported in MWCNTs [39]. Phonon scattering is one of the things that inhibits thermal conductivity. In traditional crystalline materials, scattering can occur at defect sites or grain boundaries. In an individual carbon nanotube, grain boundaries are not present. Additionally, the dimensions of carbon nanotubes and defect formation energy allow predictions of pristine defect free CNTs. However, when nanotubes reach high temperatures the phononic transport mechanism is mitigated by what is known as Umklapp scattering [36], [38]. When this process occurs, two phonons merge in a way that the momentum is conserved while essentially reversing the propagation direction. For classical physics, this process seems to be a violation of the conservation of momentum, however phonons are quasi-particles. The actual particles, the atoms, are just vibrating about their equilibrium position and therefore have zero net momentum.

2.4 Linear Assemblies

Linear assemblies created from or with carbon nanotubes incorporated into them have a wide range of applications as multifunctional materials. These materials are being investigated as current carrying wires, for sensors, thermoelectrics, and electromagnetic interference (EMI) shielding [40]–[43]. To turn these CNT structures into real world products the mechanical properties and electrical properties must be optimized, characterized, and understood.

Additionally, the production methods will need to be scalable to suit industry needs. The following sections look at batch and continuous production process used to create linear CNT assemblies, the electrical and mechanical properties of these materials, and the EMI shielding properties of CNTs.

2.4.1 Production

The most common linear assembly of CNTs found in the literature are like traditional textile yarns. Both structures have high aspect ratios and are created from high aspect ratio components twisted together providing stability to the material. Textile yarns and linear CNT assemblies both have properties that are dependent upon the base material and the processing parameters used to create them. Therefore, it is not surprising that some of the production techniques used to create linear carbon nanotube assemblies are like the traditional textile yarn production methods. In [44] carbon nanotubes grown in a CVD furnace were collected and drawn into a water bath, redirected via a roller, passed over an additional roller partially submerged in acetone and then exposed to an infrared lamp before being collected upon a collection roller.

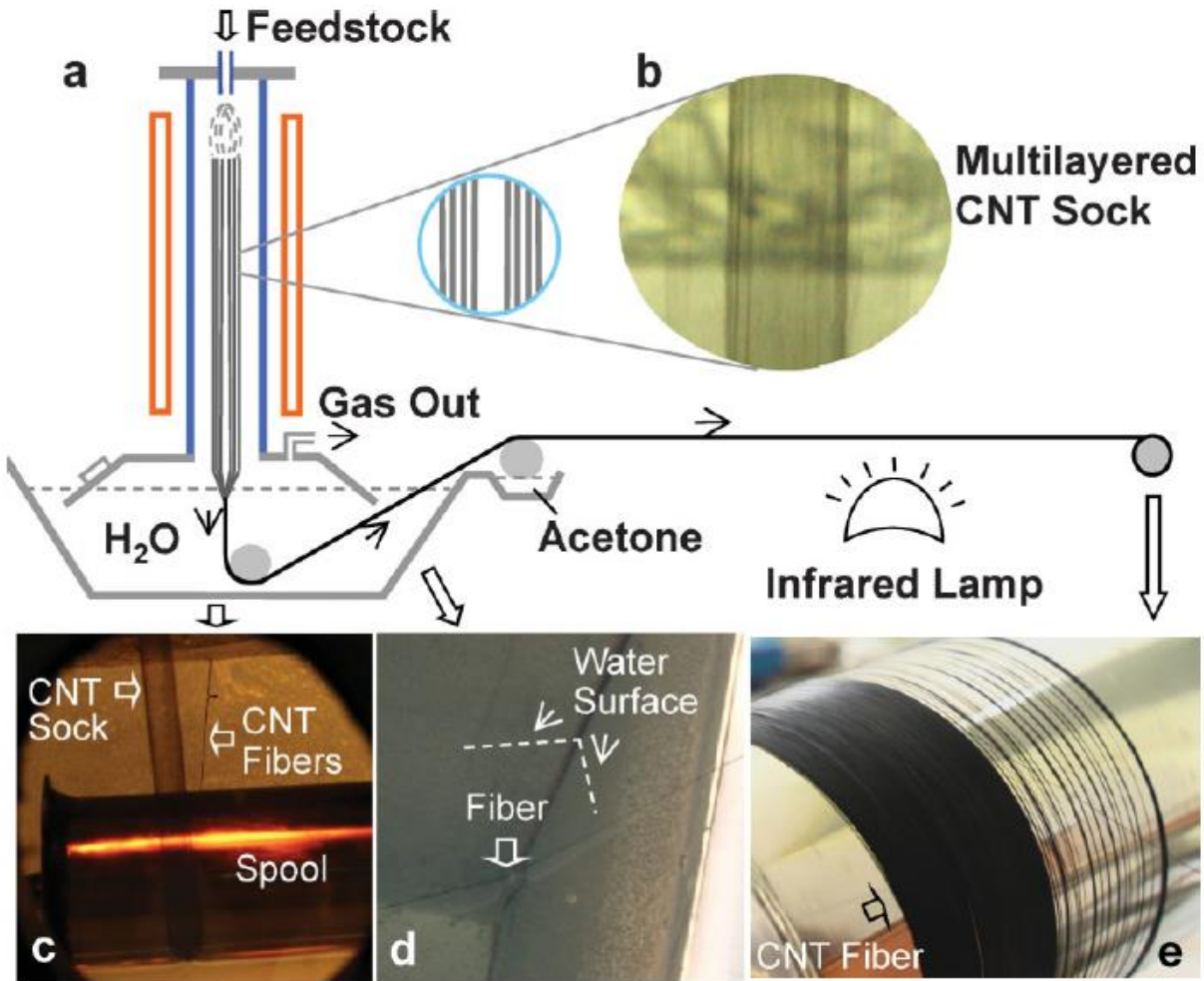


Figure 2.3: a) Schematic of continuous CNT yarn production. b) Image of the CNTs before consolidation occurs. c) CNT assembly before and after consolidation. d) Consolidated CNT exiting the water bath. e) CNT fiber wound onto the take up spool. [44]

The water bath is incorporated to cool and condense the CNTs into a denser structure. This stage is analogous to the process of transforming a sliver into a roving in traditional textiles. The initial structure is a loosely packed aligned grouping of fibers and ends denser and with some mechanical strength. The CNT assembly passing over the acetone roller serves to clean and further densify the yarn, which can be thought of as carding (for the cleaning process) and spinning to increase the density of the yarn relative to the roving. In [45] the researchers used a similar method

to produce the CNTs, using a CVD furnace, however this research does not use collection baths. But rather collects the nanotubes directly onto a spindle from within the furnaces hot zone.

A much more common technique used to create CNT linear assemblies relies upon the drawable characteristics of SVACNT arrays [11], [46]–[51]. There are some similarities between the furnace method and the research done in [46]. Both utilize liquid baths to condense the low-density nanotube assembly and then redirect the yarns with rollers through a furnace, followed by collection onto a roller. In this case, the largest difference is just that the initial source of carbon nanotubes comes from an array rather than the CVD aerosol like material found in the furnaces of [44], [45]. In [48] instead of using a full-sized solution bath the researchers just used a droplet of ethanol to condense the yarns. In [47] twist was added to the yarn by rotation of the collection bobbin during take up. Linear CNT assemblies are not limited to just single yarns, in [11] two ply and four ply yarns were also created.

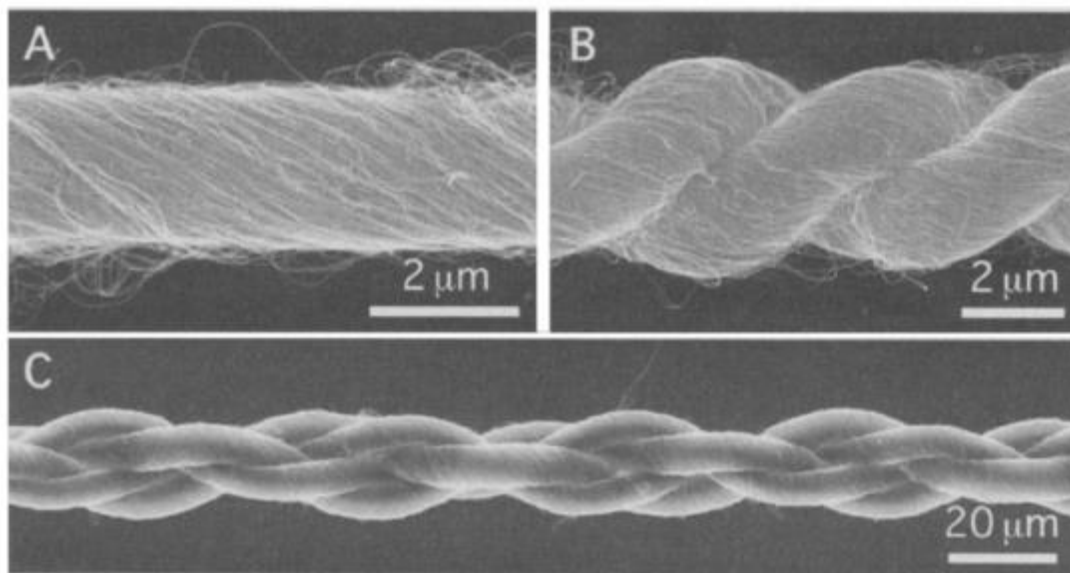


Figure 2.4: Scanning electron microscope images of A) a single CNT yarn, B) two-ply CNT yarn, and C) a four-ply CNT yarn. [11]

In another study braided CNT structures were also created, merging traditional textile structures and CNT linear assemblies [52]–[54]. It is important to note that while traditional textile structures use twist to maintain the coherency of the yarn, not all CNT research utilizes this relationship. In [49] the mechanical requirements of the yarn were minimal and therefore the alignment of the CNT axis remained parallel to the axis of the yarn.

2.4.2 Electrical Properties

The continuously spun nanotube yarns created in [44] were measured using a four-probe technique and have a conductivity of $5 \times 10^5 \text{ Sm}^{-1}$. While these properties are higher than structures created in other research, the yarns exhibited a hollow core and can therefore increase their properties by fully collapsing the structure. This will have a two-fold effect, increasing the number of tube-tube contacts and decreasing the cross-sectional area. It is important to note that in this case, a change to the cross-sectional area will not alter the amount of current passing through the yarn. The other continuously spun yarn from the CVD furnace mentioned above showed slightly higher conductivity with a value of $8.3 \times 10^5 \text{ Sm}^{-1}$ [45]. While the nanotubes produced in [44] were double wall nanotubes those produced in [45] were a mixture of single-wall and multiwall nanotubes. Study [45] also looked at the graphitic purity of these nanotubes and found that the yarns had 85-95% purity. Without purity data from [44] it makes it difficult to discern whether the increased performance is due to the present of SWNTs, purity, or some other factor.

While the novel production of these CNT yarns is important, understanding the mechanism that control the conductivity is just as important. In [47] nanotube yarns are created by direct spinning from a CNT array. In this study, the researchers varied the conductivity by changing the

twist insertion to the yarn as it was drawn from the array. In this study, yarns created with inserted twist had variable conductivities from $1.5\text{-}3.7 \times 10^4 \text{ Sm}^{-1}$ [47]. There was one yarn that did not have any twist inserted and had a very low conductivity of 0.93 Sm^{-1} . This matches up well with [50] where an un-twisted yarn had a conductivity of 1.7 Sm^{-1} and then upon twisting the conductivity increased to $4.1 \times 10^4 \text{ Sm}^{-1}$. In [47] the study calculated the porosity and number of contact points per CNT as a function of the measured density, theoretical density, and Wyk's Model.

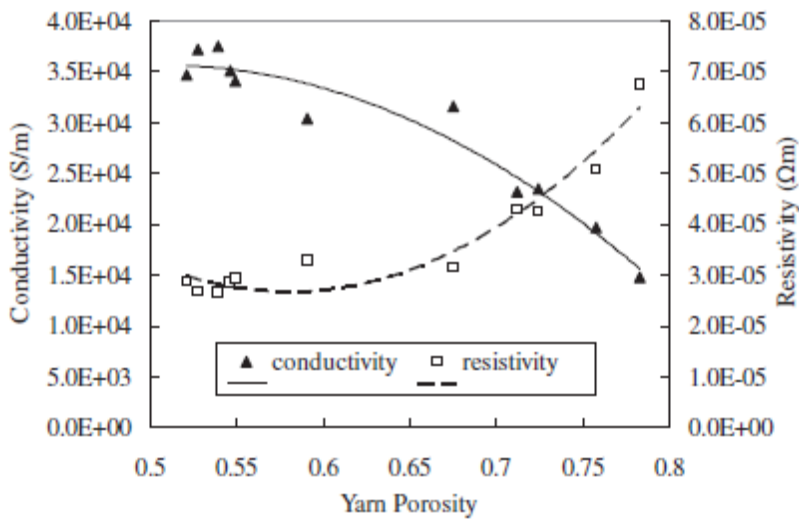


Figure 2.5: Electrical properties versus the yarn porosity, which was manipulated by changing the surface twist. [47]

There was a decreasing relationship between the yarn surface twist angle and the porosity of the yarn. There was also a fairly linear relationship with a positive slope between the number of contacts per CNT and the twist angle. This correlation makes sense, as the open space in the yarn is decreased there must be an increase in the contact between the nanotubes. What is interesting is that the specific conductivity, conductivity divided by density, shows a near linear and horizontal relationship with the porosity of the yarn. Even the zero-twist yarn matches up reasonably well with this relationship.

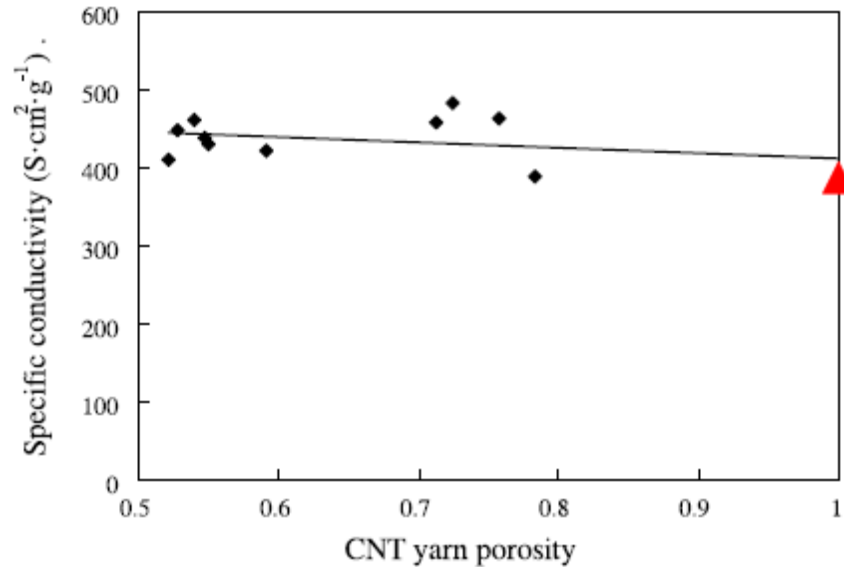


Figure 2.6: Electrical conductivity normalized by density versus the yarn porosity, which was manipulated by changing the surface twist. [47]

This correlation would make more sense if all of the yarns had the same twist angle. It would seem the anisotropic conductivity of carbon nanotubes should give yarns of different orientations different properties. An explanation for the results seen in this study could be related to the value reported as twist angle is actually the surface twist. Perhaps the interior of the yarn has a different structure that accounts for the homogeneity of the samples.

In [11] the researchers created nanotube yarns with a conductivity a of $3 \times 10^5 \text{ Sm}^{-1}$ by drawing from an array. This yarn showed a negative temperature dependence in agreement with [50]. This negative temperature dependence indicates that the CNTs are dominated by a semiconductor like performance. In [11] they were also able to maintain this conductivity after infiltrating the yarn with PVA. The conductivity remaining relatively unchanged after the infiltration of PVA indicates that whether the void space in the yarn is filled by air or a non-conducting polymer the charge carriers do not significantly enter these second phase materials and predominately stay in the carbon nanotubes.

Most of the research presented so far has just focused on measuring the conductivity of the nanotubes but with limited emphasis on unique applications of these conductive properties. What follows is a discussion of some unique application of CNT yarns. In [48] the researchers demonstrated that CNT yarns can be used as filaments for incandescent light in the visible spectrum. Interestingly, the conductivity increased after the sample was left “on” for a period of time [49]. It would be valuable to determine whether the increase in conductivity is a temperature related mechanism caused by joule heating or due to the flow of electrons through the assembly. Most carbon nanotube growths do not yield products with 100% graphitic structures, often the tubes will have regions with defective bonding. The joule heating could have caused an annealing affect that increased the graphitic nature of the tubes. Another common source of non-graphitic carbon is amorphous carbon on the surface of the tubes. The oxidative removal of this carbon could increase conductivity; however, the study was done with the carbon nanotubes under vacuum pressure so it is unlikely to have occurred. Perhaps this method could be used in other CNT yarns as a post treatment to increase the conductivity. It was also shown that these CNT yarns have sufficient alignment to act as a polarizer of ultraviolet light [49]. In [55] CNT yarns were used in a photovoltaic material and could collect holes at the junction between the yarn and silicon. CNT yarns can also be used as super-capacitors; one study showed a specific capacitance of 5 Fg^{-1} and an energy storage density of 0.6 Whkg^{-1} . Another study far exceeded these properties with a yarn showing capacitance of 79.8 Fg^{-1} when submerged into a sodium chloride solution [44].

2.4.3 EMI Shielding

There is limited research done with carbon nanotubes in linear assemblies acting as electromagnetic shielding. However, as this is one of the proposed applications in this study the following will be a brief review of the EMI properties of composite materials made with CNTs

regardless of structure. Traditionally metals are used for EMI shielding, however, CNTs are becoming part of the research field [42]. This is partially due to the fact that most metallic EMI shields function via reflecting photons while CNT based materials can absorb the incident radiation [56]. Another advantage is that traditional EMI shielding materials are heavy while CNTs have a much lower density [57]. Multiwalled carbon nanotubes have been added to a ceramic matrix and show increasing attenuation with increasing weight fraction reaching 25 dB at 9% CNT [58]. Carbon nanotube/polymer composites show good attenuation, 37-60 dB, and are close to or exceed industry required 40 dB [59], [60]. Pure carbon nanotubes show even better EMI shielding properties, 61-67 dB attenuation, in the form of a light weight 1 micron thick film [59]. 60 dB attenuation was also achieved in a CNT composite material that had a CNT weight fraction of 50% [61]. Interestingly, in one study, when CNTs were coated with metal and incorporated into a composite the EMI shielding decreased as the metal coating increased [62]. The study mentioned that the metal coated samples were difficult to disperse evenly. This suggests that for a CNT material to perform as an effective shielding agent there must be a continuous coating or at the very least uniformly distributed. Despite these advances, the current cost of nanotubes is holding CNTS back from commercial applications [41].

2.5 Electrical Properties

2.5.1 Individual CNTs

In CNTs the electrons have SP^2 bonding with 3 sigma bonds in the curved plane of the surface and one pi bonding electron perpendicular to the curved plane. The sigma bonding electrons are essentially locked into place and do not contribute to electronic current. The graphene band structure is often used as a starting point to understand why. The energy between the sigma bonding and antibonding states is much too large in the Brillouin zone of graphene. However, the

Pi bonding and Pi anti-bonding energies for a linear cusp at the K positions, which is where the atoms sit, in the Brillouin Zone. This contact point gives graphene its semimetal properties. However, this relationship becomes much more complicated when considering the curvature of a CNT. The complications arise due to the wave properties of electrons and specifically the wave vectors.

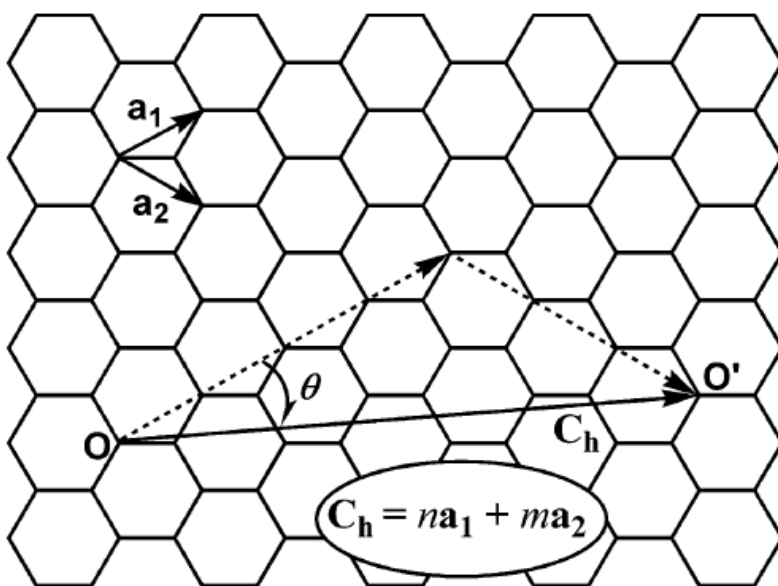


Figure 2.7: Example of the convention used to relate folded graphene to the curvature of CNTs. [34]

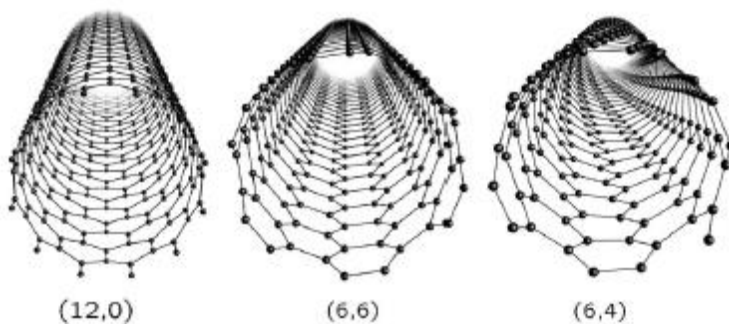


Figure 2.8: Examples of carbon nanotube folding with zig-zag $(12,0)$, armchair $(6,6)$ and chiral $(6,4)$ structures. [36]

The quantum nature of this property only allows for specific values to occur and requires dimensions that will accommodate these values. In an infinite plane of graphene, the electron is only bound in the Z, out of plane, direction and can extend indefinitely in two directions. For a cylindrical tube of with a finite diameter and infinite length the electrons can propagate without restriction along the axis. However, per zone folding theory, for the electron to travel around the curved, radial surface of the nanotube the path length must satisfy the wave vector. If the diameter of the tube does not meet the wave vector requirement, the electron will be forced to propagate around the tube at an angle other than 90 degrees to the axis. When this is the case, the pathway through a given Brillouin zone is different than for an arm chair CNT where the allowed propagation directions travel through the K points found in the Brillouin zone. It is important to note the wave vector requirement is not just a geometric construct but involves a more complicated quantum explanation that can be found in [36].

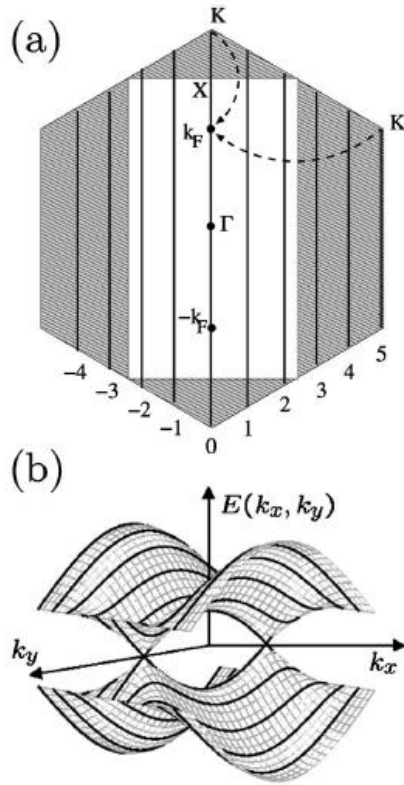


Figure 2.9: (a) Zone folding theory of allowed states in the Brillouin zone. (b) Allowed states overlaid onto the band gap diagram for graphene in the Brillouin zone. [36]

A result of this stipulation is that while the pathways that satisfy the allowed wave vector requirement are parallel to one another they are not continuous along the tube. When the graphene band structure is overlaid onto the new CNT wave vector restricted Brillouin zone, the allowed directions act as contour lines for electron energy values in the CNT. The overlaid graphene band structure is not completely accurate for a carbon nanotube, because it does not consider the fact that the nanotubes surface is curved. This curvature causes a shift in the K point within the Brillouin zone slightly away from the atom positions [63]. For arm-chair nanotubes the properties are maintained because the shift occurs in a direction along one of the allowed wave vector directions [63]. However, for other metallic, zig-zag, nanotubes a very small bandgap can be measured due to the shift of the K point [63]. These miniscule band gaps and metallic properties

were confirmed experimentally by examining single wall nanotubes with scanning tunneling microscopy [64]

These variable band structures are the reason that some nanotubes are metallic and some are semiconducting. When the allowed wave vector directions pass through K points in the graphene Brillouin zone the overlap of the Pi bonding and pi anti-bonding bands creates an energy less transition. However, if there is an offset from the K points the CNT will be a semiconductor with a bandgap whose magnitude has a rough dependence following the inverse of the diameter [65]. More accurately the bandgap depends upon the diameter and the direction the tube was rolled [66].

The band structure of a carbon nanotube and its semiconducting or metallic state is not an absolute property. It can be modulated by the application of a magnetic field as was first theorized by Aharonov and Bohm in 1959 and then experimentally measured in 1993 for a carbon nanotube [67], [68]. When a magnetic field is applied parallel to the axis of the nanotube there is a shift in the orbital momentum of the electrons [67]. This changes the wave vector and the allowed directional states along the circumference of the nanotube [68]–[70]. Interestingly, with a sufficient magnetic field the Aharonov-Bohm shift can make a full translation and return a material back to its original zero field properties. The magnitude of field required to make a full shift is not always the same for a given nanotube. A 1 nm diameter nanotube would require a 5325 T field for a full Aharonov-Bohm shift while a 40-nm diameter CNT only needs 3 T [70].

2.5.2 Assemblies

Not surprisingly the very precise and sensitive band structure is perturbed when other nanotubes are brought into the equation. In the case of a nanotube that exhibits metallic properties when isolated, a small bandgap can form when it becomes surrounded by nanotubes aligned in the

same direction. This band separation occurs due to a break down in the mirror symmetry of the now multitube system [71]. In this study the researchers found that while tube-tube interactions do cause a change in the density of states and band structure, even the most disordered system caused only minimal change called a pseudo gap [71].

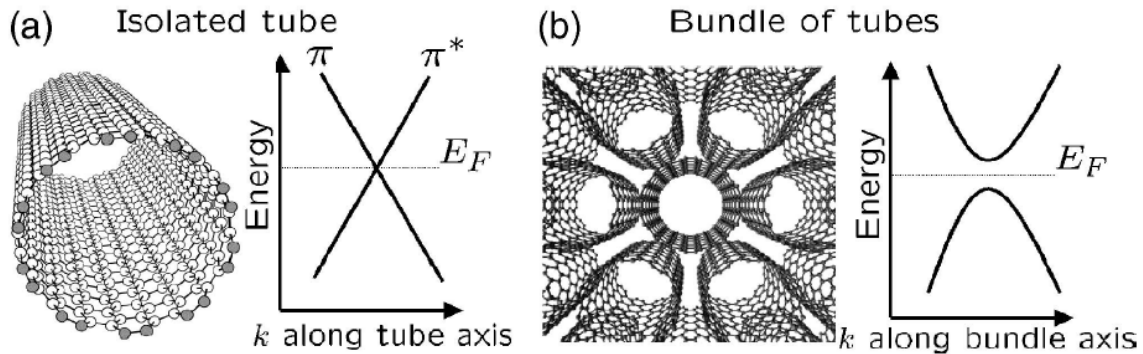


Figure 2.10: The formation of a pseudo band gap occurs when an isolated CNT (a) is surrounded by other CNTs (b) and mirror symmetry is destroyed. [36]

Interestingly, a (10,10) tube surrounded by (10,10) tubes with the exact same orientation and alignment still exhibits this pseudo gap. However, (6,6) surrounded by (6,6) tubes in the same fashion will not exhibit a pseudo band gap [71], [72]. This is because in the bundle of (6,6) tubes the bundle and the original nanotube have the same mirror symmetry, D_{6h} that is. If any of these (6,6) tubes begin to rotate, the mirror symmetry is destroyed and a band gap would be formed [36], [73]. This sensitivity to symmetry is not only present in bundles of separate tubes but is also present in multiwall nanotubes [74], [75]. This is likely why multiwall nanotubes depict semiconductor like temperature dependence even though approximately one third of nanotube folding orientations predict metallic properties. Just as with the multi-tube system, the highest degree of symmetry has the smallest effect on the band properties on MWCNTs. In high symmetry orientations, the band

gap was only slightly broken apart from the degenerate band structure. However, in the least symmetric orientation a band gap with 4 distinct bands at the fermi level was observed [74].

2.5.3 Transport Mechanisms of Individual CNTs

Carbon nanotubes are capable of electron transport down the tube axis in a way that no scattering of the electron occurs. This conduction phenomenon is known as ballistic conduction and will exhibit quantum conductance G_0 , $2e^2/h$, for every electron channel that is present [36]. However, electron scattering is a probability based event and not all scenarios give rise to ballistic conduction. Whether a scattering event will occur or not is a function of the elastic mean free path of the electron and the length the electron must travel. Factors such as topological and chemical disorder and intershell coupling decrease the mean free path and limit the length a CNT can be and still exhibit ballistic conduction [36]. When there is a defect upon the surface of a metallic nanotube, there is a probability of the electrons interacting with the defect based on the density of states. This probability is once again a mean free path. However, the comparative path length term is the circumference of the tube instead of the length of the tube. For an armchair metallic nanotube, the mean free path is 560 nm, which is much larger than the circumference of nanotubes and indicate that surface defects have a limited effect on these metallic CNTs. Unfortunately for semi-conducting tubes, these defects exhibit much lower mean free paths and can act as scattering sites [65].

2.5.4 Transport Mechanism of CNT Assemblies

When multiple nanotubes are present, additional scattering events arise. For the charge to transfer from one tube to another without a scattering event, there must be a coherent symmetry

between the two. When this condition is not satisfied the probability of transmission decreases which has been shown theoretically [76] and experimentally with scanning tunneling microscopy [77]. This symmetry requirement does not only apply to nanotube-nanotube junctions but rather to all interfaces and is generally referred to as contact resistance. The magnitude of this scattering barrier is not the same for all tube-tube interactions. For a metal-metal tube interface, the barrier is relatively small. For a metal-semi-conducting situation, research points to there being a Schottky-barrier that has variable resistance depending upon the voltage potential. Not only is there an effective resistance at these tube-tube boundaries due to coherency but it is a variable property that will increase as the pressure pushing the tubes together increases. This can be explained considering that the transmission coefficient of a single nanotube decreases as the tube is bent or under goes shear deformation. When there is significant bending strain, the SP^2 bonding and pi orbital begin to hybridize.

Another concept related to the conductivity of nanotubes is that of hopping conduction, originally theorized by Mott [78]. This theory explains how electrons can move from one discontinuous physical location to another even when there is a difference in the energy of these two states. A brief overview of this theory surmised from [79] is presented below. There is a finite amount of energy require to move from one physical location to another. If the energy state of the destination is higher the departure location, there will be an additional finite energy required to make this transition. Therefore, the probability of this transition occurring will be a function of the total energy required. By examining certain boundary conditions at minimum and maximums for the spatial and energy state separation between the two locations, along with more complicated factors provides mathematical evidence that is in alignment with the assumptions made by Mott.

The result yields that the natural log of conductivity is dependent upon $T^{(-1/(d+1))}$ where d is the dimensionality of the system.

2.6 High Volume Fraction CNT Films

2.6.1 Conductive CNT Films

The following section will cover high volume fraction, two dimensional CNT films that are electrically and thermally conductive. For a composite material with an insulating matrix to become conductive its reinforcing material must be added in a sufficient volume to form a network that extends across the material. This is commonly referred to as the percolation threshold. The amount of material that is needed to reach the percolation threshold is highly dependent upon the geometry and size of the particle [80].

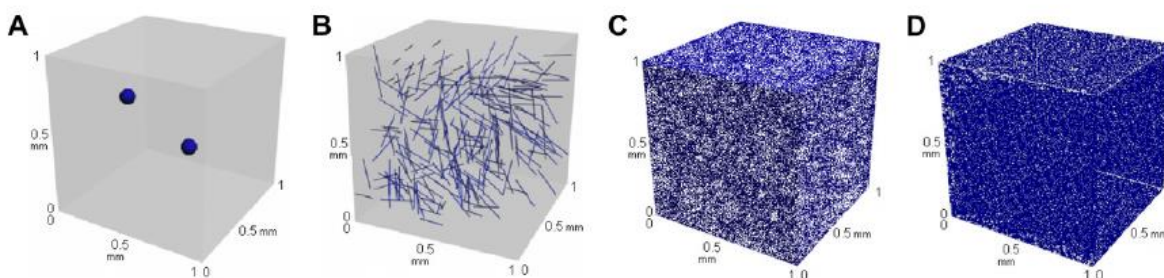


Figure 2.11: Distribution of particles with various sizes and shapes all with 0.1% volume in 1 cubic millimeter. A) Spherical alumina particles, B) carbon fiber, C) graphite nanoparticles, and D) CNTs. [80]

For spherical objects the threshold is around 16% while in carbon nanotubes the measured percolation values are much lower [81]. Even though studies agree that the threshold is much lower, there is still significant variance from study to study. Using SWCNTs, percolation has been reported at 0.1 -0.2 percent [82], while another study using multiwall nanotubes found the percolation threshold to be 0.055% [83]. Another MWCNT study showed a percolation threshold

of 0.5% [84]. An in-depth review of the factors that affect percolation can be found in [85]. While a universal value has not been determined for carbon nanotubes, there is sufficient evidence to suggest that any concentration greater than a few percent of well dispersed nanotubes will satisfy percolation requirements.

A polyimide CNT composite film was created with a conductivity of $1.8 \times 10^4 \text{ Sm}^{-1}$ [86]. This research could increase the conductivity of the sample by straining the sample before the matrix had fully cured. 6% pre-strain caused the sample to increase its conductivity to $2.7 \times 10^4 \text{ Sm}^{-1}$ [86]. The prestraining caused the network of CNTs to become denser and therefore increase the number of tube to tube contacts. Another layer by layer technique was able to create an electrically conductive film with slightly higher conductivity of $3.5 \times 10^4 \text{ Sm}^{-1}$ [87]. This method did not incorporate any polymer filler. While this might seem like it could explain the increased conductivity, it is unlikely. The polymer filler used in [86] is non-conductive, but not having a filler essentially just means that you are using an air matrix, which is also very insulating. Instead, the increased conductivity must be due to better connections between nanotubes. This increase in tube connections is probably due to the ethanol treatment applied, which increased the density of the film by 50% from 0.6 g cm^{-3} to 0.9 g cm^{-3} [87]. Conductivity can be further improved by using a technique termed “microcombing” by the authors of [88], [89]. In these studies, the nanotube ribbon drawn from the array was passed over razor blades before being collected upon a mandrel and exposed to water ethanol solution for solvent densification [88], [89].

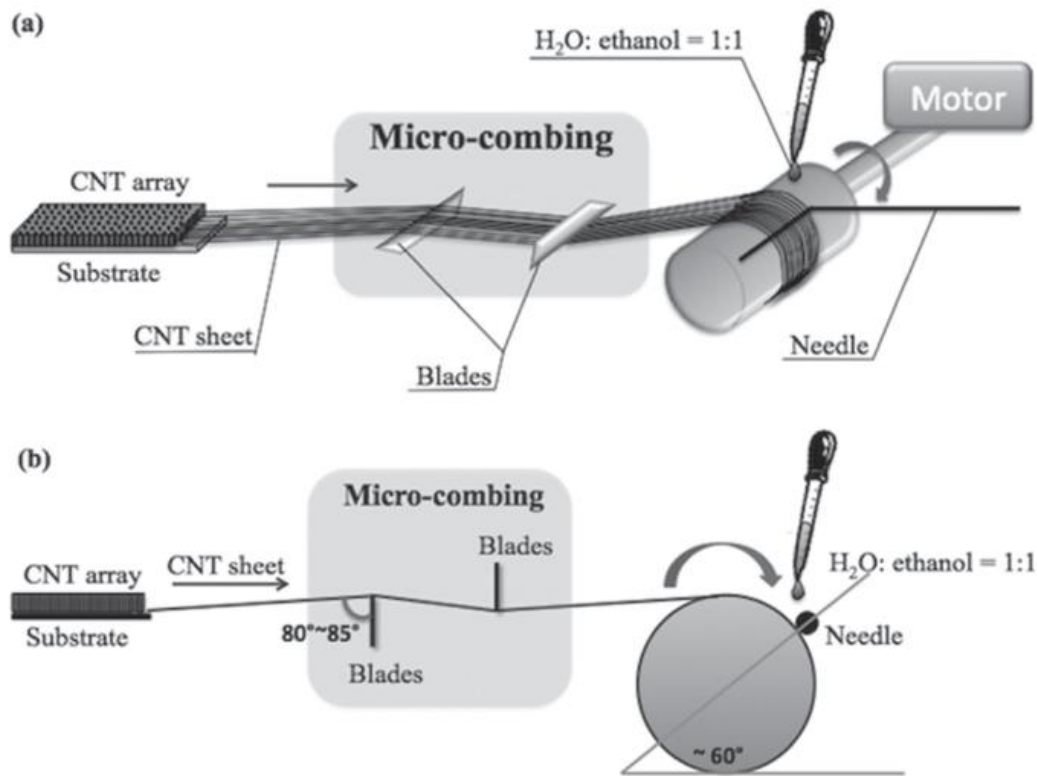


Figure 2.12: Schematic of the microcombing process (a) angled view (b) profile view. [88]

The microcombing approach mechanically increases the alignment of the nanotubes, which increases conductivity itself. Additionally, the increased alignment increases the density and therefore the conductivity because of a greater number of tube-tube contacts. Using this approach, the conductivity reached a value of $1.8 \times 10^5 \text{ Sm}^{-1}$ [88], [89]. Higher conductivity has been measured in carbon nanotube films by almost a full order of magnitude with a conductivity of $1.0 \times 10^6 \text{ Sm}^{-1}$ [90]. This research used a solution processing technique instead of dry spinning. The sample was aligned using magnetic fields while in solution and showed anisotropic properties. The conductivity was 24 times higher in the axial direction than the radial direction [90]. This low value of anisotropy indicates that the sample does not have very good alignment. Therefore, the

superior conductivity values must be because this sample was created using single wall nanotubes. This sample also showed very high thermal conductivity, $200 \text{ Wm}^{-1}\text{k}^{-1}$ [90]. This is almost a full order of magnitude higher than the prestrained polyimide composite which had a thermal conductivity of only $18.4\text{-}31.1 \text{ Wm}^{-1}\text{k}^{-1}$ depending upon the level of prestraining [91].

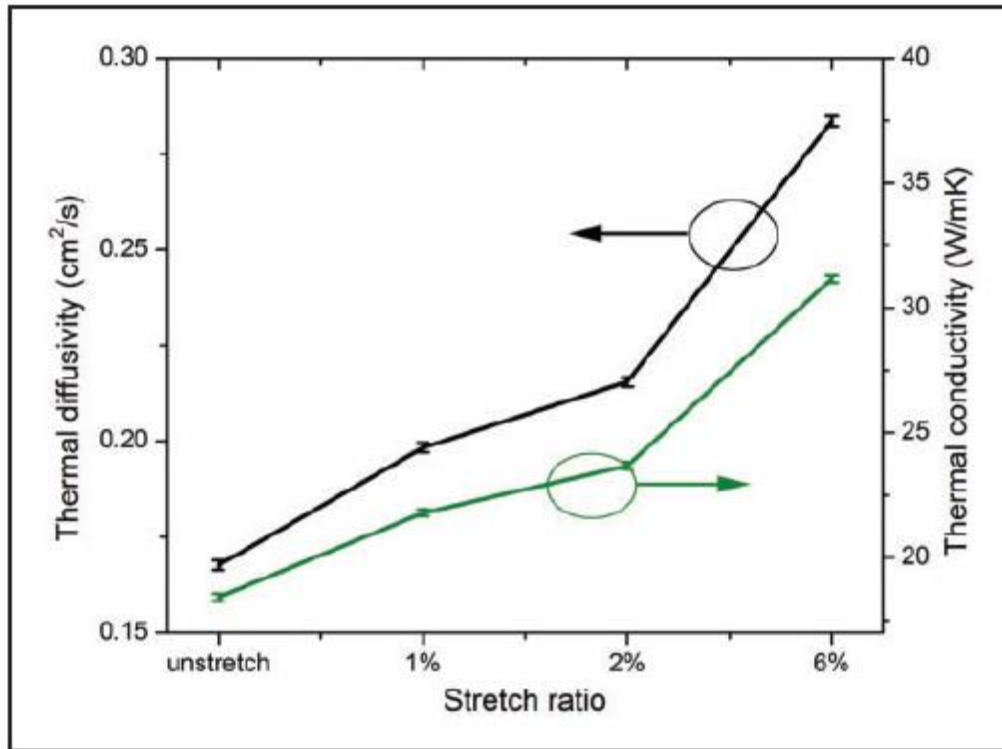


Figure 2.13: Thermal diffusivity and conductivity properties of CNTs with various amounts of prestraining. [91]

This study exemplifies the importance of having the optimal material during composite production. Despite much lower levels of orientation, SWCNTs in the above research out performed MWCNTs mentioned.

2.6.2 Electrically Conductive Adhesives

A specific application of carbon nanotubes films is in conductive adhesives designed to replace traditional lead tin solders. This section will also review electrically and thermally conductive adhesives with non-CNT additives. The thermally conductive adhesives discussed cover both electrically conducting and electrically insulating samples. Metal solders are commonly used in electronic applications and pose a significant health risk due to the lead content. Additionally, lead tin solders are much heavier than polymer based alternatives, which makes them detrimental for applications in the aerospace industry where even small weight savings can make a big difference in efficiency and performance. In commercial applications of current electrically conductive adhesives, the most common additive material are metals, specifically silver. Research is being done to determine out how to optimize these materials and have properties that vary over a wide range that are like CNT based films.

One of the big differences between metal based conductive adhesives and CNTs is the percolation threshold. Metal powders and metal nanoparticles will generally have semi-spherical dimensions and require higher loadings than high aspect ratio nanotubes. In [92] very high loadings of silver were added to epoxy precursors at value of 70 wt.%. Then the resins were cured and resistance was measured as a function of time while the resin cured in both isothermal and non-isothermal cure procedures. As the resins cured, the crosslinking caused the polymer to shrink pulling the silver particles together forming a conductive network that changed the resistance by two orders of magnitude [92]. By increasing the amount of crosslinking agent, the resin cure shrinkage and electrical conductivity also increased with values ranging from $3.3 \times 10^4 \text{ Sm}^{-1}$ to $1.7 \times 10^5 \text{ Sm}^{-1}$ [92]. This level conductivity has also been measured in a “self-healing” epoxy adhesive. The polymer sample was mechanically damaged and then allowed to heal due to the presence of

encapsulated epoxy-amine microcapsules. After healing the conductivity wasn't as high as it was before deformation. The authors indicated this was likely because the encapsulated healing material did not have any silver present. Other research showed that how the conductive additive is prepared influences the conductivity of the sample. The removal of processing lubricant from silver flakes increased conductivity as did incorporating a coupling agent to the composite material [93]. A benefit of lead tin solders is that they can be formed and reformed repeatedly by reapplying heat to the solder. Epoxies are generally one time use due to their thermoset nature and do not degrade except at high temperatures. To address this issue [86] showed that a thermoset material with a low degradation temperature can be made to function as a conductive adhesive with a conductivity of $2 \times 10^7 \text{ Sm}^{-1}$. This allows the material to be removed and fresh application reapplied when needed without damaging any temperature sensitive components. Research shows that silver can have a beneficial effect on the conductivity of carbon based conductive adhesives. In [94] the conductivity of graphene based conductive adhesives was increased when silver nanoparticles were functionalized to the surface of graphene and reached a conductivity of $2.2 \times 10^7 \text{ Sm}^{-1}$. It is quite likely that the combination of silver nanoparticles and carbon nanotubes would have a similar effect on conductivity.

2.6.3 Thermally Conductive Adhesives

Thermal management is an important concept in the computer industry as processors can generate a very high energy density at high computing loads. A good thermal conductor will take advantage of the phononic and electronic components of thermal conduction. Therefore, it is important to understand the mechanisms and make sure that any increase in electrical conductivity won't hurt phononic contributions and vice versa. Even a small addition of carbon nanotubes to epoxy adhesives can increase the thermal conductivity. In [95] as little as 1% MWCNT added to

epoxy increased the thermal conductivity by 15 percent. Research shows that the alignment of carbon nanotubes plays an important role in thermally conductive adhesives. In different epoxies, the difference between thermal conductivity for aligned versus dispersed adhesives as follows: neat epoxy $0.56 \text{ Wm}^{-1}\text{k}^{-1}$, dispersed $0.59 \text{ Wm}^{-1}\text{k}^{-1}$, aligned $1.21 \text{ Wm}^{-1}\text{k}^{-1}$ [96]. In another epoxy the values were as follows: neat epoxy $0.23 \text{ Wm}^{-1}\text{k}^{-1}$ and with aligned CNTs $0.88 \text{ Wm}^{-1}\text{k}^{-1}$ [96]. The reinforcing material is not the only parameter that can influence the thermal conductivity. In a branched epoxy thermoset, there was a drop in the thermal conductivity from 0.182 to $0.162 \text{ Wm}^{-1}\text{k}^{-1}$ when branching exceeded an optimal amount [97]. Another study involving CNTs produced an adhesive with a thermal conductivity of $5.8 \text{ Wm}^{-1}\text{k}^{-1}$ and suggested that optimizing their process could theoretically create samples with conductivity values of $25 \text{ Wm}^{-1}\text{k}^{-1}$ [98]. The importance of using an electrically conducting filler is exemplified by a study that used both graphite and boron nitride. These two materials are very similar structurally and mechanically. The biggest difference is boron nitride is insulating and graphite is conductive. In this study the graphite based sample had a thermal conductivity twice as high as the boron nitride at the various volume fractions tested [99].

However, there are some instances when a thermally conductive adhesive is needed but needs to be electrically insulating. In these situations, the additive material will need to have high phononic contributions to thermal conductivity. These materials are generally characterized by high modulus and close packing atomic structures. Generically ceramics are high modulus, insulating materials and therefore have a significant presence in the literature. For example, one study incorporated aluminum nitride into an epoxy and increased the thermally conductivity by 500% to $1.05 \text{ Wm}^{-1}\text{K}^{-1}$ about half of the theoretical value for the composite. Optimizing thermally conductivity can be quite difficult and techniques don't always transfer from one material system

to another. For example, in a study involving ceramic additives, certain particles increased thermal conduction while other particles showed a decrease [100]. For each of these reinforcing materials there was a decrease in the electrical conductivity so the explanation must be due to phonon interactions. It's likely that the introduction of these nanoparticles act as scattering sites for the phonons in the polymer. The one sample that had an increase in the thermal conductivity must either have a more strongly bonded interface, smaller scattering coefficient, or a combination of the two.

2.7 Fiber Reinforced Composites with Nanomaterial Additives

The properties of fiber reinforced polymer (FRP) composites can be modified by adding nanomaterials to the epoxy or incorporating them into or on the fiber. These 3+ phase structures are referred to as hybrid composites. Hybrid composites can also refer to a matrix with two traditional fiber reinforcements, but for this review hybrid composites will refer to fiber reinforced plastic with nanomaterial additions. In structural composites, the mechanical properties can be improved with the addition of nanomaterials. Also, the addition of nanomaterials to composites can transform single purpose composites into multifunctional materials. Multifunctional hybrid composites have higher electrical conductivity, thermal conductivity than traditional counterparts or can be use in a sensing application. As previously discussed, the mechanical properties of carbon nanotubes make them ideal reinforcing materials for composites and hybrid composites. However, achieving a high degree of orientation with significant volume fraction of evenly distributed with carbon nanotube as the sole reinforcement material has proven to be difficult. Even small volume fractions of carbon nanotubes tend to bundle within the matrix [101]. This is one advantage of hybrid composites over traditional composites made with nanomaterials. Hybrid composites

require much less volume of nanomaterial in comparison to their traditional counterparts. This compounds into a two-fold benefit of cost savings and easier processing.

2.7.1 Mechanical Properties of Composites with CNT Additions

One research group tackled the problem of a uniform distribution of carbon nanotubes by growing CNTs directly onto the carbon fiber reinforcement [102]. This study tested four different fiber treatments: without sizing, with catalyst on the surface, CVD without catalyst (which resulted in amorphous carbon), and with CNTs grown on the surface. While the study showed a 15% increase in the interfacial surface strength when carbon nanotubes were present, interestingly the catalyst and amorphous carbon caused the interfacial strength to decrease by 37% and 32% [102].

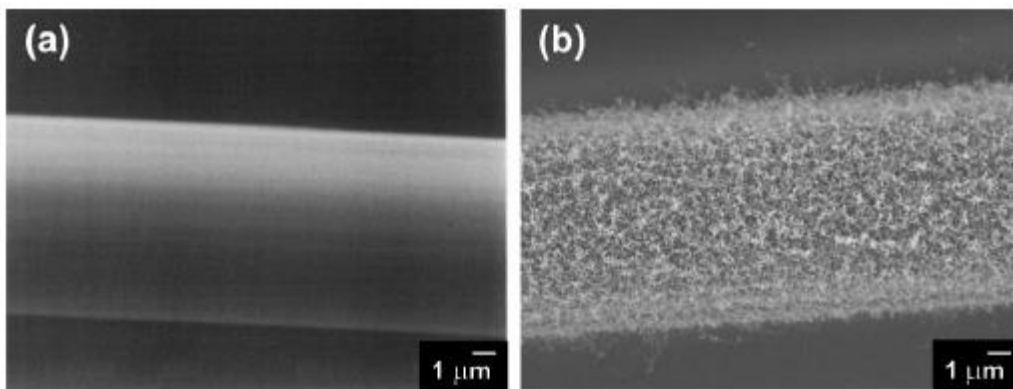


Figure 2.14: (a) Scanning electron image of bare carbon fiber and (b) carbon nanotubes grown on carbon fiber. [102]

In this study, it is possible that the increased interfacial strength isn't a consequence of the carbon nanotubes' inherent strength but rather due to how it interacts with the CF in comparison to the amorphous carbon and catalytic particles. If the CNTs grew into the graphitic regions of the carbon fiber, there would be a very strong covalently bonded interaction. In this scenario, the carbon nanotubes would essentially provide additional surface area for the load transfer between

matrix and CF. If the modulus or strength of the nanoadditive were responsible for the change in interfacial strength one might expect the iron catalyst particles to perform better than the amorphous carbon. However, the opposite trend was witnessed. This could be due to the amorphous carbon being more compatible with the carbon fiber or it could be due the volume of material added to the carbon fiber. A more rigorous study would be needed to determine the exact mechanisms on how the nanoadditions affect the interfacial strength.

The direct growth of carbon nanotubes onto fibers isn't limited to unprocessed fibers, filaments or tows. Two-dimensional cloths and as described three-dimensional carbon fiber felts have also been subjected to CVD CNT growth processes [103]. In this study the flexural strength of the tows, cloths, and felts were increased by 20%, 75% and 66% respectively while the flexural modulus was increased by 25%, 54%, and 46% respectively [103]. I believe this trend can be explained by looking at the spacing of the fibers in comparison to the length of the carbon nanotubes. In the woven structure, the weave itself likely holds the fibers together more tightly than in the simple tows. And in the carbon fiber felt it is almost assuredly the case that the largest spacing between two fibers is greater than of that the woven fabric. However, there are also some locations where the carbon fibers are well entangled and the separation is not very large, as is the nature of felts. As produced the CNTs are grown from the surface of these structures and reach a terminus in the epoxy. However, imagine and hypothetical scenario where the CNTs terminated at a second fiber. In this scenario, a three-dimensional reinforcement network would be created, likely with very strong properties. Now as we return to our produced materials, we must remember that the CNTs have a finite length. If this finite length approaches the spacing between fibers, the properties could approach that of a 3D network. However, if they're much shorter than the spacing distance there will be regions of pure matrix that will have lower strength and modulus than the

CNT reinforced regions. If this is the case, why the felt is in the middle of the fabric and tow is unclear. It could be that the average spacing of the felt is lower than that of the tows. Another possibility is that there is some sort of non-linear response and very tight knit regions in the felt increase the properties more than having spacing greater than the tow hurts it. Another study showed an increase in the toughness of a woven cloth composite with nanotubes grown on the material by 76% [104]. It's likely that the similarity in percent increase is just a coincidence between these two studies and not a fundamental property. What is clear is that the addition of carbon nanotubes to FRPs has a significant change upon performance. In [104] the failure mechanism without CNTs was a matrix dominated shear-out failure, while the sample with CNTs exhibited tensile fracture.

One drawback to the direct growth of CNTs onto fibers is that it can only be used for certain reinforcing fibers. Specifically, only fibers that can undergo high temperatures are available for this technique. Any polymeric material with a degradation temperature below a minimum of 600 C degrees will breakdown during typical CNT CVD growth processes. It's been shown that high temperatures can reduce fiber properties even when kept below degradation and melt temperatures [105].

To get around the high temperature processing parameters, electrophoretic deposition can be used to deposit nanotubes on the reinforcing fiber in radially aligned sheets [106]. Unfortunately, this process requires the CNTs to be easily dispersed in solution, which required the researchers to oxidize the CNTs [106]. This is unfortunate because functionalization of CNTs is known to decrease the mechanical properties of the individual nanotubes. However, despite the detrimental oxidation, this research increased the tensile strength 157% by and the modulus by 70% greater than the tensile strength and modulus of the traditionally produced FRP in the study

[106]. Another approach that avoids high temperature is to add the CNTs directly to the epoxy. In [107] the researchers impregnated glass fiber reinforced composites with MWCNT-epoxy suspensions. Unfortunately, like in the case of electrophoretic deposition, to achieve this distribution of CNTs in nanotubes acid-oxidation had to take place [107]. However, once again despite the oxidation of the nanotubes the interlaminar shear strength was increased by 33% with only the addition of approximately 0.25-1 wt.% nanotube [107]. A low temperature approach that does not require oxidation for dispersion in a solution was reported in [108]. In this study CNTs were grown in a CVD furnace and then applied to a prepreg fabric by a transfer printing method [108].

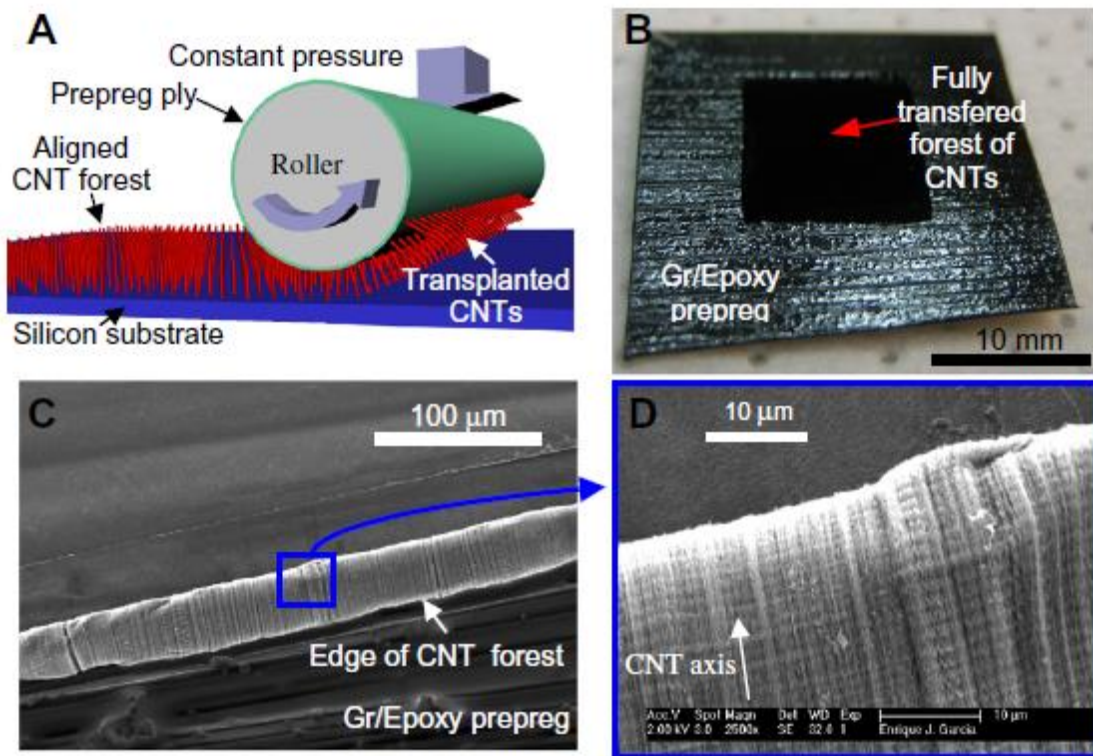


Figure 2.15: A) Schematic of the printing transfer process used to apply CNTs to a prepreg ply. B) Prepreg after transfer of CNTs. C) Scanning electron microscope of the CNT prepreg interface. D) Magnified image of the transferred CNTs showing the retained alignment. [108]

This approach has the benefit of being low temperature, non-oxidative, and even more importantly, it maintains the orientation of the nanotubes in a single direction. This study showed that the mode two delamination of laminates can be increase by approximately 300% using this method [108].

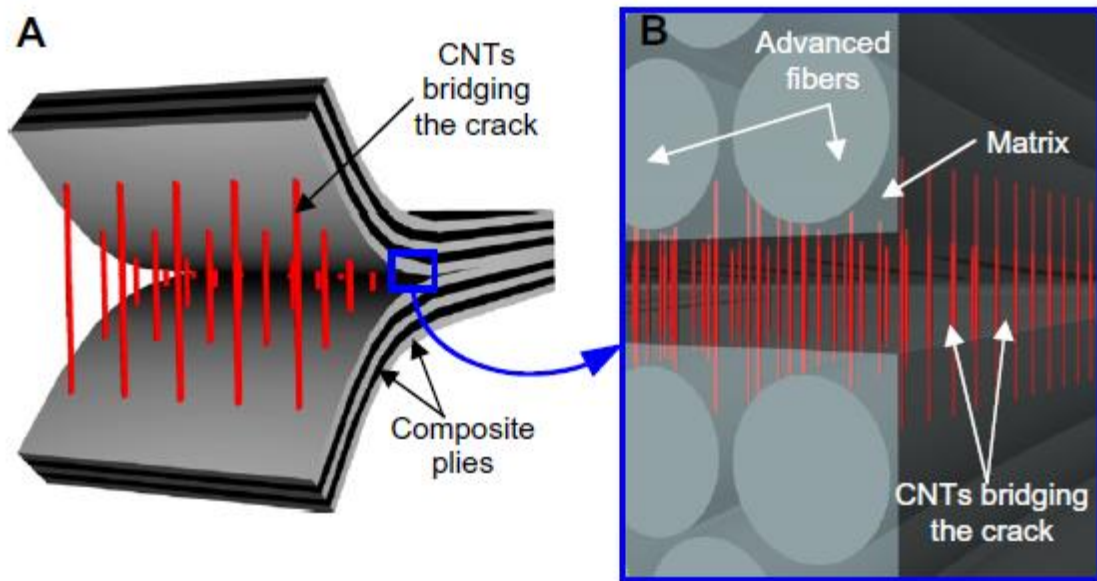


Figure 2.16: Representation of aligned CNTs in a laminated composites A) during mode 1 delamination and B) before delamination. [108]

The authors of that paper do comment that the results are preliminary and samples sizes were small. Even though carbon nanotubes have not reached their full potential, the capabilities they provide are still quite impressive.

2.7.2 Mechanical Properties of Composites with Non-CNT Nanomaterial Additions

Nanomaterials other than CNTs are being researched as additives to FRPs designed to modify mechanical properties. Even though CNTs have higher theoretical properties than other nanomaterials there are many advantages in studying these “inferior” materials. Thinking of the

nature of composites, materials with multiple phases, brings forth one benefit nanomaterials have over CNTs. This is because in a typical FRP the matrix phase can be thought of as a three-dimensional structure, and the fibers are one dimensional. If we incorporate CNTs, one dimensional structures, we've done nothing to increase the dimensionality of the composite. However, zero dimensional nanoparticles and 2 dimensional planar materials such as graphene flakes can operate in different fashions. Determining which properties non-linear nanomaterials can improve and mechanisms behind these increases is an important task being addressed in the research community. As the materials created in this research project involve linear nanomaterials this section will kept brief in comparison.

Nanoclay added to carbon fiber reinforced epoxy composites can increase static tensile strength in comparison to neat composites. Additions of 1%, 3%, and 5% nanoclay increased the tensile modulus with a direct relationship between modulus and weight percent [109]. Interestingly the 3% and 5% samples were almost identical in the plastic deformation region. However, the 3% sample was slightly more ductile than the 5% sample and both were more ductile than the 1% or 0% sample [109]. Regarding fatigue, the nanoclay has proved to increase the number of cycles until failure and the material had better properties after a given number of cycles [109]. Similar increases in mechanical properties were found in a unidirectional FRP with 20 nanometer diameter silica nanoparticles and 15 wt.% loading in the composite [110]. While unidirectional composites were also used in [109] that study created laminates with 0 degree 90 degree orientations. However, nanoclay particles are not only beneficial for unidirectional FRPs. In [111] 2% loading of clay nanoparticles on woven glass fiber composites increased flexural strength and flexural modulus by 15% and 10% respectively. Clays are not always used as the sole additive to FRPs to increase the fatigue properties. In [112] rubber particles were added to a FRP

laminated composite in addition to silica nanoparticles at 9 wt.% and 10 wt.% loadings respectively. Interestingly in this study there was a decrease in the tensile modulus of the material, while exhibiting an increase in the tensile strength. However, while these inclusions only caused a few percent change in modulus in strength, the nanomaterial treatment did have a significant effect upon the fatigue life increasing by 400% [112]. Nano silica and a reactive liquid rubber added to a carbon fiber laminate in [113] caused the fracture toughness to increase. The modified resin and modified composite were both tested for fracture toughness and exhibited a near linear relationship [113]. One note about the rubber particles in [111]–[113] is that the dimensions are in the micron range rather than nanoscale. While these values fall outside of the theme of this review, because of the nano silica particles these articles were discussed. For comparative reference in [114] a glass fiber reinforced plastic was mixed with micron sized rubber particles without nano silica. In this study the fatigue life was also improved and crack propagation rates were decreased [114]. While the mechanical properties of composite materials are promising, adding in multifunctionality can improve the materials desirability significantly.

2.7.3 Properties of Multifunctional Fiber Reinforced Composites

Carbon nanotubes once again provide significant promise in creating multifunctional FPR composites. The most common attempt to make a multifunctional material is to increase the electrical conductivity. In the previous sections, we saw that functionalized nanotubes were incorporated into resins and solutions to increasing mechanical properties. And while functionalized nanotubes do not have as high mechanical properties as pristine nanotubes, there were still significant improvements in mechanical properties. In [115] hybrid composite materials were made with pristine and functionalized carbon nanotubes. The epoxy CNT combination and the pristine-CNT-epoxy glass fiber composite had resistivity values that were approximately 10

orders of magnitude below that of the epoxy glass fiber composite. When CNTs were oxidized and used with epoxy and glass fiber there was only a decrease in the resistivity of about 2 orders of magnitude. Another consideration that needs to be considered is the anisotropy of carbon nanotube conductivity. In [116] CNTs were added in between layers of E-glass with preferential CNT orientation. The CNT layers were oriented parallel to the warp of the woven fabric and perpendicular to the warp. In these respective orientations, the in-plane resistances varied by over an order of magnitude with 0.079 kilo-ohms and 1.23 kilo-ohms respectively [116]. Measurements were taken in the direction of the warp. Another interesting result from this study was that the through thickness resistance was much lower than that of the E-glass. For this to have been accomplished the CNTs must have diffused through the prepreg epoxy when placed under pressure and before the epoxy hardened. Like the studies on mechanical properties, *in situ* growth of carbon nanotubes has been studied to create multifunction hybrid composites [117]. In this study, there was an increase in the conductivity of the material as the percent CNT increased. At just 3% loading of CNTs there was an approximately 8 order of magnitude decrease in the resistance. These drastic changes in resistance occur when CNTs are added to insulative materials such as glass fiber. However, research has shown that MWCNTs can be added to conductive carbon fiber (CF) FRPs and there is an increase in the conductivity by about 50% in plane and about 30% increase in out of plane conductivity [118]. While changes to the conductivity of the original composite can be made, the total resistivity is still much higher than that of CNT theoretical properties. However, even with the small loadings of CNTs additional functionality can be incorporated. Even at just, 0.3 wt.% CNT, hybrid composites gain antistatic properties and make CNTs an ideal additive for sensing application [119].

In one study 3D braid hybrid composites were created with small amounts of CNTs, 0.5 wt.%, and could discern different mechanisms of failure within the braid [120]. This is due to the fact that small disruptions in the electrical pathways created by the CNTs in the original state cause large changes in the resistance of the braid. As the hybrid composite was stretched researchers determined 5 distinct regions: Stage 1, resistance stable near R_o levels; Stage 2-4, increasing resistances with various slopes; and Stage 5, stable resistance at value much higher than R_o [120].

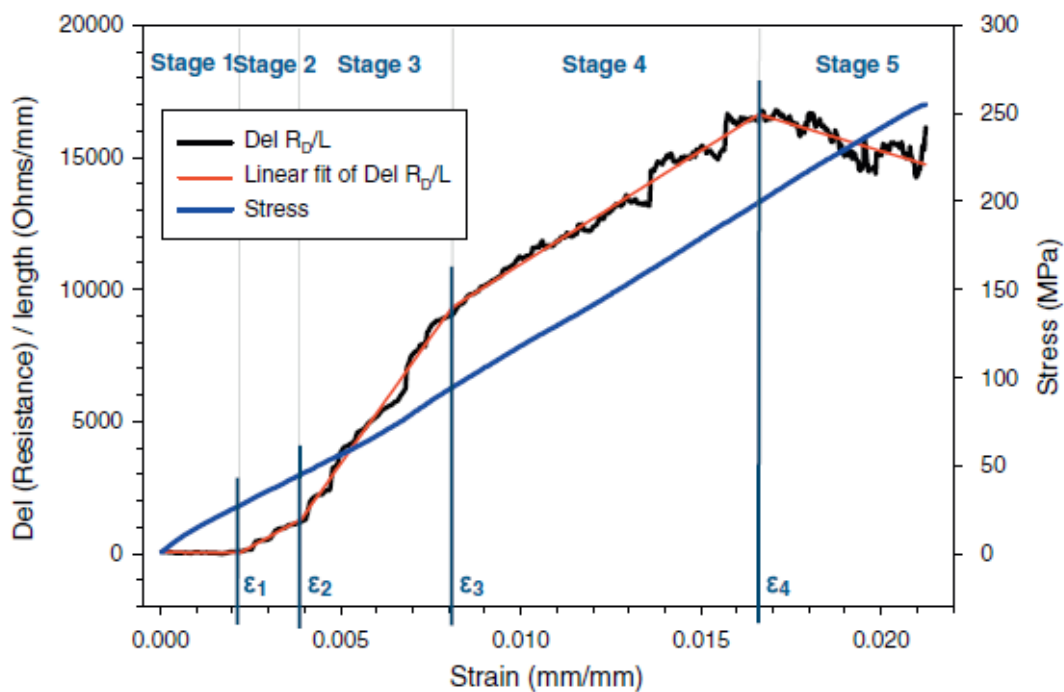


Figure 2.17: Various deformation stages: Stage 1, resistance stable near R_o levels; Stage 2-4, increasing resistances with various slopes; and Stage 5, stable resistance at value much higher than R_o . [120]

The mechanism responsible for stages 2-4 are listed in order as follows: micro crack formation, formation of microcrack interactions, saturated microcracks growing at a steady rate [120]. The ability to detect damage was also shown in another study using glass fiber reinforce polymers, CNTS and carbon black [121]. This study also showed that the conductivity of these hybrid

composites could be used for load detection, fatigue monitoring, and detection of microscale damage undetectable by other methods [121]. It is important to note that carbon nanotubes do not only increase the electrical conductivity but they also affect the thermal properties of hybrid composites. In one study, thermal conductivity was increased by 50% in comparison to the neat hybrid due to the addition of carbon nanotubes [122]. The coefficient of thermal expansion was also reduced by 38% which is important when trying to use composites in combination with other materials. Large differences in CTE can cause materials to separate from one another due to thermal strain.

2.8 Critical Summary

Carbon nanotubes have remarkable mechanical and conductive properties that make them a novel choice for composites. There are a variety of reasons and challenges that have prevented CNTs from becoming a common commercial product. To begin with, there are variations in the properties of carbon nanotubes that have different chiral angles, diameters, or the number of walls. In theory, armchair single wall carbon nanotubes are the optimum material for most composites applications. However, controlling growth to solely produce armchair nanotubes has not been achieved at the commercial level. Even once an economic process is developed, CNT composites will have different electrical properties than those of individual tubes. This is partially due to boundary effects where charges have to transfer from one CNT to another. It is also due to the fact that when carbon nanotubes are surrounded by other materials there is a change in the electronic structure of the CNTs themselves.

Additionally, single wall carbon nanotubes cannot easily be uniformly dispersed in solution or composite matrices without functionalizing the surface. This chemical modification of the SWCNT generally decreases the mechanical and conductive properties. Another problem with

using functionalized nanotubes is the random distribution in the matrix limits the volume fraction that can be achieved. Using spinnable carbon nanotubes for composite manufacturing allows high volume fractions with very good alignment to be achieved. Highly aligned CNTs in a composite material give the material anisotropic properties. This can be beneficial in some cases. When isotropic performance is needed, laminate composite processing allows for quasi-isotropic performance in the planar directions.

Alignment not only allows composites to have higher volume fraction than a randomly dispersed composite but also increases the electrical conductivity. The increased conductivity is due to having more tube-tube contacts which allows for the facile transfer of charges. While pulling spinnable CNTs from an array provides much higher alignment than solution dispersed CNTs there are processes that can improve it even further. Higher alignment can be achieved simply by finding the optimum speed the CNTs are pulled from the array. Micro-combing of the CNT ribbon before it enters the matrix increases alignment. Using solvent to consolidate the CNTs before the matrix is added will also increase the number of tube-tube connections. Once the CNTs have made it into the matrix, pre-straining the material before the matrix fully cures can increase alignment and material properties. Despite these challenges, CNTs are still an excellent reinforcement for composite materials but more research needs to be done to harness the potential of CNTs.

The studies presented in the subsequent sections will examine merging traditional filament winding techniques with spinnable vertically aligned carbon nanotubes. A novel method for creating conformal, aligned CNT coatings for small diameter fibers with tunable conductive properties will be presented. The processing parameters that affect the conductivity and conductance will be examined. This will be followed by an in-depth analysis of the conduction, transport, and magnetoresistance properties of 2-dimensional planar CNT epoxy films.

3. Tunable Electrically Conductive Carbon Nanotube Coatings for Monofilaments Applied via Filament Winding

Brian Wells,^{a,b} Junghyun Wee,^c Kara Peters,^c and Philip Bradford^{a*}

^aDepartment of Textile Engineering, Chemistry, and Science, North Carolina State University, Campus Box 8301, Raleigh, North Carolina 27695, USA

^bDepartment of Materials Science & Engineering, North Carolina State University, Campus Box 7907, Raleigh, North Carolina 27695, USA

^cDepartment of Mechanical and Aerospace Engineering, North Carolina State University, Campus Box 7910, Raleigh, North Carolina 27695, USA

*Corresponding Author, Phone: 919-515-1866, Email: philip_bradford@ncsu.edu

3.1 Abstract

This work details a method of applying a conductive carbon nanotube coatings to small diameter linear assemblies. Multiple layers of aligned carbon nanotube sheets were drawn onto a rotating nylon monofilament from a traversing carriage. The method allows for the formation of coatings with tunable electrical resistivity and resistance. Resistivity was varied by manipulating the angle between the carbon nanotube axis and the axis of the monofilament, the thickness of the coating, and the amount of consolidation between the CNTs. Resistivity was tuned over approximately an order of magnitude from 4.3×10^{-4} to $3.7 \times 10^{-3} \Omega\text{m}$. Coating resistance was manipulated by changing the cross-sectional area of the coating and was increased approximately 7-fold from 52 Ω to 350 Ω for a given probe spacing. It was also found that the resistivities of two samples, with the same coating thickness and angle, are different when processed at different winding speeds. This novel approach allows users to apply a light weight, flexible conductive coatings to filament or wire like structures with tailored electrical properties which may be useful in areas of electronic textiles or lightweight wire shielding.

Keywords: Carbon Nanotubes, Filament Winding, Conformal Coatings, Electrical Properties

3.2 Introduction

Carbon nanotubes (CNTs) have been used to create electrically conductive products through a variety of methods yielding different structures, shapes, and properties. One dimensional yarns, two dimensional films [45], [87]–[89], and three dimensional networks [123], [124] can all be created from carbon nanotubes. Electrically conductive coatings have a wide range of applications such as current carrying, sensing, smart textiles, and static dissipation. Depending on the application, the electrical resistivity requirement varies. For current carrying applications, the minimum resistance possible is desirable to increase efficiency. However, the dissipation of static charge only requires resistivity in the range of $100 \Omega\text{m}$ [119]. Electromagnetic interference (EMI) can disrupt electrical signal traveling through conductive wires coated with an insulating layer. Carbon nanotubes films exhibit excellent EMI shielding properties, 61-67 dB attenuation, in the form of a light weight $1 \mu\text{m}$ thick film [60]. High EMI shielding performance is also present in a CNT composites. In a ceramic matrix the attenuation reached 25 dB at 9% CNT, and in a polymer matrix, 37-60 dB was achieved which is close to or exceeding industry required 40 dB [58], [60], [61].

Conductive coatings have been produced through a variety of methods using different types of nanotubes. Spray coating methods utilize and airbrush to spray nanotubes dispersed in a polymer solution onto a substrate [125]. This method produces coatings with poor alignment and randomly oriented nanotubes. Spin casting methods use shear forces to create alignment between CNTs [126]. However, this method produces a radial symmetry and therefore has zero net orientation. Functionalized CNTs can be used to create coatings with controlled thicknesses via a layer by layer deposition [127]. Dip coating methods can create coatings with some orientation in the direction of motion as the substrate is pulled through the solution [128]. Magnetic fields can also

be used to slightly increase the alignment of CNTs in solution [90]. However, a problem with dispersing nanotubes in solution is that it generally requires the use of functionalization, which decreases the electrical conductivity [129]. The use of ultrasonication can create CNT films without functionalizing nanotubes but coatings remain without orientation [129]. Due to the anisotropic properties of CNTs, a highly-oriented CNT structure will have higher conductivity. Yarns created from CNTs have very high levels of alignment and can be produced with controllable orientation relative to the yarn axis. Unfortunately, these yarns are independent structures and are not feasible for use as coatings.

CNT yarns can be made by drawing vertically aligned CNTs from an array. Using this method, one research group produced CNTs assemblies with near linear current-voltage curves from zero to seventy volts and demonstrated use as an incandescent light source and as an ultraviolet light polarizer [49]. More traditional textile like yarns have been created by introducing twist by rotating a spindle to collect the CNTs from a CVD furnace [44], [45] or by rotating a variable-speed motor as the yarns were drawn from the array [11], [46]–[48], [50], [51], [130]. Twisted CNT yarns with varying twist angles have been shown to have varying electrical properties. The twist angle changes the porosity and density of the yarn changes. Samples with the highest conductivity, had the lowest porosity but all samples found to be almost equivalent when examining the specific conductivity, which is the conductivity divided by the yarn density [47]. Additionally, it was concluded that the interconnects between CNTs that form during growth dominate the charge transfer mechanism and additional tube-tube connections formed during twisting have limited effect on the conductivity [47]. In addition to the ability to vary the conductivity of yarns, yarn diameter can be changed over an order of magnitude from 10 – 200 microns [44]. The properties of these pure CNT yarns can be increased via post processing techniques. The addition of the

pyrolytic carbon for example serves to bond CNTs together, provide additional pathways, and decrease void space [130].

This paper introduces a method of applying a conformal CNT coating to small diameter filaments. CNTs are applied via dry processing without functionalization, preserving the conductivity of the nanotube. This method provides control over the thickness of the coating by limiting the number of layers applied. The orientation of the CNTs is controlled by changing the winding speed and carriage velocity. The combination of these factors provides control over the resistance and the resistivity along the axis of the filament.

3.3 Material and Methods

The vertically aligned spinnable CNTs with a height of approximately 2 mm used in this experiment were synthesized using a floating catalyst chemical vapor deposition (FCCVD) method described in previous work [131], [132]. The monofilament that the CNT coating was applied to is a nylon fishing line with negligible conductivity and .736 μm diameter. The CNT coatings were drawn from CNT arrays using a modified filament winding apparatus, X-Winder, and software. The modifications were implemented so that flexible, small diameter filaments could replace rigid, large diameter mandrels. This was accomplished by reconstructing the machine, shown in Figure 3.1, with fiber chucks, and providing powered, simultaneous rotation of both fiber chucks. The chucks were added for alignment and effective gripping purposes. The simultaneous rotation was necessary to allow the filament to be kept under tension without implementing shear forces within the filament that would twist the filament into a coil instead of enabling rotation.

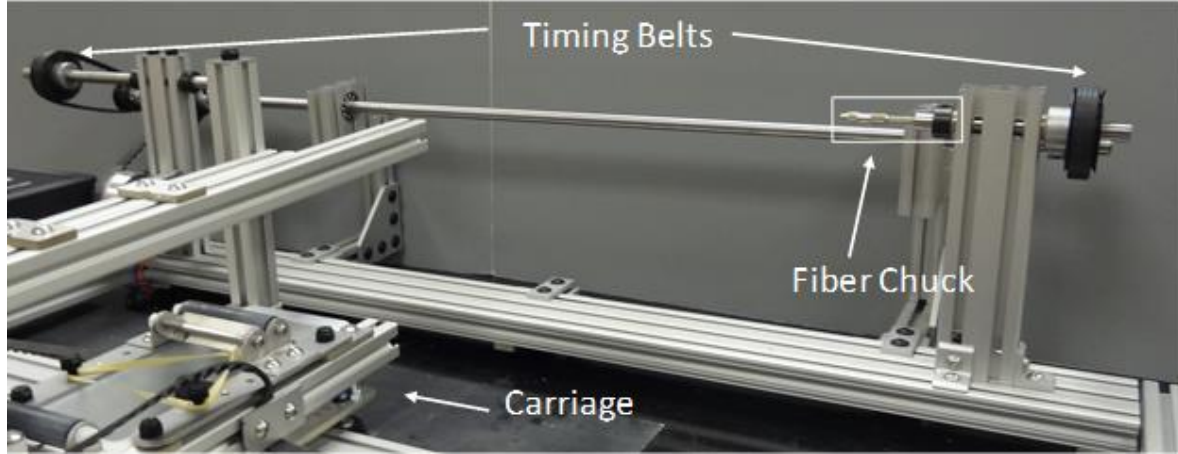


Figure 3.1: Modified X-winder for use with polymer filament mandrels. Timing belts allow for synchronized rotation of fiber chucks which grip the filaments.

The CNT ribbon was initiated by dragging a razor blade over the array and then transferred to the filament. As the filament began to wind, the van der Waals forces between the CNTs drew the subsequent CNTs from the array onto the monofilament. Due to the dimensions of the filament and the nature of the CNTs, a traditional filament winding coating could not be used because too much slack forms in the ribbon when transitioning directions. Instead, a continuous helical coating was applied to the sample. The helical winding angle was changed by varying rotational velocity of the chucks holding the filament. As the ratio of the tangential rotational velocity (ω_t) to the carriage velocity (v_c) changes, the winding angles also changes. The tangential rotational velocity, ω_t , was calculated according the Equation 1, ω filament rotational velocity, d filament diameter.

$$\omega_t = \omega \pi d \quad (1)$$

The carriage velocity was kept constant at 0.762 mm per second for all samples. This value was low due to the limited angular velocity provided by the setup. A tailor-made machine could apply the coatings at a much higher rate with the proper motors and control software. The angular

velocity was set to 20, 25, 35, 50, and 75 rpm to get the corresponding angles of approximately 45, 52, 60, 68 and 75°, relative to the filament axis. The angle of 45° was chosen as the minimum because the ratio of ω_t to v_c is 1.0 and values below 1.0 do not wind smoothly onto small diameter filaments. In Figure 2 scanning electron microscope (SEM) images of filaments coated with CNTs at angle approximately 45°, 60°, and 75° to the filament axis is shown.

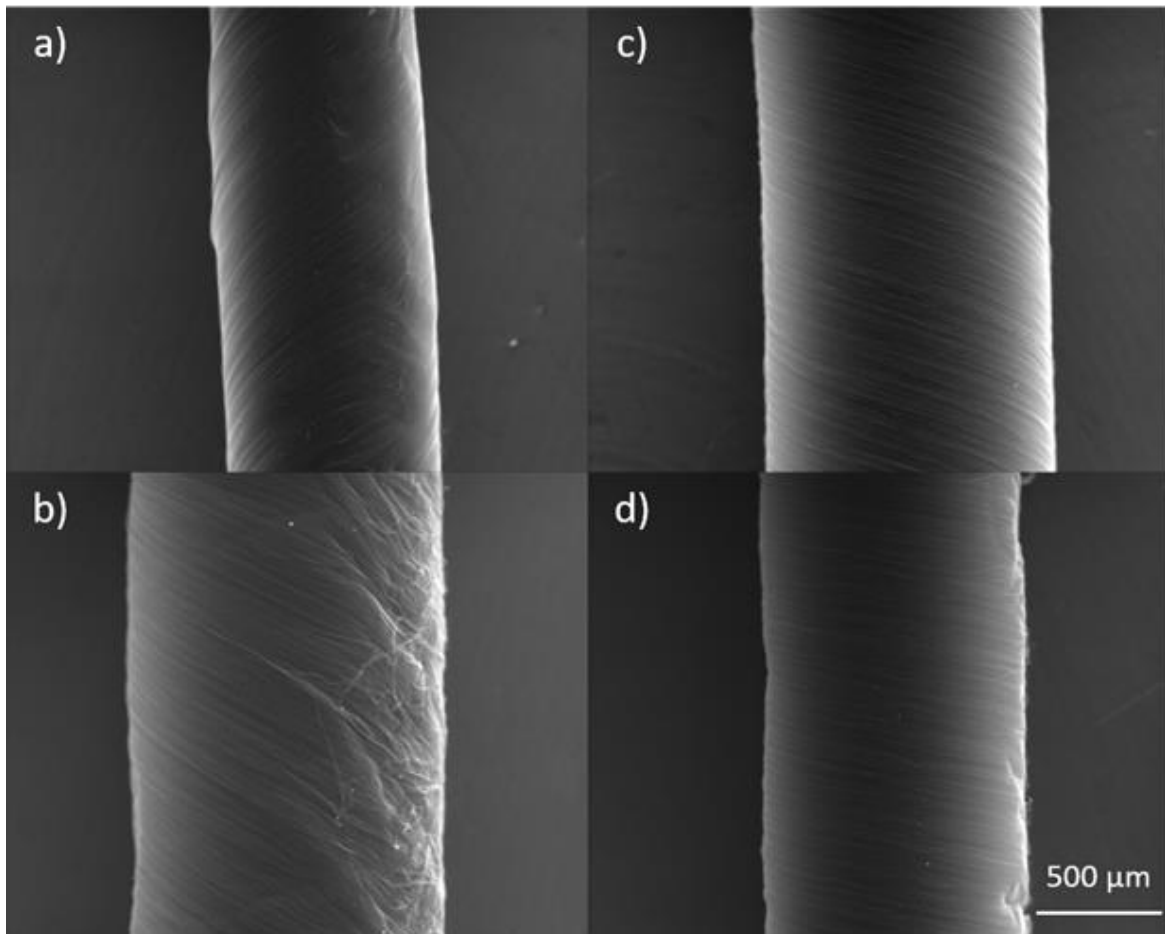


Figure 3.2: SEM images of a CNT coated filaments with CNTs oriented a, b) 45° c) 60° and d) 75° to the fiber axis. All images were taken at the same magnification, note the different in diameter between the two 45° samples a, b). The coating in image a) is approximately 11 layers thick while the coating in image b) is approximately 88 layers thick.

The angle of 75° was chosen as the maximum value because the motors are limited to 90 rpm and corresponds to an angle of 77.62° when the v_c is set to 0.762 mm per second. Due to the helical winding, multiple layers of CNTs were added to the filament for a single traverse. The number of layers per traverse (N_l) is a function of the width of the CNT array (w_a), the rotational velocity, and the linear velocity according the Equation 2. Figure 3 shows this relationship with images of an actual coating (a-b) and a simplified schematic (c-g). A summary of the samples created can be found in Table 3.1.

$$N_l = w_a * \omega / v_c \quad (2)$$

Table 3.1: Summary of the processing parameters and characteristics for each sample. *Note sample 5 and 7 are the same sample but listed separately because of different parameter investigated.

Sample	Angle (Degrees)	RPM	Carriage Velocity (in/s)	Number of Layers
1	45	20	0.03	11
2	45	20	0.03	22
3	45	20	0.03	44
4	45	20	0.03	67
5	45	20	0.03	89
6	45	20	0.03	111
Sample	Angle (Degrees)	RPM	Carriage Velocity (in/s)	Number of Layers
7*	45	20	0.03	89
8	52	25	0.03	83
9	60	35	0.03	78
10	68	50	0.03	83
11	75	75	0.03	83

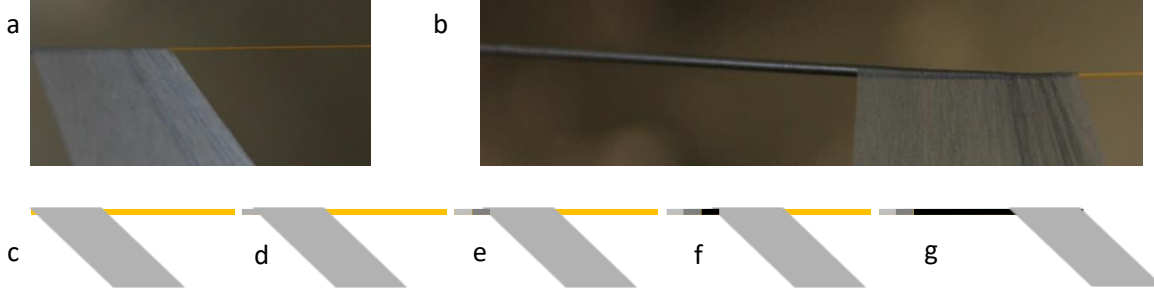


Figure 3.3: a) CNT array attached to the mandrel before winding commences, b) CNT array at the end of the winding process showing the decrease diameter along the leading edge, c-g) schematic representation of winding process, as the array traverses sequential layers are deposited as characterized by the darker sections applied to the fiber.

An Agilent 34410a 6 ½ digit multimeter was used to measure the resistance of each sample listed above. Measurements were taken at different spacings along the filament in a four-point probe method configuration with U1163A SMT Grabbers as the contact probe. Because of the non-uniform application of CNTs at the edges of the coating, all measurements were taken at least 2.54 cm, the width of the array, from the ends of the coating.

The diameters of the coating were measured using a digital stereo microscope (Motic). The coated filament was imaged next to a section of uncoated fiber to serve as a size reference. The diameter of the uncoated fiber was measured using ABS digimatic calipers (Mitutoyo) at various locations and averaged. The cross-sectional area was calculated using the diameter of the coating and then subtracting the cross-sectional area of the filament. This was done to calculate the resistivity of the samples per Equation 3, where R is the electrical resistance, ρ the resistivity, A is the cross-sectional area of the coating, and ℓ is the distance between the probes [1].

$$R = \rho\ell/A \quad (3)$$

There is significant open space between the CNTs, which means the resistivity calculated is representative of the coating rather than the base material properties of the CNTs.

3.4 Results and Discussion

3.4.1 Resistance Versus Coating Thickness

The resistance and resistivity was measured for six identical samples created without varying the processing parameters, to examine the repeatability of the winding process. This group of samples showed 2.85% and 5.49% standard error for resistance and resistivity respectively. Due to material and time constraints, all the subsequent data points in this work for samples with various thicknesses and winding angles, were taken from individual samples.

According to Equation 3, the resistance of an Ohmic resistor will vary linearly with one over the thickness and with the length of the sample change respectively. Figure 4 shows that the measured resistance of each sample varies linearly as the spacing between electrodes changes. The linear regressions for each sample correspond to R^2 values greater than .99 and thus are obeying Equation 3 and the coating is very consistent along the length of the filament.

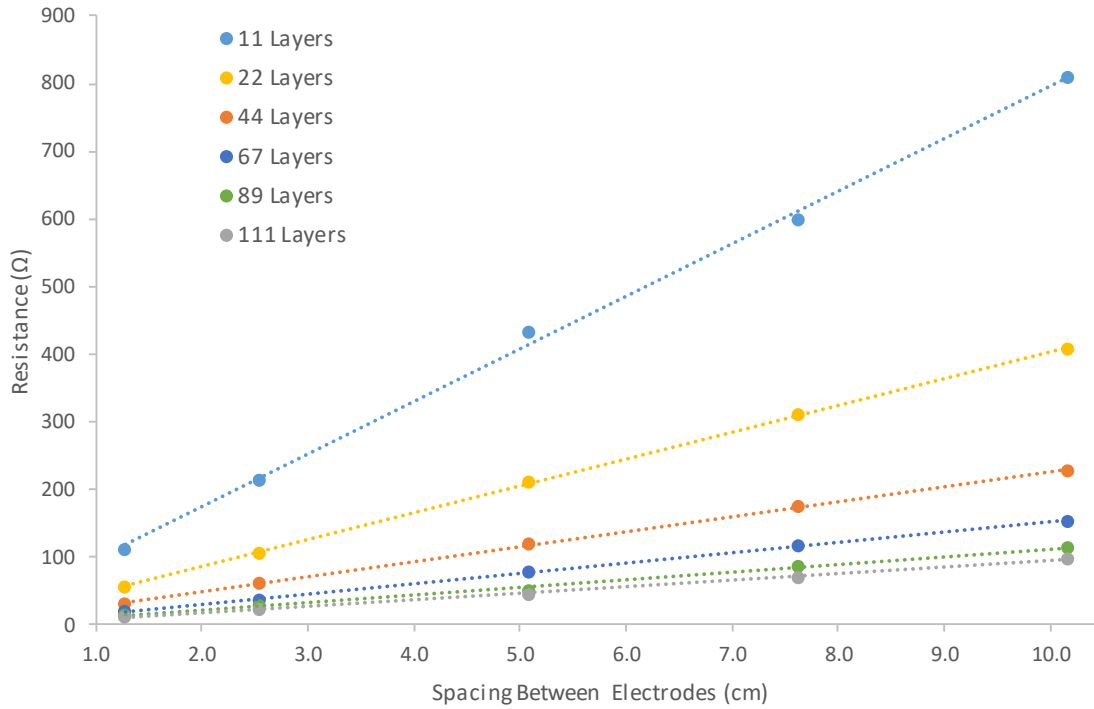


Figure 3.4: Resistance versus probe spacing for 45-degree samples with various number of layers applied to the mandrel.

The different slope of each sample shows that there must be a difference in either the resistivity or the cross-sectional area of the samples. As shown in Figure 5, the resistance is plotted as a function of the number of layers, at a given spacing. The plot shows that the resistance changes with a power law relationship. This relationship correlates very well to the changes in the cross-sectional area of the CNTs coating as a function of the number layers.

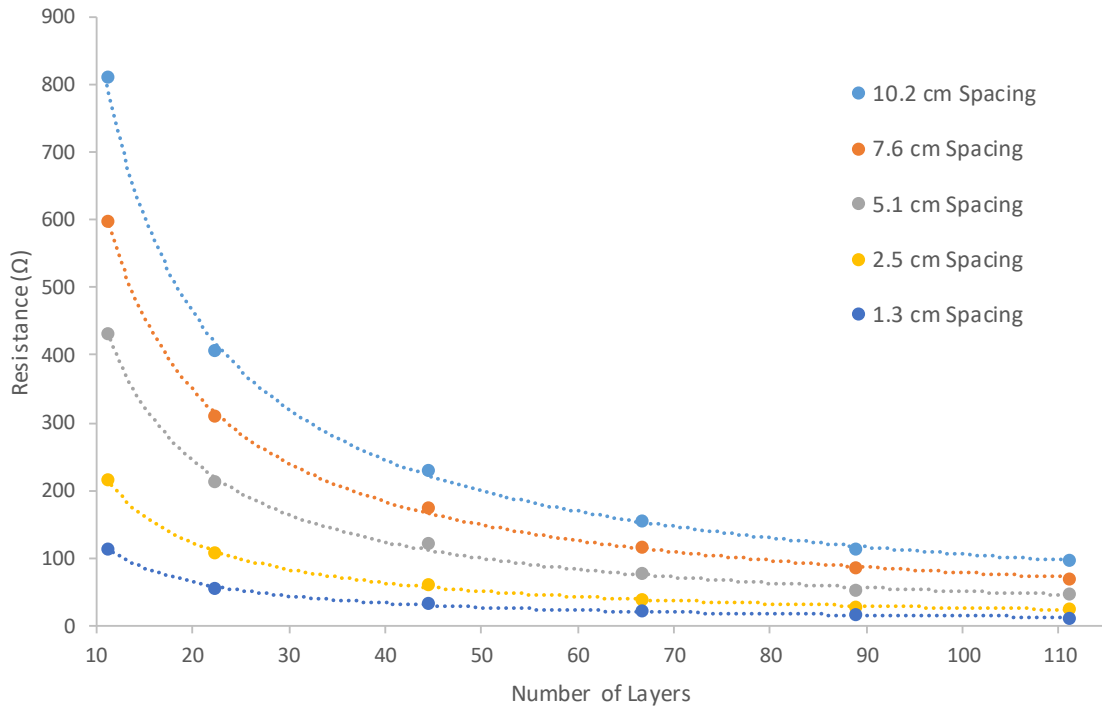


Figure 3.5: Resistance versus the number of layer for various spacings between electrodes for samples with 45-degree winding.

Interestingly, Figure 6 shows that the resistivity also changed as the number of layers increased. This was an unexpected result as the processing parameters of the CNTs was kept constant for each of the coatings.

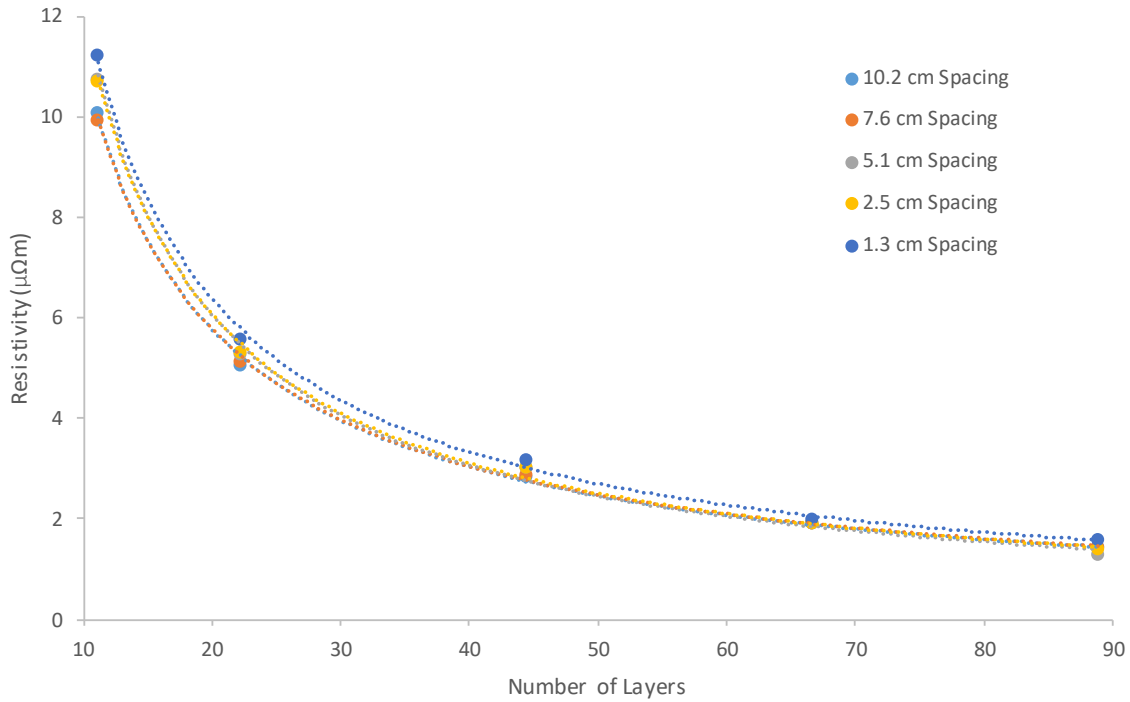


Figure 3.6: Resistivity versus the number of layers for 45-degree samples for various spacings between electrodes.

An important consideration to note is that the processing parameters were calculated for the diameter of the bare filament. As the coating grows in thickness, the tangential linear velocity increases because of the constant rotational velocity. Therefore, the winding angle will be slightly higher at the outer surface of the coating than next to the filament. The change in angle would be approximately less than 1° for the 45° sample and 4° for the 75° sample at a coating thickness of 88 layers. While this could explain a difference in the resistivity of the samples, it would predict an increase in resistivity as the coating thickness increases. However, the measured values followed the opposite trend as shown in Figure 6.

The increase in tangential velocity could be causing the unexpected decrease in resistivity. A comparison to a traditional yarn manufacturing process, roller drafting, is used to understand this

phenomenon. During roller drafting, cotton fibers are accelerated by cylindrical rollers with different tangential velocity. The difference in tangential velocity has a net force that momentarily pulls on the leading end of the fiber while effectively holding the trailing end stationary. This process causes the fibers to align and change the linear density. The greater the difference in the tangential velocity the more aligned the fibers become and the more the linear density increases. Similarly, because the CNTs in a thick coating are winding at a higher velocity, they must be undergoing a larger acceleration. A process similar to roller drafting could be occurring where the “pulling force” is applied by the acceleration and the “holding force” is due to the van der Waals forces with successive tubes and the interfacial bond between the CNT and the substrate. This variable pulling force, as a function of acceleration, could change the amount of overlap between surrounding CNTs in the drawn web.

For coatings with a larger diameter, the last CNTs to be applied will experience greater acceleration than those at the surface of the filament. If these CNTs have better alignment between themselves the overall coating would show lower resistivity. To test this theory 5 samples were made with a 45° winding angle, 22 layers thick, but all with different winding velocities. The averaged resistivity values, shown in Figure 7, generally follow the expected trend of decreasing resistivity with increasing winding velocity. A source of variation in this experiment could have arisen due variable tension in the CNT ribbon. As the CNT array is depleted, the distance between the polymer filament and the CNT array the length of the web increases. To maintain a taught web there must additional tension applied. This additional tension may act as extra “pulling force” which would be compiled into this experiment. To isolate this affect additional equipment would have to be added to the instrument so the array is moved toward the filament as the winding occurs maintaining a given spacing.

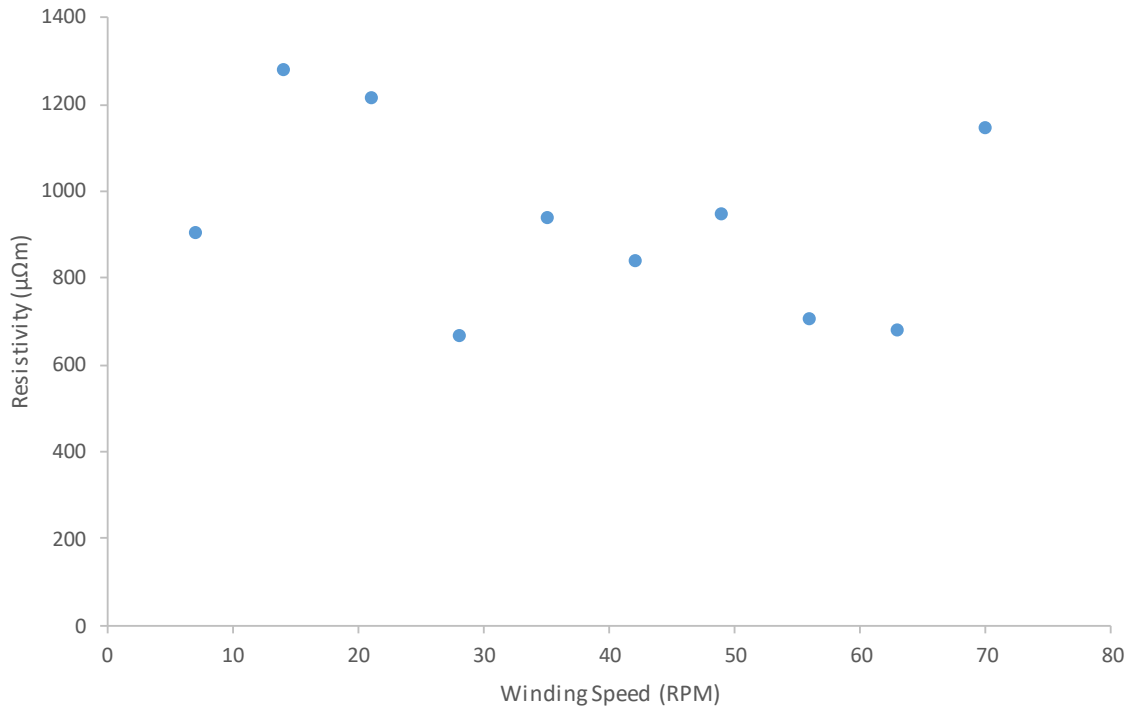


Figure 3.7: The effect of winding speed versus the resistivity on samples with 45-degree winding angle and 22 layers.

If the high acceleration has drafted the CNTs to the point where the overlap between CNTs begins to decrease, there would be a decrease in resistivity. These results correspond well with other research that showed an increase in the tensile strength and modulus of CNT films as winding speed increased [133]. In that study, the sample exposed to the highest winding speed also saw a deviation from the trend that the other samples exhibited [133]. In that study, the authors contributed the increase in performance to an increase in alignment of CNTs.

Tube to tube contact plays a role on the resistance of the CNT coatings and can be manipulated by changing the density of the films. To demonstrate this affect, the 45-degree sample with 111 layers was submerged into acetone and the capillary forces caused the CNT coating to visibly condense as it dried. The resistance values are shown in Figure 8 before and after consolidation. This post

processing liquid consolidation technique could be used in combination with dilute polymer solutions to create CNT polymer composite coatings.

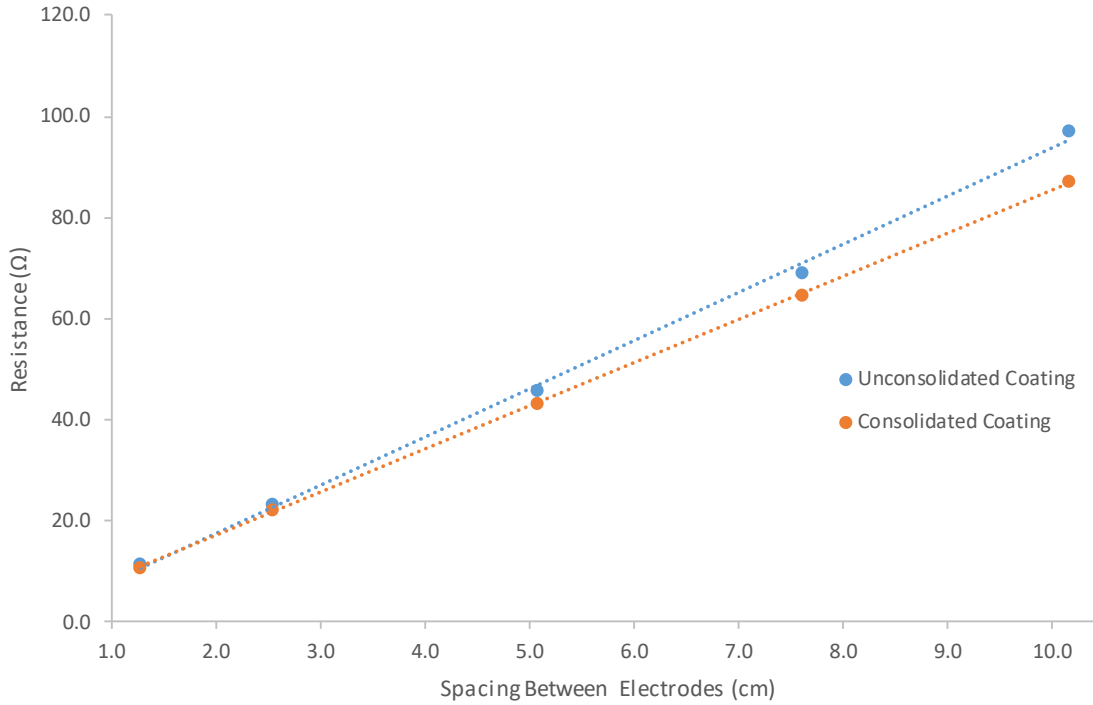


Figure 3.8: The effect of consolidation on the resistance of filament coatings.

The introduction of polymeric matrix material would bolster the wear resistance and other mechanical properties of the coating. Additionally, the added coating should not have a negative effect upon the electrical properties of the coating. The electrical pathway established through the CNT network would likely remain intact as the dissolved polymer chains fill the void spaces between CNTs. An alternative approach to encapsulating the CNT coating with a dilute polymer solution would be to use a heat shrink tubing. This method would consolidate the nanotubes mechanically and prevent the coating from abrasive damage.

While the decrease in cross-sectional area typically causes an increase in the resistance of a material, these results show the opposite trend. This is because when the CNTs are forced to consolidate there are more contacts between CNTs and therefore there is an effective change in the resistivity of the sample. The magnitude of the decrease in resistivity must be larger than the decrease in cross-sectional area because there was a measured decrease in resistance. The diameter of the consolidated assembly decreased by 3.8%, but because the diameter of the assembly is dominated by the monofilament, the change in wall thickness is much greater. The wall thickness of the CNT coating decreased by 11% and which equated to a 13% change in the cross-sectional area of the CNT coating.

The unconsolidated density of the coatings ranged from 0.03-0.23 g/cm³. Interestingly, as the coating thickness increased the density did as well. However, this range of values contrasts with CNT foams created in previous research [123] where the density was as low as 0.0038 g/cm³ and there was significantly more void space between the nanotubes. In this work, the near two order of magnitude higher density is likely due to the fact that the CNT sheets were wrapped around very small diameter fibers (smaller than the length of the CNTs). In contrast in [5] the sheets were taken up across parallel rods and the lowest density of the sheet corresponded to an area where no wrapping forces were present.

3.4.2 Resistance Versus Winding Angle

In the second part of the experiment, the angle between the filament and the CNT axis was varied from 45 to 75 degrees. These samples also exhibited Ohmic behavior, resistance varying linearly with changes to the probe spacing, as shown in Figure 9.

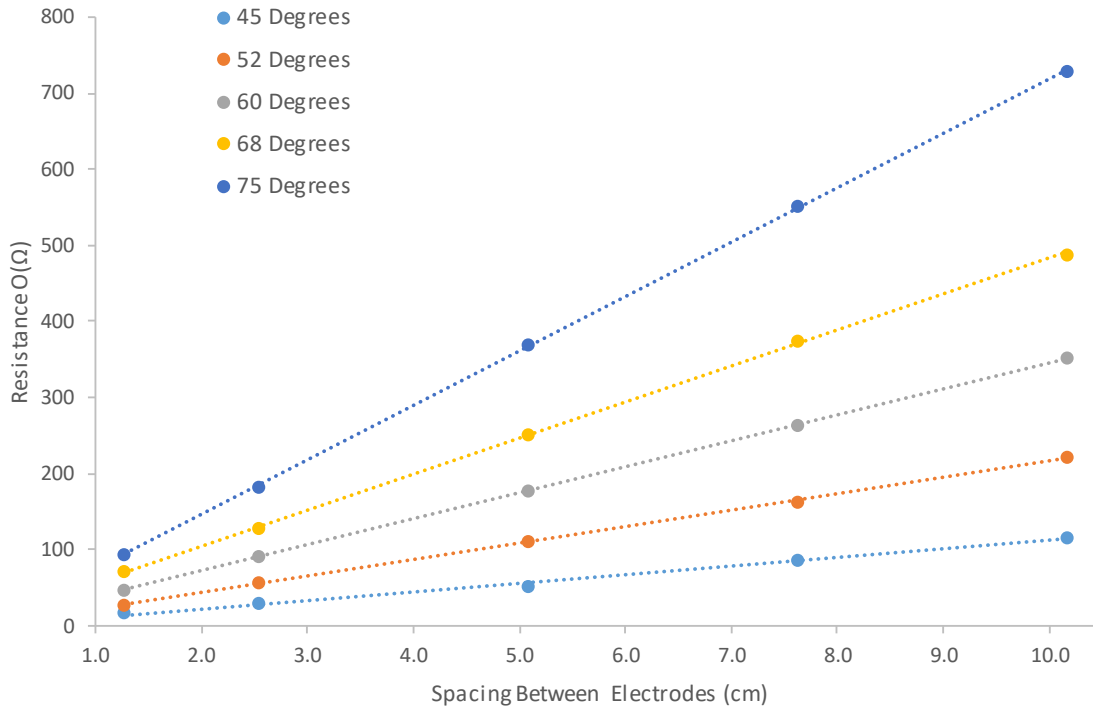


Figure 3.9: Resistance versus probe spacing for samples with various winding angles and approximately 83 layers applied to the mandrel.

For each sample in Figure 9 the number of layers was kept approximately constant, in order to achieve a consistent cross-sectional area between sample types. Therefore, the difference in slope can be explained by a different resistivity in each sample. The resistance and resistivity as a function of winding angle are shown in Figure 10 and Figure 11 respectively.

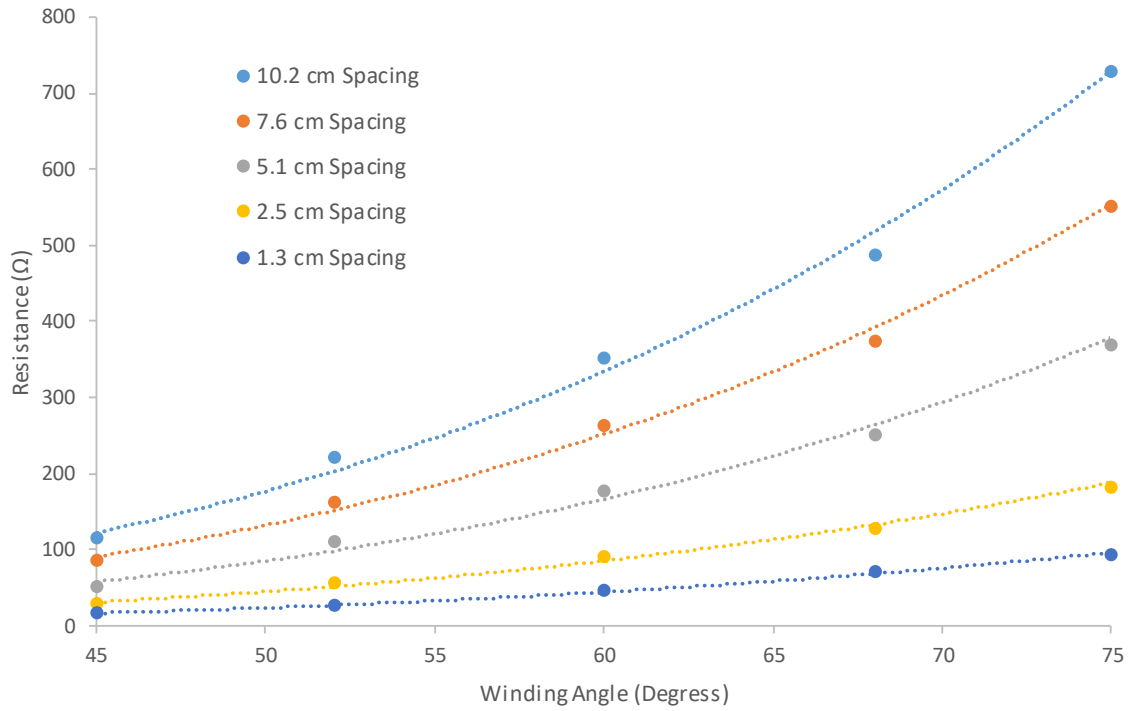


Figure 3.10: Resistance versus winding angle for various spacings between electrodes for different samples with approximately 83 layers applied.

The large discrepancy could be associated with a change in the charge conduction mechanism. As the winding angle approaches 90 degrees, the charge carriers may begin to become dominated by hopping radial conduction instead of ballistic axial transport [134]–[136].

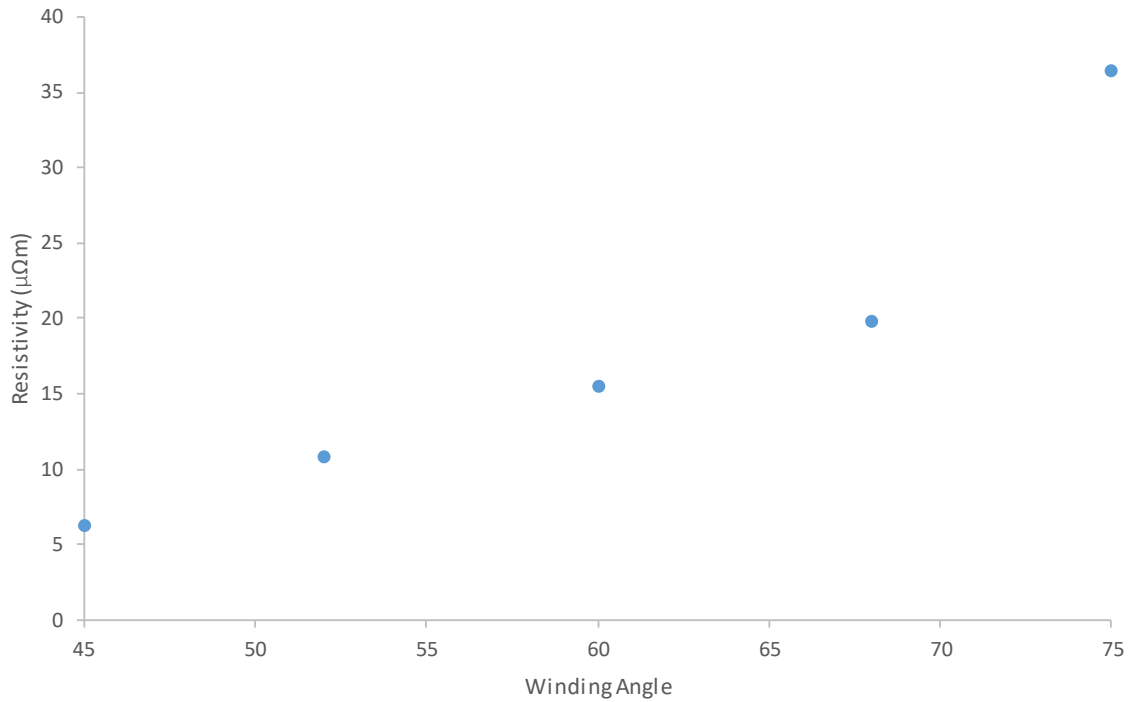


Figure 3.11: Resistivity versus Winding Angle.

3.5 Conclusions

Electrically conductive conformal coatings can be created by the direct winding of carbon nanotubes onto small diameter filaments. The resistance of these coatings was measured at different locations along the filament and increased linearly in good relationship to Equation 3. The resistivity was calculated from the resistance, probe spacing, and thickness of the coating. The resistivity of the samples varies over approximately an order of magnitude from 4.3×10^{-4} to $3.7 \times 10^{-3} \Omega\text{m}$. Interestingly, the resistivity decreased as the thickness of the coating increased for a given winding angle. It is assumed to be related to tube-tube overlap. It was also possible to manipulate the resistivity by changing the angle between the axis of the carbon nanotubes and the axis of the filament. It was shown that the resistivity decreases when the CNT coatings were consolidated and the number of tube to tube contacts increases. From 45 to 68 degrees the change in the resistivity

appeared to follow a smooth continuous function, but when the winding angle reached 75 degrees there was a large shift. It is assumed that at high angles there is a transition to carrier motion dominated by a higher number of hopping conduction events. It is assumed that the CNTs coating would form an effective shield against electromagnetic interference, because of the conductivity and conformal nature of the coating. Further testing should be done verify these claims. By modifying the chucks to provide rotation and translation this process could be turned into a continuous production process with a static carriage.

4. Highly Anisotropic Magneto-transport and Aharonov-Bohm Oscillations in Carbon Nanotube/Epoxy Composites

Brian Wells,^{1,2} Raj Kumar,² Lew Reynolds,² Kara Peters,³ and Philip Bradford^{1*}

¹Department of Textile Engineering, Chemistry, and Science, North Carolina State University, Campus Box 8301, Raleigh, North Carolina 27695, USA

²Department of Materials Science & Engineering, North Carolina State University, Campus Box 7907, Raleigh, North Carolina 27695, USA

³Department of Mechanical and Aerospace Engineering, North Carolina State University, Campus Box 7910, Raleigh, North Carolina 27695, USA

* Corresponding Author

4.1 Abstract

Carbon nanotubes (CNTs) have been widely investigated as an additive material for composites and have potential applications in electronic devices due to their extremely large electrical conductivity and current density. In this work, highly-aligned carbon nanotube composite films were created using a sequential layering fabrication technique. The degree of CNT alignment leads to anisotropic resistance values that vary by over 400x in orthogonal directions. Similarly, the magnetoresistance (MR) of the CNT composite differs depending upon the relative direction of current and applied magnetic field. A suppression of negative to positive MR crossover was also observed due to the modified band structure in these CNT-epoxy composites. More importantly, an oscillatory positive magnetoresistance (MR) behavior is discovered at low fields which persists up to room temperature when the current and in-plane field are parallel to the axis of CNT (B||I||CNT). This behavior is consistent with the presence of Aharonov-Bohm oscillations in our CNT/epoxy composites. When the current, applied magnetic field and nanotube axis are aligned, the in-plane MR is positive instead of negative as observed for all other field, current and tube

orientations. Here, we provide in-depth analysis of the conduction mechanism and anisotropy in the magneto-transport properties of these CNT-epoxy composites.

4.2 Introduction

Individual carbon nanotubes (CNTs) have shown very high electrical conductivity and current density compared to conventional conductors due to their nanoscale diameter and near quantum conductance [24], [36], [137], [138]. These properties have been utilized to create field effect transistors (FETs) with current densities higher than Si and GaAs FETs [138]. This discovery is potentially critical for fabrication of next generation devices that will be required as the semiconductor industry approaches the theoretical quantum limits in silicon-based structures. These CNT FETs are also being considered for sensing applications and they have been shown to detect DNA in concentrations as low as 1 pico-molar [139]. However, the electrical properties of CNTs are affected by numerous factors and can exhibit significant variance. One such factor is the diameter of CNTs, which can vary from a few angstroms in single wall nanotubes to tens of nanometers in multiwall nanotubes [140], [141]. This means that the conductivity can vary over several orders of magnitude. Furthermore, CNTs with different diameters usually exhibit different electron band structures, which are determined by the chiral angle and how the nanotube is folded. It is well known that CNTs can be metallic for armchair and zig-zag configurations whereas they can be semiconducting with a wide range of band gaps depending on chirality [34]. Similar to traditional metals and semiconductors, the resistivity of CNTs is a function of temperature [51], [134], [137], [142]. Carbon nanotubes also exhibit magnetoresistance (MR) [143], [144]. Interestingly, the sign of the magnetic field, positive or negative, does not have a significant effect on the change of the resistance. For both field directions magnetoresistance increases or decreases accordingly and is nearly symmetric about zero magnetic field. While the sign of the magnetic

field does not have significant effect on magnetoresistance, the directionality of the field relative to the current does play a major role. The perpendicular field magnetoresistance and in-plane magnetoresistance (MR) of CNT-based materials have been studied to achieve insight on the magnetotransport properties of CNT-based materials for potential applications in next generation sensing and switching devices [145]. The magnetoresistance effect was initially investigated by Thomson and is common in magnetic materials as it relates to spin coupling between electrons and the applied magnetic field [146]. When moving electrons in CNTs are exposed to a magnetic field applied normal to the plane of the sample they are subjected to the Lorentz force. This causes the charge carriers to accumulate on one surface of the nanotube and is referred to as the Hall effect, and a quantized version of the Hall effect known as the quantum Hall effect (QHE) has also been reported in carbon nanotubes [147], [148]. One particular magnetic field orientation can have significant impact on the electrical and magneto-transport properties of carbon nanotubes; when the magnetic field is applied parallel to the long axis of the carbon nanotube, there is a shift in the electron wave-function. This interaction is known as the Aharonov-Bohm effect (AB) and affects electrons travelling on the surface of a cylindrical conductor. An oscillating magnetoresistance with increasing magnetic field is an indicator of Aharonov-Bohm interactions for surface conduction in the solid materials [149], [150]. However, theoretically a single carbon nanotube exhibiting ballistic conduction will have a resistance value equivalent to the quantum resistance, $R_q = h/2e^2 = 12.9 \text{ k}\Omega$ [137]. Since only the outer tube is carrying charge in MWCNTs, the resistance must increase with an increase in diameter. Another source of variation in the electrical properties of CNTs arises when current flows from one tube to another. In this scenario, the orientation of the carbon nanotubes becomes very important. Carbon nanotube assemblies with high degrees of alignment have highly anisotropic conductivity, which varies over several orders

of magnitude in orthogonal directions [85]. For carbon nanotubes adjacent to one another, evidence of hopping conduction has been reported in electrical measurements [51], [78], [79]. The application of high pressure and chemical treatment can modify the band structure of the CNTs in a manner that induces a change in the MR and a positive to negative crossover of the MR at high fields that is suppressed in CNT systems [151], [152]. Here, we report a significant anisotropy in the magneto-transport characteristics of CNT/epoxy composites and the observation of Aharonov-Bohm oscillations up to 300 K.

4.3 Experimental

The vertically aligned spinnable carbon nanotubes used in this experiment were synthesized using a floating catalyst chemical vapor deposition method described in previous work [131], [132]. The CNTs were then drawn onto a 5-inch diameter glass mandrel wrapped in PTFE using a modified filament winding apparatus, X-Winder, that is controlled by software. The mandrel was set to a rotational velocity of 0.7 RPM and the CNTs were drawn onto the mandrel from the bottom. This orientation was used so that solution could be dropped onto the assembly without the solution destroying the fragile CNT ribbon. The solution was 1% Epotek 301-2 dissolved in 99% acetone and was applied at a constant rate via a syringe pump. The drop rate and rotational velocity were chosen so that consecutive droplets would spread and form a continuous coating on the nanotubes while allowing the acetone to evaporate before the next layer of nanotubes was added. After 30 minutes, the nanotube epoxy film was removed from the mandrel and folded upon itself twice to increase the thickness. The sample was outgassed at room temperature in a vacuum oven at a vacuum pressure of approximately 10 Torr for 30 minutes to ensure that the acetone had been removed from the sample; this procedure is similar to that

described by others [91]. Once removed from the vacuum oven, the sample was covered in a PTFE film and placed in a hot press under pressure < 0.5 MPa and cured at 80°C for three hours.

Once the CNT composite film had cured, resistance was measured as a function of temperature and magnetic field in a Quantum Design Physical Property Measurement System (PPMS) with a base temperature of 1.9K and magnetic fields to $\pm 9\text{T}$. All electrical measurements were made using a four-point probe technique in the van der Pauw configuration with a square probe geometry and the measurements were carried out with the current flowing perpendicular ($\perp\text{CNT}$) and parallel ($\parallel\text{CNT}$) to the axis of the carbon nanotubes. Ohmic contact between the sample and the probes was verified by measuring the current-voltage relationship from -10 to 10 mA. Subsequent to demonstration of good Ohmic contact, the sample was cooled to 5K . Resistance measurements were taken in 5 -degree increments from 5 - 300K . Then the magnetoresistance (MR) was investigated by applying magnetic fields to $\pm 5\text{T}$ (in 1kOe increments) at 5 , 25 and 300K to the sample. For each current direction, ($\perp\text{CNT}$) and ($\parallel\text{CNT}$), the (MR) was measured with an applied out-of-plane magnetic field and an in-plane MR measurements were performed along ($\perp\text{CNT}$) and ($\parallel\text{CNT}$) current directions with the applied field in the plane of the samples.

4.4 Results and Discussion

4.4.1 Electrical transport:

A linear current- voltage relationship demonstrated good Ohmic contact to the samples over the current range measured (not shown). Figure 6.1 shows the resistance versus temperature behavior for current applied perpendicular (a) and parallel (b) to the nanotube axis, respectively. The temperature dependence in both directions reveals semiconductor-like behavior with

resistance decreasing as temperature increases. One should note that the magnitude of the measured resistance in the perpendicular direction is $\sim 400\times$ that in the parallel direction over the entire temperature range. The nature of the anisotropy is shown in the inset of Fig. 2 by the ratio of the resistance in the perpendicular $R(\perp)$ and parallel $R(\parallel)$ directions. This anisotropy in resistivity has been observed previously in thin films of aligned carbon nanotubes [142]. Some SWCNTs exhibit metallic-like temperature dependence of resistivity at low temperatures and then switch to semiconducting like behavior at a variable transition temperature [134].

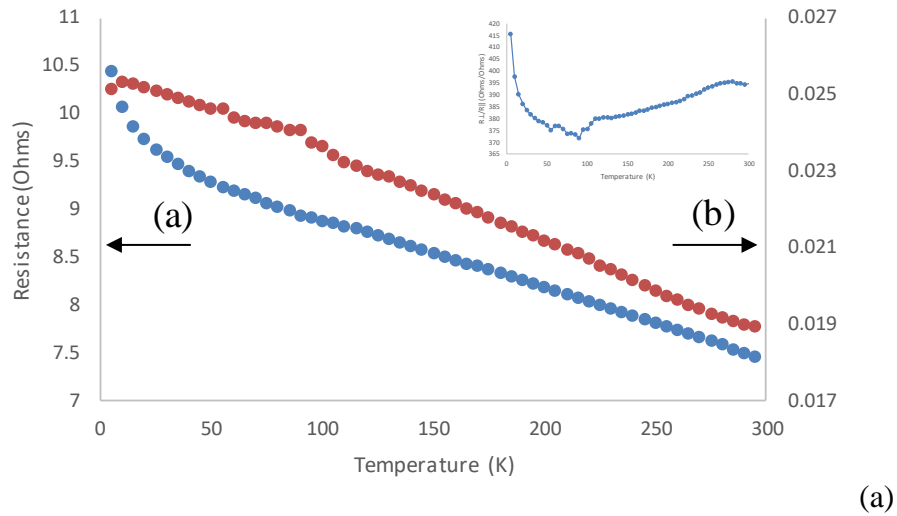


Figure 4.1: Temperature dependence of resistance with the current flowing (a) perpendicular and (b) parallel to the CNT axis. The inset shows the ratio of resistance perpendicular to that parallel to the CNT axis.

Despite the large anisotropy in resistance values along the two current directions, charge transport in both current directions exhibits evidence of hopping conduction, as demonstrated by the plot of $\ln(\sigma T^{1/2})$ versus $T^{-1/4}$ in Fig. 2 that is a signature of hopping conduction. There is a strong linear correlation over the entire temperature range 5-300 K with R^2 values of 0.94 and 0.96. If we restrict our data to the same temperature range of anisotropy as reported in reference [51], then our R^2

values increase to 0.99. Any contribution from the epoxy is assumed to be negligible since its resistivity is $\sim 10^{12} \Omega\text{-cm}$.

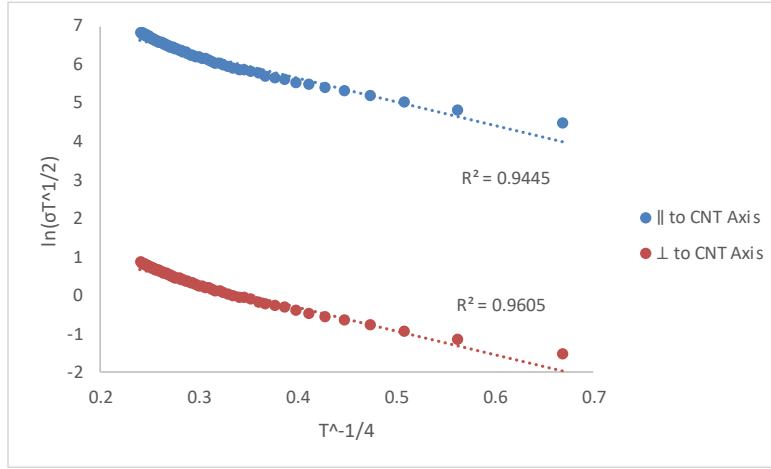


Figure 4.2: Approximately linear relationship between the $\ln(\sigma T^{1/2})$ versus $T^{-1/4}$ indicating charge carriers undergo hopping conduction from 5 to 300K.

It is also interesting that the slope of the resistance ratio is negative from 5 - 100 K, then becomes positive at higher temperatures (see inset in Fig. 1). To explain the observed anisotropy in the resistance values along two different directions and their temperature dependence, we followed the methods described in references [142] and [144].

The overall electrical transport behavior of the CNT-epoxy composites can be explained by considering the resistance as a combination of two components, the intrinsic resistance of the CNTs and the resistance associated with hopping conduction, $R = R_i + R_h$. The latter, $R_h = N\gamma \frac{\Delta}{k_B T}$ depends on the number of intertube hopping events (N) which take place at temperature T(K) with an energy barrier (Δ), where γ has the dimension of resistance. The existence of hopping conduction in these CNT/epoxy composites has been confirmed by the $\ln(\sigma T^{1/2})$ versus $T^{-1/4}$

behavior as shown above in Figure 2. The observed high $R(\perp)/R(\parallel)$ ratio, 415 at 5K, is attributed to the high aspect ratio of the CNTs in our CNT/epoxy composites.

The reported magnitude of the barrier height (Δ) for intertube hopping is 10 meV [144]. At a temperatures > 100 K, (Δ) $< K_B T$ and the resistance curve is no longer thermally activated; consequently, the $R(\perp)/R(\parallel)$ plot in Fig. 1 shows a negative slope. Down to 100 K where the barrier height (Δ) $> K_B T$, intertube hopping events are suppressed that results in a positive slope of resistance vs. temperature plot from 100 to 5 K. The $R(\perp)/R(\parallel)$ ratio increases $\sim 10\%$ as temperature is lowered from 100 to 5 K as shown in the inset of Fig. 1. Additionally, as mentioned previously the best fit of $\ln(\sigma T^{1/2})$ versus $T^{-1/4}$ ($R^2 \sim 0.99$) is observed along the $R(\perp)$ direction within the low temperature regime, 5 - 75 K, which again supports our hypothesis that hopping events are suppressed, and the resistance curve is thermally activated down to 100 K where the barrier height (Δ) $> K_B T$.

4.4.2 Magnetotransport Measurements:

To understand the elusive transport mechanism of the CNT systems, magneto-transport studies of the CNT systems have been performed and reported in the published literature [153], [154]. But a detailed systematic study of the CNT systems with both in-plane and out-of-plane applied magnetic field is lacking. We have performed detailed out-of-plane and in-plane field magneto-resistance (MR) measurements on our CNT-epoxy composite samples in which aligned carbon nanotubes are embedded in the epoxy in an α geometry.

Figures 3a and b show out-of-plane field MR plots with current parallel to the axis of the CNT's ($I \parallel \text{CNT}$) and perpendicular to the axis CNT($I \perp \text{CNT}$), respectively (insets show the relative orientation of the current with out-of-plane applied field). Here, the applied magnetic field is

perpendicular to the plane of CNT-epoxy composite and to the axis of the CNT's embedded in the composite.

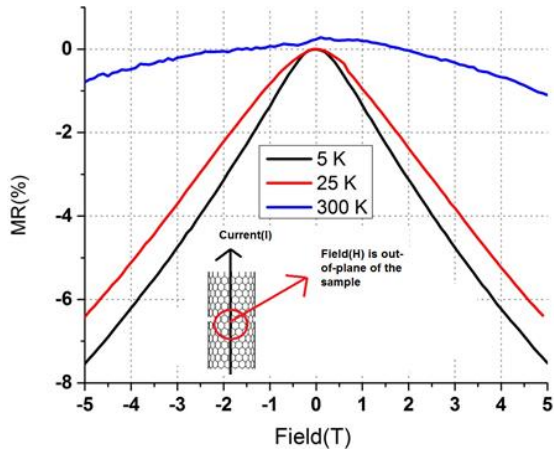


Figure 4.3(a)

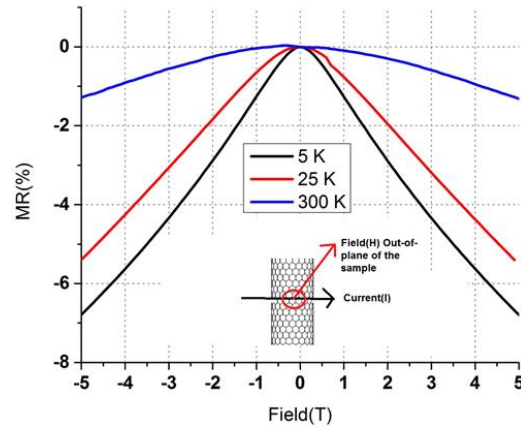


Figure 4.3(b)

Figure 4.3: (a) MR with current flowing along the CNT axis and the applied out-of-plane field is normal to the current and CNT axis, (b) MR with current flowing perpendicular the CNT axis and the applied out-of-plane field is normal to the current and CNT axis.

The observed MR is negative for both orientations of current with respect to the CNT axis, but the magnitude of the MR is higher for the current parallel to the axis of CNT ($I \parallel \text{CNT}$) case. The intriguing feature of the MR plots is that there is no crossover from negative to positive MR to 5 T field over the 5-300K temperature range investigated. However, a change in the sign of MR from negative to positive has been reported at ~ 4 T for CNT systems: with decreasing temperature, the magnitude of negative contribution increases at low field [155], [156]. The crossover from negative to positive MR can be suppressed by the application of high pressure and acid treatment to CNT composites, which was attributed to significant changes in the band structure that enabled suppression of the crossover [151], [152]. In our samples this crossover is completely suppressed and there is no change in the sign of the MR at 5 K up to fields of 5 T without any applied pressure

and acid treatment. This suppression of crossover suggests that our sample preparation method modifies the band structure of the CNT's in the CNT-epoxy composite.

The observed negative MR may originate from weak-localization of carriers. In the weak-localization effect, a quantum correction to Drude conductivity is observed due to destructive interference of the quantum wave function around a scattering center in a localized system where transport occurs via variable range hopping [156], [157]. The observation of negative MR at 300 K rules out the possibility of negative MR due to Landau level quantization in graphitic systems.

In-plane MR measurements were also performed in four different current and field relative orientations, and the results are shown in Figure 4(a, b, c and d); the insets show the relative orientation of the current with the in-plane applied field.

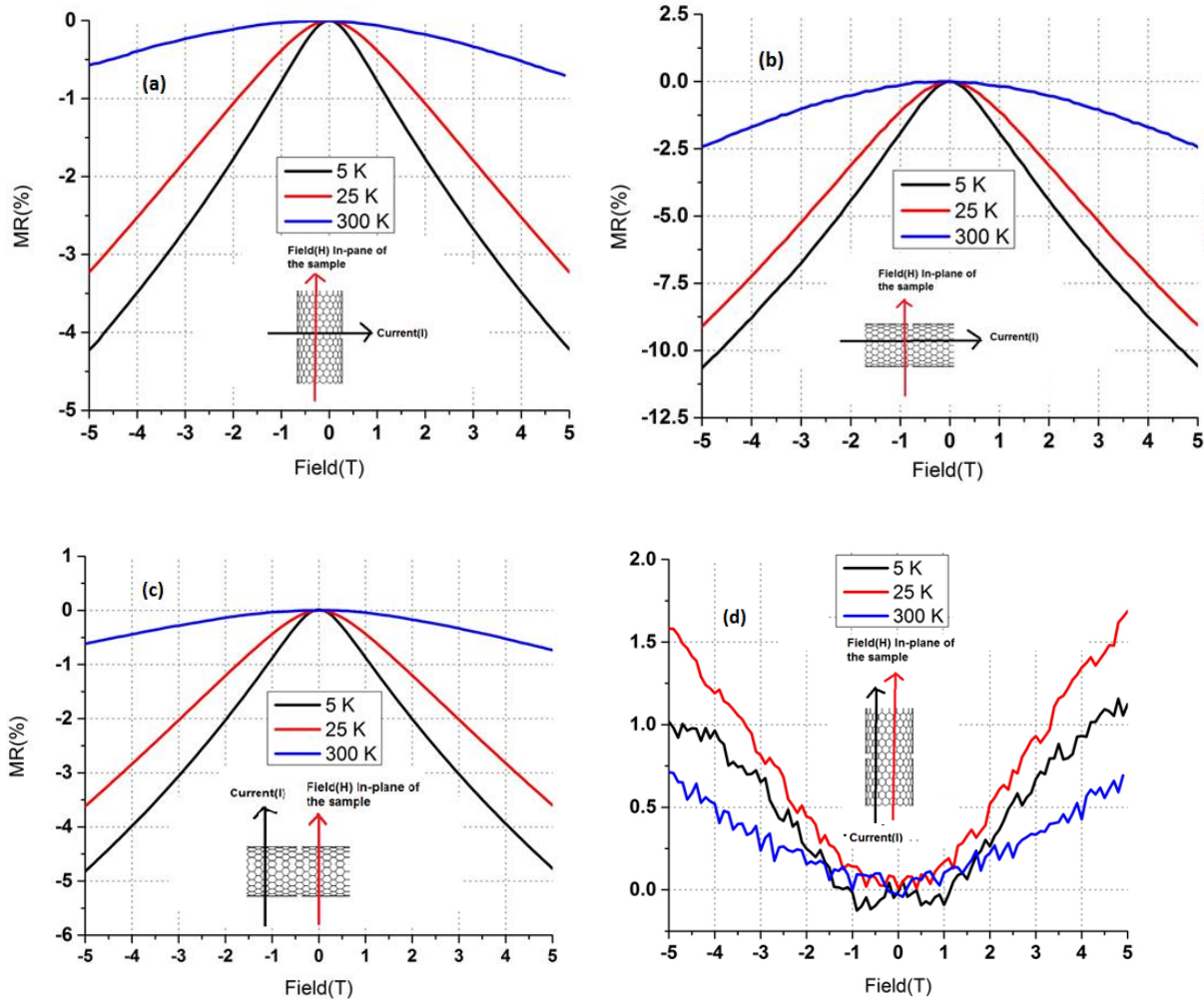


Figure 4.4: (a) In-plane MR with current flowing perpendicular to the CNT axis and the applied in-plane field is normal to the current and parallel to the CNT axis, (b) In-plane MR with current flowing along the CNT axis and the applied in-plane field is normal to the current direction and the CNT axis. (c) MR with current flowing perpendicular to the CNT axis and the applied in-plane field is parallel to the current direction and normal to the CNT axis and (d) MR with current flowing along the CNT axis and the applied in-plane field is along the current direction and the CNT axis.

The observed in-plane MR is negative when the current and the in-plane field are normal to each other ($I \perp \text{CNT}$ and $B \parallel \text{CNT}$) and the largest MR, $\sim 10.5\%$ at 5 K, is observed when the current is along the axis of the CNT ($I \parallel \text{CNT}$) in the CNT-epoxy composite as shown in Figure 4(b). The $B \perp \text{CNT}$ and $I \perp \text{CNT}$ configuration also showed the negative in-plane MR as shown in Figure 4(c).

The most novel and intriguing finding of this study was observed when the current and the applied in-plane field are parallel to the axis of CNTs in CNT-epoxy composites. A positive oscillatory in-plane MR signal is observed as shown in Figure 4(d) when the current flows along the axis of CNT and the in-plane field is also applied along the axis of the CNT's (B||I||CNT). To the best of our knowledge, this is the first reported observation of oscillatory low field positive MR in carbon nanotube systems which persist up to room temperature. While a high field positive MR has been reported [151], [156], a low field positive oscillatory MR signal has not been reported thus far in the literature on CNT systems.

There are three potentially relevant theories to explain the unique positive MR behavior of our CNT-epoxy composites in the B||I||CNT configuration: variable-range hopping (VRH), wave function shrinkage effect and the Aharonov-Bohm (AB) effect can generate a positive MR in disordered materials such as CNT-epoxy composite [155]. The wave function shrinkage theory can be excluded on the basis of existence of low field and high temperature positive MR. Additionally, the positive MR is only observed in B||I||CNT configuration whereas in all other orientations the observed MR signal is negative. But, we cannot completely rule out the possibility of a VRH mechanism playing a role in the positive MR as it is supported by the variable temperature resistance measurements.

A plausible explanation for observation of an oscillatory positive MR is formation of an Aharonov-Bohm (AB) quantum phase in our CNT-epoxy composites when the current and field are parallel to the axis of CNT (B||I||CNT). In the Aharonov-Bohm effect, an Aharonov-Bohm phase is formed, and the band gap is tuned and modulated periodically by the flux quanta, $\phi_0 = e/h$. The periodic modulation of the band gap mediated by the location of the Fermi level produces an oscillatory behavior in magnetic and magneto-transport properties of CNT materials with

formation of an AB phase. [149], [158]. In order to estimate various parameters to confirm the presence of an Aharonov-Bohm phase in our samples, a detailed temperature and field dependent study of the positive MR is required.

4.5 Conclusion:

Carbon nanotube/epoxy composite films have been fabricated with highly anisotropic electrical properties. Conductivity varies over 400x in directions parallel and perpendicular to the nanotube axis. The temperature dependence of resistance for these two directions is negative for both across the temperature range investigated. However, the magnitude of this dependence is different in terms of absolute and percentage change. Both directions show evidence of hopping conduction with a linear $\ln(\sigma T^{1/2})$ versus $T^{-1/4}$ dependence. A high resistance ratio is attributed to the number of hopping events which is a function of temperature and the barrier height. The resistance curve is thermally activated down to 100 K and shows a positive slope. Negative out-of-plane field MR is observed for both orientations and negative to positive crossover of the MR is suppressed due to the modified band structure of CNTs in our CNT-epoxy composites. The in-plane field MR shows negative trends in all orientations except when current, in-plane field and the axis of CNTs are parallel. An oscillatory positive MR behavior at low field and room temperature is observed when the current and field are parallel to the axis of CNT (B||I||CNT). All other five relative orientations of the current and field show the typical negative MR signals with the maximum MR% when the field is parallel to current (B||I) and a unique and novel behavior was observed in (B||I||CNT) orientation only.

5. Filament Wound Multifunctional Carbon Nanotube Adhesives

Brian Wells,^{a,b} Kara Peters,^c and Philip Bradford^{a*}

^aDepartment of Textile Engineering, Chemistry, and Science, North Carolina State University, Campus Box 8301, Raleigh, North Carolina 27695, USA

^bDepartment of Materials Science & Engineering, North Carolina State University, Campus Box 7907, Raleigh, North Carolina 27695, USA

^cDepartment of Mechanical and Aerospace Engineering, North Carolina State University, Campus Box 7910, Raleigh, North Carolina 27695, USA

*Corresponding Author, Phone: 919-515-1866, Email: philip_bradford@ncsu.edu

5.1 Abstract

Commercially available electrically and thermally conductive adhesives are dominated by those that are filled with metallic particles. Silver is one of the most common fillers materials, but is very expensive and heavy. In the aerospace industry, even modest weight reductions can result in large savings over the lifetime of a craft. Carbon nanotube (CNT) adhesives have been created via a variety of mechanical mixing techniques with promising results. However, these structures have randomly oriented CNTs and generally low volume fraction. This paper introduces a technique that can create adhesives with a wide range of volume fractions, 9 to 45% in this study, and have controlled orientation/alignment of CNTs from 0-90 degrees. These structures had a measured conductivity that ranges from 11,000-61,000 S/m and a specific conductivity higher than a commercially available silver filled epoxy tested for comparison. The CNTs not only introduced electrical conductivity to an insulating epoxy ($<5 \times 10^{-11}$ S/m), but the addition of these nanofillers also showed a maximum increase in the lap shear strength (LSS) by approximately 57.5% compared to the neat epoxy. This increase was for a specific sample and a specific CNT orientation. In the orthogonal in-plane direction of this sample the LSS was approximately the same as the neat epoxy. By changing the angle of alignment between the CNTs, the ratio of

electrical properties in the in-plane orthogonal directions could be manipulated. The ratio of lap shear strengths in the in-plane orthogonal directions was found to be heavily affected by the fiber volume fraction.

5.2 Introduction

Using carbon nanotubes to create electrically and thermally conductive adhesives has many advantages over metal filled adhesives and traditional lead tin solders. Lead tin solders are commonly used in electronic applications and pose a significant health risk due to the lead content. Additionally, metal solders are much heavier than polymer based alternatives, which makes them detrimental for applications in the aerospace industry where even small weight savings can make a big difference in efficiency and performance. In commercial applications of current electrically conductive adhesives, the most common additive material are metals, specifically silver.

One of the big differences between metal based conductive adhesives and CNTs is the percolation threshold. Metal powders and metal nanoparticles will generally have semi-spherical dimensions and require higher loadings than high aspect ratio nanotubes. In [92], very high loadings of silver were added to epoxy precursors at a value of 70 wt.%. As the resins cured, the crosslinking caused the polymer to shrink pulling the silver particles together forming a conductive network that changed the resistance by two orders of magnitude [92]. A benefit of lead tin solders is that they can be formed and reformed repeatedly by reapplying heat to the solder. Epoxies are generally one time use due to their thermoset nature and do not degrade except at high temperatures. To address this issue the authors in [86] showed that a thermoset material with a low degradation temperature can be made to function as a conductive adhesive with a conductivity of $2 \times 10^7 \text{ Sm}^{-1}$. This allows the material to be removed and fresh application reapplied when needed without damaging any temperature sensitive components. CNTs are being used in epoxies

as the sole conductive material and samples have been produced with CNT contents as high as 35% in [159].

Research shows that silver can have a beneficial effect on the conductivity of carbon based conductive adhesives. In [94] the conductivity of graphene based conductive adhesives was increased when silver nanoparticles were functionalized to the surface of graphene and reached a conductivity of $2.2 \times 10^7 \text{ Sm}^{-1}$. The combination of silver nanoparticles and carbon nanotubes has been shown to have a similar effect on conductivity increasing electrical conductivity of CNTs by approximately 600% and four order of magnitude in CNT composites compared to pristine nanotubes [160]. CNTs chemically plated with silver have also shown higher conductivity than pristine nanotubes [161].

5.2.1 Thermally Conductive Adhesives

Thermal management is an important concept in the computer industry as processors can generate a very high energy density at high computing loads. A good thermal conductor will take advantage of the phononic and electronic components of thermal conduction. Therefore, it is important to understand the mechanisms and make sure that any increase in electrical conductivity won't hurt phononic contributions and vice versa. The importance of using an electrically conducting filler is exemplified by a study that used both graphite and planar boron nitride. These two materials are very similar structurally and mechanically. The biggest difference is boron nitride is insulating and graphite is conductive. In this study the graphite based sample had a thermal conductivity twice as high as the boron nitride at the various volume fractions tested [99]. CNTS are being studied for use in electronics packaging due to their electrical and thermal conductivity. [162]

Even a small addition of carbon nanotubes to epoxy adhesives can increase the thermal conductivity. In [95] as little as 1% MWCNT added to epoxy increased the thermal conductivity by 15%. A similar increase was seen in [163] where MWCNTs caused an increase in thermal conductivity by 18%. Interestingly, this study also tested functionalized nanotubes which had even greater increases in thermal conductivity than the raw MWCNTs. This is interesting considering functionalization decreases electrical and thermal conductivity of the nanotubes themselves [115], [164]. The increased thermal conductivity of the acid functionalized CNTs is likely due to better dispersion of the nanotubes in the matrix material. The amine functionalized CNTs were also better dispersed than the raw CNTs but have higher thermal conductivity due to crosslinking between the epoxy and the functionalized CNTs. This effect was also seen in [165] where benzenetricarboxylic acid functional groups added to MWCNTs increased the thermal conductivity.

Research shows that the alignment of carbon nanotubes plays an important role in thermally conductive adhesives. The difference between thermal conductivity for aligned CNTs versus randomly dispersed CNTs is as follows: neat epoxy $0.56 \text{ Wm}^{-1}\text{k}^{-1}$, dispersed $0.59 \text{ Wm}^{-1}\text{k}^{-1}$, aligned $1.21 \text{ Wm}^{-1}\text{k}^{-1}$ [96]. This increased thermal conductivity was also seen in a different epoxy for aligned CNTs; the values were as follows: neat epoxy $0.23 \text{ Wm}^{-1}\text{k}^{-1}$ and with aligned CNTs $0.88 \text{ Wm}^{-1}\text{k}^{-1}$ [96]. Another study involving CNTs produced an adhesive with a thermal conductivity of $5.8 \text{ Wm}^{-1}\text{k}^{-1}$ and suggested that optimizing their process could theoretically create samples with conductivity values of $25 \text{ Wm}^{-1}\text{k}^{-1}$ [98]. One study utilized a single layer of aligned CNTs in an adhesive between two graphitic joints and was able to achieve a thermal conductivity of $250 \text{ Wm}^{-1}\text{k}^{-1}$ [166]. In [167] the CNT polymer composites were created and it was determined that electrical conduction was the main mechanism for heat transfer in CNT and polymer. In this

system the phonon contribution was limited due to phonon scattering at the boundary between polymers and CNTs. It was noted that higher volume fraction would likely decrease phonon boundary scattering.

5.2.2 Mechanical Properties and Synthesis

The mechanical properties of epoxy adhesives can also be increased by incorporating CNTs into the resin. The simplest way to do this is through mechanical mixing and is a quite common approach found in the literature. Unfortunately, this approach does not yield high volume fractions of well dispersed nanotubes. Often only fractions of a percent are added to the resin such as in [168] where 0.25 wt% CNTs added to resin for epoxy adhesives. Higher fractions, 3%, have been achieved using a high shear mixing homogenizer [169]. A modified approach is to disperse the nanotubes and epoxy in solvent separately before mixing together which can help with dispersal as was done in [170]. And finally, the use of ultrasonication combined with heating the matrix can help dispersal as well due to the decreased viscosity when heat is applied [171]. The benefit of a solvent on the dispersal of nanotubes is further magnified when the nanotubes have been functionalized [172]. In that study samples with CNT loadings of 2, 5, and 10% were created with pristine and functionalized nanotubes. Interestingly these higher weight fractions actually decreased the properties compared to the neat epoxy and only the small weight percentages increased properties. Each of these studies were able to increase the mechanical properties of the adhesives using CNTs but showed evidence that the dispersal and processing parameters play a large roll on the performance.

5.3 Experimental Methods

5.3.1 Sample Production

The vertically aligned spinnable carbon nanotubes used in this experiment were synthesized in our laboratory using a floating catalyst chemical vapor deposition method described in previous work [131], [132]. The CNTs were then drawn onto a 5-inch diameter glass mandrel wrapped in PTFE using a modified filament winding apparatus, X-Winder, and software. The mandrel was set to a rotational velocity of 0.7 RPM and the CNTs were drawn onto the mandrel from the bottom. This orientation was used so solution could be dropped onto the assembly without the solution destroying the fragile CNT ribbon. The solvent quickly evaporated before the coated ribbon reached the point where the CNT ribbon met the mandrel. The software was also used to create adhesives where the CNTs were aligned various angles relative to the mandrel axis as shown in Figure 5.1.

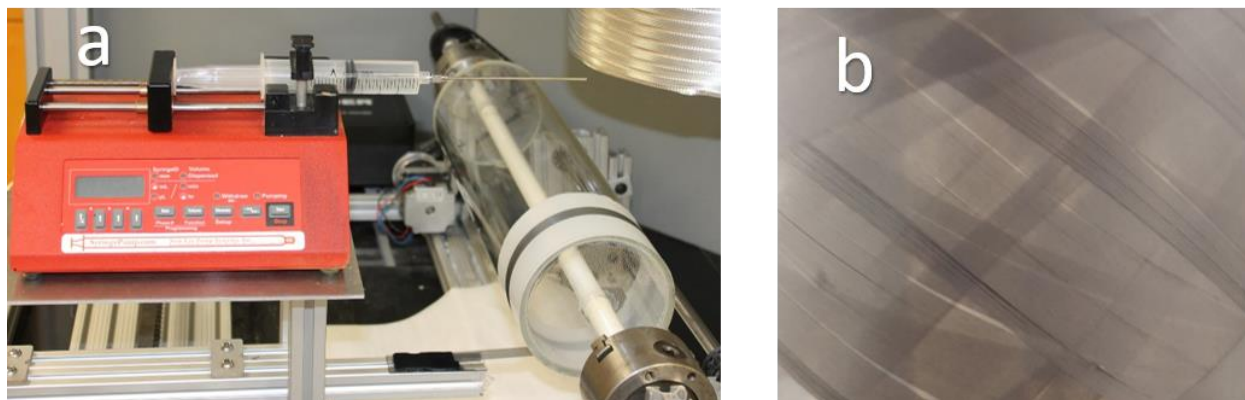


Figure 5.1: a.) Picture of the modified X-winder filament winding apparatus and epoxy dropper set up used to create the 0-90 orientation CNT epoxy films. b.) Optical image of the CNT coatings applied at 45 degree angles.

The solution dropped on to the mandrel was constituted of Epotek 301-2 dissolved into acetone and was applied at a constant rate via a syringe pump. This epoxy system was chosen, as it is a structural adhesive, has a long pot life, has a low viscosity when dispersed in acetone. The drop rate and rotational velocity were chosen so that consecutive droplets would spread and form a continuous coating on the nanotubes while allowing the acetone to evaporate before the next layer of nanotubes was added at the bottom of the mandrel. To change the volume fraction of nanotubes, the concentration of epoxy in acetone was varied, using solution concentrations of 1%, and 5% epoxy by weight.

The angular samples had orientations of 30°-60° and 45°-45° and were wound onto Teflon film without the epoxy/acetone solution being dropped during winding. This is because the amount of time the winding would have required to wind a sufficient number of layers was outside of the pot life of the epoxy. Instead the dry windings were removed from the mandrel and the epoxy/acetone solution was added subsequently. The mass of epoxy used was chosen to correspond to approximately 9% CNT mass fraction. The concentration of the solution was set to 10% to ensure there a sufficiently low viscosity, and to keep the total volume of solution low to minimize evaporation time of the epoxy.

After the windings were completed, the film was removed from the mandrel and samples were prepared for lap shear strength (LSS) testing, electrical/thermal conductivity measurements, and thermal gravimetric analysis. LSS samples were created using 25.4 mm wide aluminum coupons, 1.50 mm thick, with 12.7 mm of overlap connected by the CNT epoxy composite in accordance with recommendations in ASTM D1002 – 10. The samples were cured in a hot press at 80°C for three hours under constant pressure of approximately 1 MPa. The samples prepared

for electrical/thermal conductivity measurements, and thermal gravimetric analysis were cured in a vacuum oven at 80°C and approximately 10 Torr.

5.3.2 Measurements

Lap shear strength testing was carried out with an extension rate of 0.5 inches per minute in a FDI 20000 tensile tester with attached Fracture Diagnostics International software that measured the load and displacement on a 20,000 pound test frame. The mass fraction of the CNTs was determined by thermal gravimetric analysis with a Seiko TG/DTA 6200. The sample was heated from room temperature to 1000°C at a rate of 10°C/min in a nitrogen atmosphere with a flow rate of 100 ml/min. Electrical conductivity was determined by measuring the resistance using an Agilent 34410A Digital Multimeter, 6½ Digit and normalizing to the dimensions of the samples. Copper foil was added to the ends of the composite samples to serve as contact points for the electrodes. The assembly was then cured in an oven at 80°C with the copper foil in place. Thermal conductivity was calculated using the measured density and thermal diffusivity. Thermal diffusivity was measured using a nanoflash method. The samples were tested at room temperature, with a laser voltage of 400 V and a pulse width of 0.3 ms. 5 measurements were made for each sample and the average value was reported as the diffusivity. Literature values for the heat capacity of CNTs and epoxy were used, 700 J/kg-K and 1000 J/kg-K were used in a rule of mixtures approximation based on the measured mass fraction for the specific heat capacities of the CNT adhesives.

5.4 Results and Discussion

From the thermal gravimetric analysis, the composition of the composite was determined and weight percent filler is shown in Table 5.1. In Table 5.1, we see that as the concentration of

epoxy dropped onto the CNTs increases by a factor of 5 from 1% to 5% the weight percent filler decreases by a factor of 5 from 45% CNT to 9% CNT. Additionally, the electrical conductivity changes by approximately the same magnitude as the concentration of the solution is changed. This is reasonable considering that the CNT fraction is well above the percolation threshold and the CNTs have the same orientation in both samples. Essentially, the change in the amount of matrix material present just affects the dimensions of the sample as the conductivity of the matrix is negligible compared to the composite adhesive with an over 10 orders of magnitude difference. What is interesting is that the dry (meaning no epoxy), unconsolidated CNT ribbon shows an electrical conductivity that is lower than both epoxy composites despite being composed of 100% CNT. However, this can be explained by considering the void space between the CNTs and the air that fills these spacings as the “matrix material”. Using this definition, the weight percent filler would remain close to 100%, however the volume fraction of filler would decrease substantially. When the dry CNT ribbon was consolidated with pure acetone, the CNTs realigned and a significant amount of void space was removed. This has a twofold effect on the conductivity: increasing the number of CNT-CNT contacts and also decreasing the dimensions, which results in near 34x increase in conductivity. However, this value is still lower than the measured conductivity of the adhesive with 45% CNT filler. There are several possible explanations for this relationship and further testing would be needed to discern the nature of this performance. For the CNT composite material, the acetone/epoxy solution is applied sequentially with the application of nanotubes while the acetone consolidated sample was consolidated all at once. Perhaps the sequential application of nanotubes results in better alignment between the tubes. This may also be affected by the rotational forces of the mandrel during the winding. Another possibility is that the presence of the epoxy molecule actually helps the alignment of the CNTs and hold them in

place preserving conductive pathways. Finally, the thickness of these dry CNT films samples is quite low in comparison to the other dimensions. Any measurement error in this direction could have a negative effect on the accuracy of the results. The size of these samples also meant that the measured mass was very small. When examining the calculated densities, it appears that there is an error in these values. Creating significantly thick samples would be very time intensive and have expensive materials cost. Using electron microscopy to measure the samples dimensions could provide more insight into this issue.

Table 5.1: Mass fraction of filler material for CNT epoxies and commercial silver filled epoxy. *The electrical resistivity of the silver epoxy varies as a function of the temperature profile used during the curing schedule.

Sample	Weight Percent Filler	Density (g/cm³)	Electrical Conductivity (S/m)	Specific Electrical Conductivity (S/m)/(g/cm³)	Thermal Conductivity (Wm⁻¹k⁻¹)
Commercial Silver Epoxy	66% Ag	2.876	1.1-20 x10 ⁴ *	3.82x10 ³ -6.95x10 ⁴	2.5
1% Epoxy Solution	45% CNT	0.511	6.135 x10 ⁴	1.21 x10 ⁵	0.162
5% Epoxy Solution	9% CNT	0.734	1.142 x10 ⁴	1.56 x10 ⁴	0.786
Dry CNT Unconsolidated	100% CNT	1.57x10 ⁻⁵	0.127 x10 ⁴	8.06 x10 ⁷	---
Dry CNT Consolidated	100% CNT	4.97x10 ⁻⁴	4.285 x10 ⁴	8.62x10 ⁷	---

The through thickness thermal conductivity of the CNTs is much lower than that of theoretical values for CNTs. However, these values are in the axial direction, radially the thermal conductivity of carbon nanotubes is much lower at 1.52 Wm⁻¹k⁻¹[173]. However, even taking this into account, it is surprising the high-volume fraction sample has a thermal conductivity lower than that of pure epoxy. The low density of this sample provides clues as to why this value is so low. If there are voids in the CNT epoxy adhesives, these gaps will act as scattering sites for the

phonon motion. These voids would also explain why the density is below that of both CNTs and epoxy. From comparing the density of the dry, unconsolidated CNT ribbon to the CNT ribbon consolidated by acetone we see that there is a significant amount of void space in the CNTs as they're drawn from the array. Even when consolidated with acetone, these gaps decrease in size, but still remain and create a structure that is much lower density than that of a single CNT. It's possible that the total volume required to fill these voids is less than the amount applied during the winding. While these samples were cured under vacuum to remove the acetone, it's possible the resin molecules did not have time to diffuse into these gaps. This could be due to the initiation of the thermosetting reaction causing the resin molecules to increase in molecular weight and become more resistant to motion at the atomic level. The samples that were prepared for lap shear strength were cured under pressure, which likely would have removed the majority of this void space as the pressure forces the resin molecules into gaps whether partially cured or not.

The lap shear strength of each of the CNT epoxy samples, neat epoxy, and silver filled epoxy is shown in Figure 5.2. The hypothesis was that while the introduction of nanotubes would impart electrical conductivity, they would decrease the lap shear strength of the epoxy. This assumption was based on the idea that the CNTs at the interface of the adherends would not chemically bond the two surfaces together and the sample would undergo adhesive failure. However, the low volume fraction sample exceeded expectations and sustained a higher load than the pure epoxy and the silver filled epoxy.

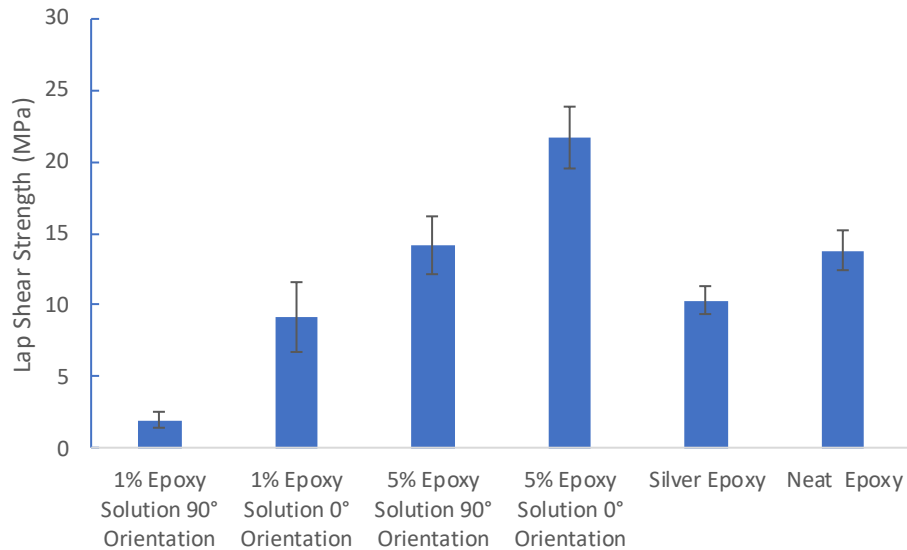


Figure 5.2: Lap shear strength of CNT epoxy adhesives and reference neat epoxy.

Examining the failure surfaces provides an explanation for these results. For the pure epoxy sample, the sample shows evidence of cohesive failure. This failure is characteristic of the sample's interfacial strength with the adherend being greater than the mechanical strength of the epoxy. When this occurs, the cohesive failure is characterized by the uniform presence of adhesive on both faces of the adherends.

An alternative situation is known as adhesive failure and occurs when the mechanical strength of the epoxy is higher than the interfacial strength with the adherend. Adhesive failure is characterized by the presence of the adhesive on one adherend and a bare surface on the other adherend. Optical examination of the CNT epoxy samples showed that there was partial coverage of the epoxy composite on both adherends signifying the failure mechanism was a combination of adhesive and cohesive failure as shown in Figure 5.3. This indicates that the mechanical strength and interfacial strength are on a similar order of magnitude.



Figure 5.3: Images of the failure surface after shearing showing the cohesive failure. The two samples on the left had the CNTs oriented in the direction perpendicular to the strain and the two samples on the right had the CNTs oriented in the direction of strain.

The difference in performance between the horizontally aligned and vertically aligned samples can be understood by examining fiber reinforced composite theory. When the load is applied in the same direction as the fiber axis there is a significant load transfer from the matrix material to the reinforcement. When the load is applied in the direction perpendicular to the nanotubes the load transfer is not as efficient and the failure mechanism is dominated by the strain of the matrix material at a given stress. In Figure 5.2 we see that the pure epoxy and the sample with the nanotubes perpendicular to the strain sustained approximately the same maximum LSS before failure.

Only the neat epoxy showed any significant amount of plastic deformation in comparison to the epoxies with filler material. All the filled epoxies underwent a sudden brittle failure as seen in Figure 5.4. The style of grip that was used for the tensile test meant that there was initial strain associated with a near zero increase in stress. This was due to the sample aligning within the grips until it reached a point where the friction force was great enough to hold the specimen stable. Therefore, the extension values shown in Figure 5.4 were adjusted so zero extension represented the point in the data where the stress began to increase substantially and is representative of the sample.

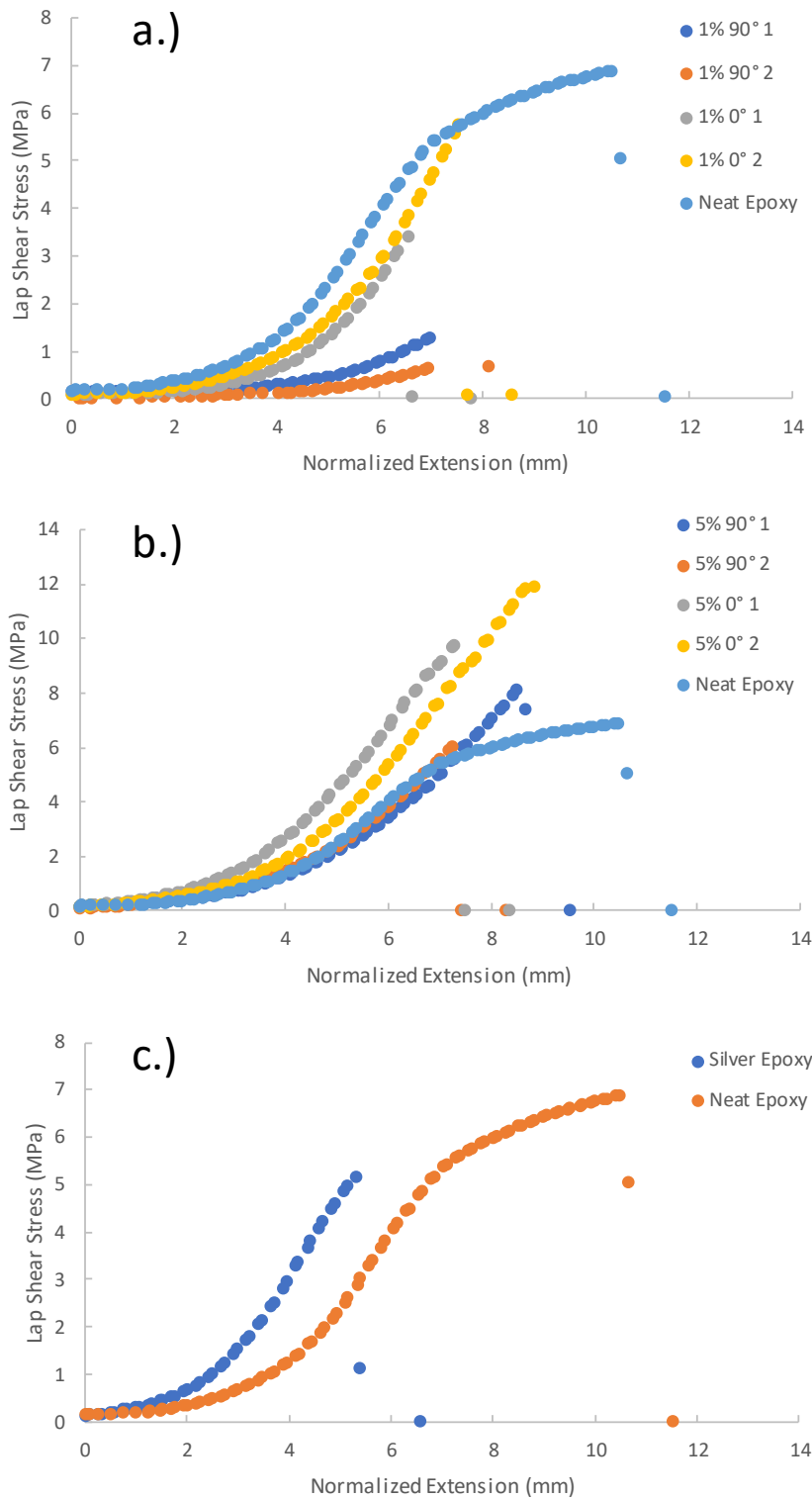


Figure 5.4: Load vs Extension with extension normalized to exclude non-representative data. a.) high volume fraction CNT sample, b.) low volume fraction CNT sample, c.) silver reference sample

Another interesting feature of these load vs normalized extension graphs is the information it tells about the modulus of the material as represented by the slope of the data. It would have been expected that the addition of carbon nanotubes would increase the modulus of the material significantly. However, for all the samples the modulus appears to be relatively constant. The exception to this is for the high-volume fraction sample where the CNT axis was oriented perpendicular to the extension. In this orientation, the modulus has decreased relative to the epoxy. These results could be explained by insufficient load transfer from the epoxy matrix to the carbon nanotubes. In theory, the high aspect ratio of the carbon nanotube, approximately 10,000:1, should provide ample surface area for the Van der Waals forces to create significant load transfer. However, this assumes that the CNTs are completely surrounded by epoxy. From the electrical conductivity measurements, there is evidence that there is at least some amount of nanotube-nanotube contact between the samples. These epoxy deficient regions would effectively lower the aspect ratio of the CNTs, which would decrease load transfer to the CNT. Also, while the CNTs are very well aligned and distributed uniformly in each layer that is applied, the spacing between nanotubes laterally and in the through thickness direction is different. Perhaps there are epoxy rich regions in between the CNT layers.

This conclusion brings up the questions why does the addition of CNTs increase the shear strength of the epoxy in the case of the low volume fraction sample. This strengthening is likely due to the presence of the CNTs preventing crack propagation. In the case of the low volume fraction sample, the spacing between CNTs is small enough that microcracks are deterred against growing to a critical failure length. However, there is still sufficient amount of epoxy to sustain a substantial load, 3500 Newtons. In the case of the high-volume fraction adhesive, the spacing between the nanotube will be even closer than the low volume fraction sample. When the load is

in the direction perpendicular to the nanotubes there is a continuous pathway of epoxy that the crack can grow along parallel to the CNT axis and therefore the strengthening has a muted effect. Despite this, the low volume fraction sample was still stronger than the silver filled epoxy.

To further examine the effect of CNT orientation on the properties of adhesives films samples, with approximately 9% CNT mass fraction, were created cross ply $\pm 60^\circ$ and $\pm 45^\circ$ orientations to compliment the unidirectional 0° and 90° samples. Because the fabrication process was not the same for the angled samples versus the 0-90 samples the values should not be used for direct comparison. However, it was expected that the ratio of the properties in the respective directions would show the relative degrees of isotropy for the different samples and that the 0 and 90 sample would have the highest, followed by the ± 60 and the ± 45 sample would approach a ratio of 1:1. The sheet resistance of a single layer of CNTs was measured and the ratio of the orthogonal directions, rotational (RD) and carriage (CD). These directions are depicted in Figure 5.5.

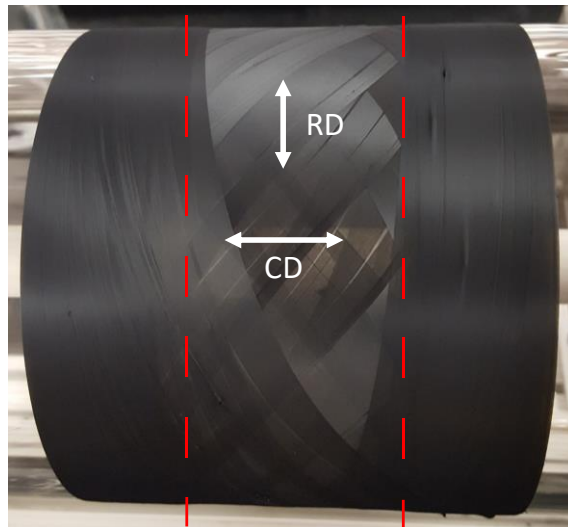


Figure 5.5: Image of a $\pm 45^\circ$ cross ply CNT coating applied to the glass mandrel with the CD and RD directions labeled. The areas outside of the red dashed lines represent the transition points during the winding and were discarded since their alignment doesn't represent the programmed alignment.

Table 5.2: The ratio of the sheet resistance of a single layer of CNTs in orthogonal directions.

+/- 45° CD/RD	+/- 60° CD/RD	0° and 90° CD/RD
2.36	4.94	58.45

The electrical properties followed the general trend that was expected, however the ratio for the 45° sample is higher than the predicted 1:1 ratio. These measurements show that the direction that is aligned with the mandrel's rotation has a lower resistance than the orthogonal direction. This may be due to the curvature of the mandrel in the rotational direction while the carriage direction is flat at a single tangential location. This curvature could be affecting the alignment or density of CNTs in the subsequent passes.

5.5 Conclusion

The addition of carbon nanotubes to epoxy adhesives via filament winding has produced electrically conductive samples with specific conductivity on the same range or greater than commercial silver filled epoxies. The addition of CNTs can be used to increase the lap shear strength of the adhesive and change the failure mechanism from cohesive to a mixture of cohesive and adhesive. The through thickness thermal conductivity as estimated to be greater than that of neat epoxy, but still much lower than metallic filled commercial options. It is assumed that better consolidation would result in an epoxy with higher through thickness conductivity. Also, the in plane thermal conductivity should be much higher when aligned with the CNT axis. The electrical and mechanical properties are sensitive to the volume fraction of nanotubes present and reached their respective maximums at different values. This technique allows users to create adhesives with properties that vary over a wide a range and can be engineered to match the application.

Additionally, the technique can create adhesives with electrical properties and lap shear strengths with a varying degree of directionally dependence.

6. Filament Winding Vertically Aligned Spinnable Carbon Nanotubes and E-Glass to Create Hybrid-Nano Composites

Brian Wells,^{a,b} Karim Aly^a, Kara Peters,^c and Philip Bradford^{a*}

^aDepartment of Textile Engineering, Chemistry, and Science, North Carolina State University, Campus Box 8301, Raleigh, North Carolina 27695, USA

^bDepartment of Materials Science & Engineering, North Carolina State University, Campus Box 7907, Raleigh, North Carolina 27695, USA

^cDepartment of Mechanical and Aerospace Engineering, North Carolina State University, Campus Box 7910, Raleigh, North Carolina 27695, USA

*Corresponding Author, Phone: 919-515-1866, Email: philip_bradford@ncsu.edu

6.1 Abstract

Nano-composites made with carbon nanotubes (CNTs) often have much smaller volume fractions than fiber reinforced composites. These low volume fraction composites are far from reaching the maximum theoretical properties and even their traditional fiber counterparts. A common approach to this problem is to create a hybrid composite from a matrix material, fiber reinforcement, and a nanomaterial. This technique increases composite performance when limited to adding small amounts of CNT. However, by merging traditional filament winding techniques with vertically aligned spinnable carbon nanotubes (VASCNTs) we present a brand new method for creating hybrid composites with controlled CNT alignment, uniform/even disbursement, controlled-volume fractions and that can be used with temperature sensitive fibers. These filament wound hybrid composites were electrically conductive with a conductivity on the range of 11-83 S/m. The mechanical properties showed a maximum increase of 25% for the axial compressive yield strength and of 18.5% for the radial compressive yield strength compared to a sample created without any CNTs.

6.2 Introduction

Carbon nanotubes have been used to create a variety of textile structures, such as yarns, braids, knits, and woven fabrics [52], [53]. CNTs have been studied as a reinforcing material for composites to create high strength lightweight materials. Unfortunately, these composites often exhibit mechanical properties well below the theoretical values [174]. Even in high volume fractions, 70%, the measured performance lags behind traditional composites [175]. However, using CNTs as an additive to resins and composite materials shows promise in improving the mechanical properties [176], [177]. The properties of fiber reinforced polymer (FRP) composites can be modified by adding CNTs to the epoxy or incorporating them into or on the fiber. These 3+ phase structures are referred to as hybrid composites and have significant potential in the aerospace industry [178]. This is because the addition of CNTs can not only improve the mechanical properties of structural composites but can also transform single purpose composites into multifunctional materials.

In the aerospace industry, the move to composite materials over traditional aluminum has been motivated by fuel efficiency as a function of decreased weight. However, transitioning to fiber reinforced composites decreases the conductivity and makes the craft more vulnerable to lightning strikes even when using conductive carbon fibers [178]. CNTs are an ideal reinforcing material to solve that problem because they are very electrically conductive. In [115] hybrid composite materials were made with pristine and functionalized carbon nanotubes. The epoxy CNT combination and the pristine-CNT-epoxy glass fiber composite had resistivity values that were approximately 10 orders of magnitude below that of the epoxy glass fiber composite. When CNTs were oxidized and used with epoxy and glass fiber there was only a decrease in the resistivity of about 2 orders of magnitude. *In situ* growth of carbon nanotubes on fibers has been studied to

create multifunction hybrid composites. In [117] study, there was an increase in the conductivity of the material as the percent CNT increased. At just 3% loading of CNTs there was an approximately 8 order of magnitude decrease in the resistance [117]. These drastic changes in resistance occur when CNTs are added to insulating materials such as glass fiber. However, research has shown that when MWCNTs are added to conductive carbon fiber (CF) FRPs and there is an increase in the conductivity by about 50% in plane and about 30% increase in out of plane conductivity [118]. MWCNTs and heat treated carbon nanofibers were embedded in epoxy resin separately and together showed the highest conductivity when mixed together [179]. While changes to the conductivity of the original composite can be made, the total resistivity is still much higher than that of CNT theoretical properties.

However, even with the small loadings of CNTs additional functionality is incorporated. At even just, 0.3 wt.% CNT, hybrid composites have been shown to gain antistatic properties [119]. Concentrations at values less than 1.0 wt.% can be used for sensing applications and structural health monitoring. In one study 3D braid hybrid composites were created with small amounts of CNTs, 0.5 wt.%, and could discern different mechanisms of failure within the braid [120]. This is due to the fact that small disruptions in the electrical pathways created by the CNTs in the original state cause large changes in the resistance of the braid. As the hybrid composite was stretched researchers determined 5 distinct regions: initial state, micro crack formation, formation of microcrack interactions, saturated microcracks growing at a steady rate, and a disrupted CNT pathway [120]. The ability to detect damage was also shown in another study using glass fiber reinforce polymers, CNTS and carbon black [121]. That study also showed that the conductivity of these hybrid composites could be used for load detection, fatigue monitoring, and detection of microscale damage undetectable by other methods [121]. Structural health monitoring can reduce

maintenance costs and avoid failures before they occur. At slightly higher loadings, less than 10% MWCNT in an epoxy resin, incorporating CNTs provides electromagnetic shielding over a wide range of frequencies up to 26.5 GHz [180]. Another study used MWCNTs to provide a specific shielding of $163 \text{ dBcm}^3\text{g}^{-1}$ in the x-ray band of light [181]. The ability to shield against x-rays is particularly desirable in space craft where cosmic radiation, has not been mitigated by the atmosphere and can harm crew and equipment.

Another factor that needs to be considered is the anisotropy of carbon nanotube conductivity. To get the highest theoretical conductivity, the composite needs a high packing factor and volume fraction. To accomplish this the nanotubes must be arranged in an aligned manner. In [116] CNTs were added in between layers of E-glass with preferential CNT orientation. The CNT layers were oriented parallel to the warp of the woven fabric and perpendicular to the warp. In these respective orientations, the in-plane resistances varied by over an order of magnitude with 0.079 kilo-ohms and 1.23 kilo-ohms respectively when measurements were taken in the direction of the warp [116]. Randomly oriented CNTs distributed in a matrix will decrease the anisotropic conductive properties but will not be able to achieve the volume fraction possible with aligned CNTs. While anisotropy is sometimes desirable, an optimal processing method would have the ability to create CNT composites with anisotropic or quasi-isotropic electrical properties as needed.

Additionally, incorporating CNTs for multifunctionality often has a positive effect on the mechanical properties and can contribute to further weight savings in the aerospace industry. This is due to the outstanding mechanical properties of carbon nanotubes making them ideal reinforcing materials for hybrid composites. Theoretically, an ideal structure would have a high-volume fraction of pristine CNTs, evenly distributed, and with controlled alignment of the CNT axes.

There are different fabrication methods in the literature that have tried to achieve this optimal composite structure. However, in many cases optimizing one parameter comes at the detriment of another.

For example, one research group tackled the problem of a uniform distribution of carbon nanotubes by growing CNTs directly onto the carbon fiber reinforcement [102]. The study showed a 15% increase in the interfacial surface strength when carbon nanotubes were present, and a decrease of 37% and 32% when catalyst and amorphous carbon are on the surface of the carbon fiber [102]. Unfortunately, because the axis of the CNTs are not aligned in the fiber direction, the CNT's inherent strength is not being utilized most effectively. The direct growth of carbon nanotubes onto fibers isn't limited to unprocessed fibers, filaments or tows. Two-dimensional cloths and as described three-dimensional carbon fiber felts have also been subjected to CVD CNT growth processes [103]. In that study the flexural strength of the tows, cloths, and felts were increased by 20%, 75% and 66% respectively while the flexural modulus was increased by 25%, 54%, and 46% respectively [103]. Another study showed an increase in the toughness of a woven cloth composite with nanotubes grown on the material by 76% [104]. In [104] the failure mechanism without CNTs was a matrix dominated shear-out failure, while the sample with CNTs exhibited tensile fracture. When CNTs are grown on fibers they provide additional surface area for load transfer between matrix and carbon fiber, but likely do not have their axis oriented in the direction of the applied load.

A major drawback to the direct growth of CNTs onto fibers is that it can only be used for certain reinforcing fibers. Specifically, only fibers that can undergo high temperatures are available for that technique. Any polymeric material with a degradation temperature below a minimum of 600 C degrees will breakdown during typical CNT CVD growth processes. Even if the growth can

be completed it has been shown that high temperatures can reduce fiber properties at temperatures below degradation and melt temperatures [105].

To get around the high temperature processing parameters, electrophoretic deposition can be used to deposit nanotubes on the reinforcing fiber in radially aligned sheets [106]. Unfortunately, that process requires the CNTs to be easily dispersed in solution, which required the researchers to functionalize the CNTs [106]. This is unfortunate because functionalization of CNTs is known to decrease the mechanical properties of the individual nanotubes. However, despite the detrimental oxidation, that research increased the tensile strength 157% by and the modulus by 70% greater than the tensile strength and modulus of the traditionally produced FRP in the study [106]. Another approach that avoids high temperature is to add the CNTs directly to the epoxy. A low temperature approach that does not require functionalization for dispersion in a solution was reported in [108]. In that study CNTs were grown in a CVD furnace and then applied to a prepreg fabric by a transfer printing method [108]. This approach has the benefit of being low temperature, non-oxidative, and even more importantly, it maintains the orientation of the nanotubes in a single direction. That study showed that the mode two delamination of laminates can be increase by approximately 300% using that method [108]. However, that approach does not evenly distribute the nanotubes as there are CNT rich regions in-between each layer of prepreg ply. SEM analysis shows that the CNTs do not significantly diffuse into the regions near the fiber reinforcements. Functionalized nanotubes have been used in filament winding by mixing the functionalized CNT to the epoxy resin [182]. CNTs with long functional groups have also been used to create a liquid like CNT solution, which was then mixed into epoxy resin during filament winding [183]. In [107] the researchers impregnated glass fiber reinforced composites with MWCNT-epoxy suspensions. Unfortunately, like in the case of electrophoretic deposition, to

achieve even distribution of CNTs, acid-oxidation had to take place [107]. However, once again despite the oxidation of the nanotubes the interlaminar shear strength was increased by 33% with only the addition of approximately 0.25-1 wt.% nanotube [107]. That approach has also been used with pristine nanotubes to create filament wound epoxy/e-glass tubes and was shown to increase the fatigue life [184]. However, only small concentrations of CNTs were used, 0.5 and 1.0 wt.%, because even small volume fractions of carbon nanotubes tend to bundle within the matrix [101]. This means either the volume fraction of CNTs must be kept low or a uniform distribution will be sacrificed. Additionally, the CNTs will be randomly oriented instead of distributed with a controlled orientation.

Even though these processing techniques have not created an optimal structure, the addition of CNTs has improved mechanical properties in the respective studies. A process that can create an optimized CNT FRP composite is highly desirable and will benefit the aerospace industry significantly. By merging traditional filament winding techniques with vertically aligned spinnable carbon nanotubes (VASCNTs) we present a method for creating hybrid composites with controlled CNT alignment, uniform/even disbursement, and that can be used with temperature sensitive fibers.

6.3 Experimental Methods

6.3.1 Materials and Fabrication

The vertically aligned spinnable CNTs with a height of approximately 2 mm used in this experiment were synthesized using a floating catalyst chemical vapor deposition (FCCVD) method described in previous work [131], [132]. The reinforcement filaments were glass fiber E-glass 2400 Tex, 3920 filaments per two and 17 microns/filament. The epoxy was IN2 Epoxy Infusion

Resin with the AT30 slow hardener. This resin system was chosen for its low viscosity, 500-800 centipoise at room temperature and pot life exceeding the programmed winding time.

The composite tubes characterized in this study were created using a modified desktop filament winder called the X-Winder. The modifications included self-centering chucks and with simultaneous powered rotation of each chuck to provide accurate alignment and prevent slippage in the timing belts. A flexible plastic tube was also added to guide glass filaments to the mandrel as they leave the resin bath. A clamping mechanism was applied to this tube to squeeze excess resin from the filaments. For the offset co-winding to be described subsequently, the carriage's delivery arm was modified to support the CNT array by adding an 80/20 extruded aluminum bar, in plane to the delivery arm and parallel to the mandrel's axis.

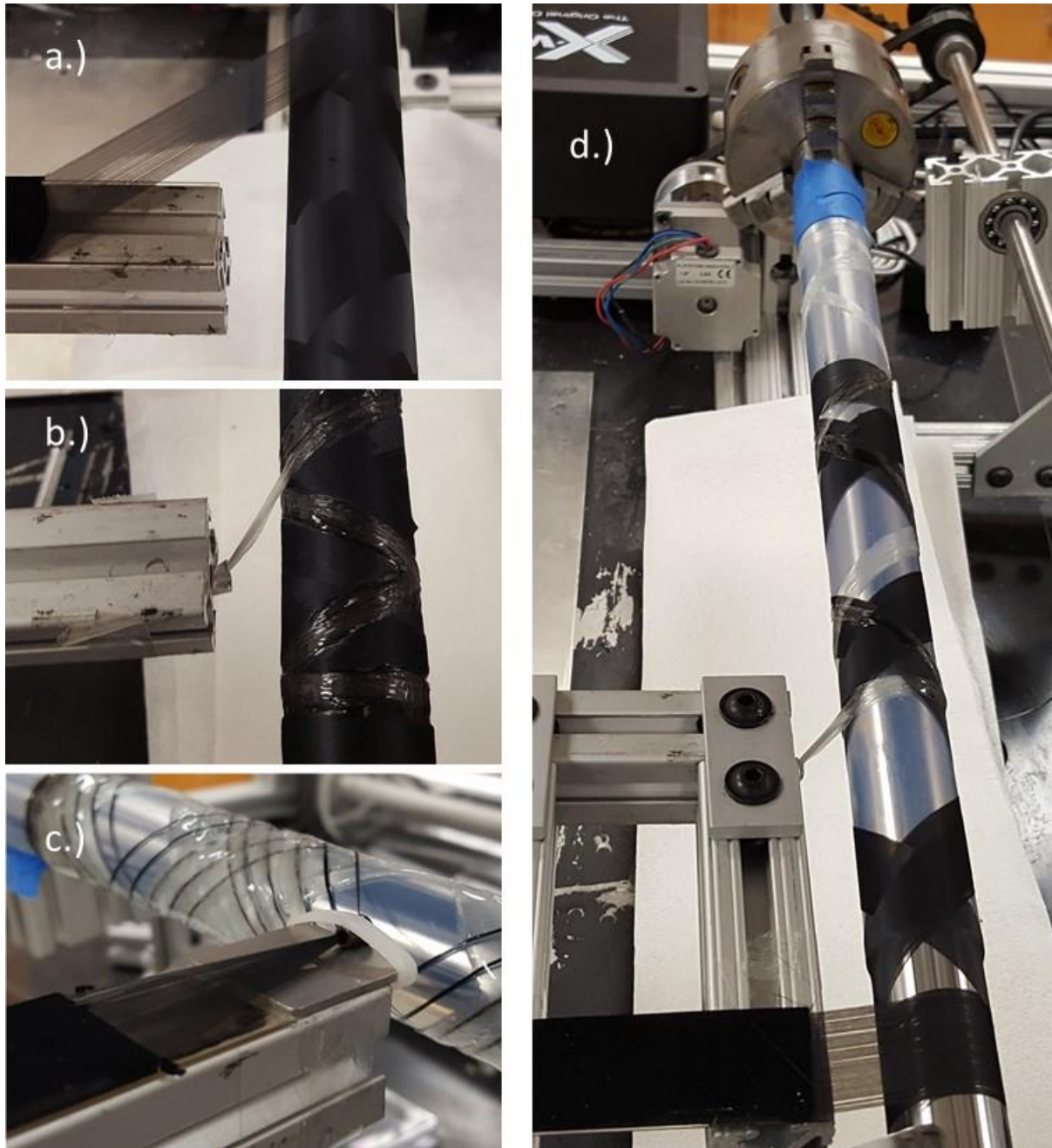


Figure 6.1: a.) Filament wound CNTs applied to a mandrel at a 45° orientation prior to b.) glass fiber filament winding. In c.) a co-wound structure is shown where the CNTs are wound throughout the thickness of the tub and consolidated through a small knitting eyelet. In d.) the offset co-winding composite tube structure with the CNTs in an unconsolidated state.

Table 6.1. Summary of the orientation and distribution of glass fiber and CNTs for the composites created. *4XS had 4 time the number of CNTs as the other structures by pre-winding 4 full layers prior to the application of the glass fiber.

Sample Name	Sample Reference	Winding Angle	CNT Location	Distribution
Neat Sample	NS	45°	No CNTs present	Unconsolidated
Inside Sample	IS	45°	Inside	Unconsolidated
Outside Sample	OS	45°	Outside	Unconsolidated
Co-Wound Sample	CUC	45°	Throughout	Unconsolidated
Co-Wound Consolidated	CMC	45°	Throughout	Medium Consolidation
Co-Wound Consolidated 2	CLC	45°	Throughout	Large Consolidation
4x CNT Sample	4XS	45°	Inside*	Unconsolidated
4 Layer Sample	4LS	45°	Inside and Interior	Unconsolidated
30° Sample	30S	30°	Inside	Unconsolidated
60° Sample	60S	60°	Inside	Unconsolidated

A variety of tubes were created with various orientations and distributions of fiber glass with a summary of these samples found in Table 6.1. Tubes with CNTs located on the inside surface were fabricated by pre-winding the CNTs before the fiberglass. Consequently, tubes with CNTs located on the outside surface were fabricated by post-winding the CNTs after the fiberglass. And tubes with CNTs located throughout the tube were fabricated by co-winding the CNTs and fiberglass simultaneously. Knitting eyelets were used to consolidate the VASCNT ribbon. Two arbitrary sizes were used for medium and large consolidation. The unconsolidated ribbon does not pass through a knitting eyelet.

The X-winder software was used to program the winding patterns for the mandrel diameter, filament width, part length, and a maximum rotational velocity of 20 RPM. During initial fabrication trials, the filaments were prone to slipping out of place during the first pass of the carriage. To compensate for this problem, the X-winder was programmed to rotate the mandrel an additional 360 degrees to prevent the filaments from slipping when the carriage's motion reversed. All the tested samples were created using this additional rotation and have proper filament distributions. When the winding was complete, the filament was disconnected from the supply and secured to the mandrel. The composite tube was then rotated on the mandrel until at least the epoxy had reached its gel time, 8-10 hours. This was done to maintain an even distribution of epoxy and prevent the epoxy from dripping off the composite for more consistent fiber mass fractions. The composites cured in room temperature ambient conditions for at least 24 hours and then underwent a 3-hour post cure at 80°C. After post cure heat treatment, the composites were cooled to room temperature and removed from the mandrel using a 40-ton press and a steel tube with an inner diameter of 32 mm and an outer diameter of 41 mm. After removal from the mandrel the composites were cut to their testing dimensions using a wet saw. For the electrical measurements, the ends of the composite where the filaments did not have a 45° orientation were cut off. For the compression testing the composites were cut to have a 1:1 aspect ratio as described in ASTM D696.40075 to prevent buckling. Wall thicknesses were approximately 3.7 mm thick, and tubes of approximately 10 inches in length weighed around 30 grams. The mass of CNT added to each sample was estimated to be maximum of 0.2 grams for all of the samples except for 4XS which would have has approximately 0.8 grams of CNT. This estimate was based on the measured mass of CNTs wound onto a mandrel, then normalized to the linear distance that was applied to the

mandrel, and calculated based on the linear distance of CNT applied to the mandrel during composite fabrication.

6.3.2 Measurements

An Agilent 34410a 6 ½ digit multimeter was used to measure the resistance of each sample listed above. ABS digimatic calipers (Mitutoyo) were used to measure the inside diameter and outside diameter of the composite tubes. Using these values the axial resistivity of the samples was calculated per Equation 1 where ρ the resistivity, R is the electrical resistance, A is the cross-sectional area of the tube, and ℓ is the distance between the probes [1].

$$\rho = RA/\ell \quad (1)$$

To ensure good electrical contact between the probes and the part, the faces of the tubes were covered with an acetone based silver paint with an acrylic binder. The through thickness electrical resistance was also characterized by applying silver paint to the interior surface of one end of the composite tube and the exterior surface of the other end of the tube.

The compression tests were performed using a MTS Landmark servo hydraulic 250 kN test system in a controlled laboratory environment. These tests included axial and radial compression loading tests at a fixed displacement speed of 1.3 mm/min as prescribed in ASTM D695.40075. The force and displacement data were recorded by the testing machine load cell. Certain samples were also tested while measuring the electrical resistance in real time as a function of compression. It is essential to point out that both the testing machine data acquisition software and the multimeter program used for recording the CNT sheet resistance change were started simultaneously with a data collection frequency of 10 Hz to guarantee precise correlation of mechanical and electrical resistance data. Axial yield strength was calculated according to Equation 2 in accordance with

ASTM D695.40075 where σ_a is the axial yield stress, F is the maximum load, and A is the minimum initial area. Hoop yield strength was calculated according to Equation 3 where α is .866 and is a correction term to compensate for non-ring geometries where α is equal to 1.0, P_{cr} is the maximum load, r_o is the initial outer radius, t_o is the initial thickness, and l is the length of the cylinder [185], [186]. 2-3 replicates were tested for each sample for each directions, axially and radially.

$$\sigma_a = F/A \quad (2)$$

$$\sigma_h = \alpha P_{cr} r_o / t_o^2 l \quad (3)$$

6.4 Results and Discussion

The electrical conductivity of the samples varied over a range of 11.0-83.8 S/m with the most conductive sample having the highest concentration of nanotubes and the least corresponding to the sample with medium consolidation wound throughout the thickness. As expected, the through thickness conductivity measurements showed that only samples with any significant conductivity were those which had CNTs wound throughout the sample. The four-layered tube, 4LS, showed very slight conductivity between the two layers however, there was still over 7 orders of magnitude difference between this value and the axial conductivity for the individual CNT layers. Samples 8 and 9 were created to show the difference in the axial conductivity as a function of the winding angle. In Figure 6.2 the various winding angles and alignments can be seen.

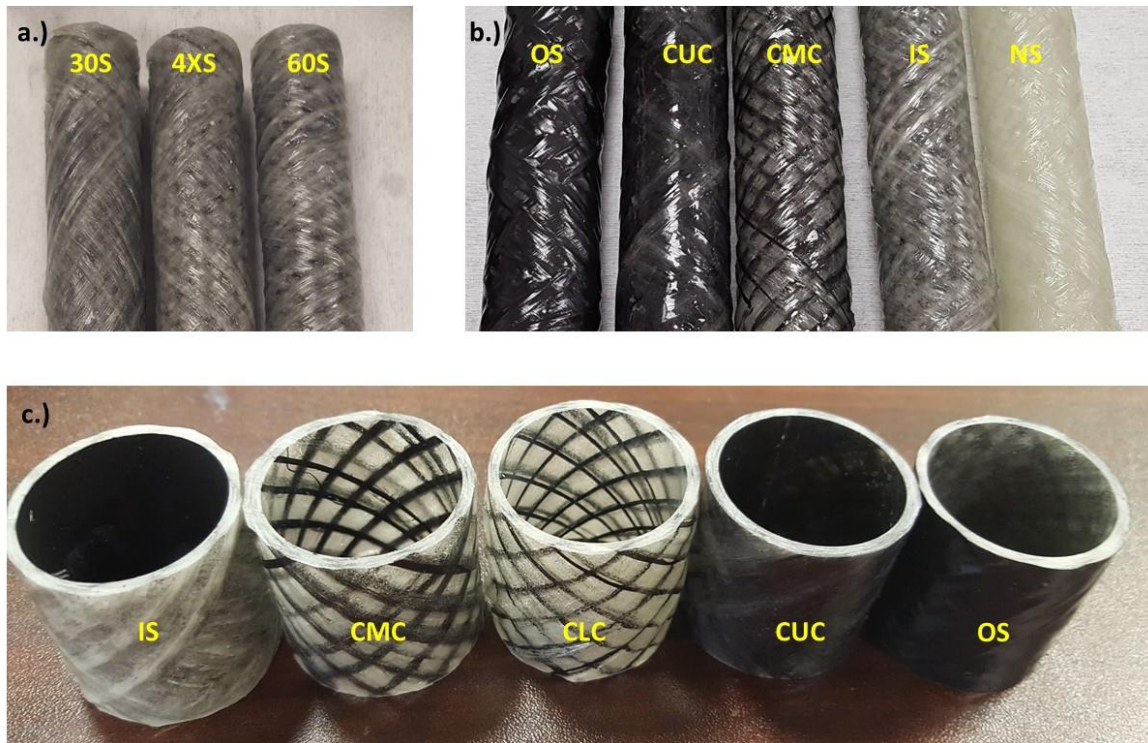


Figure 6.2: a.) Filament wound composites with various winding angles. Left to right 30°, 45°, 60° winding orientations. b.) Filament wound composite tubes with various CNT locations and distributions. c.) Filament wound composite tubes cut down for compression testing.

It was expected that the lower the winding angle the greater the electrical conductivity would be. However, the opposite was recorded when measuring Samples 8 and 9. Additionally, the sample wound with a single layer of nanotubes located on the interior surface of the tube with a 45° orientation had a conductivity that fell outside of the values for Samples 8 and 9. These unexpected results could be due to the inherent differences in the nanotube growths from one array to another. It's possible that the winding speeds played a role on the electrical conductivity, however this is likely a negligible affect since they only varied between 19.3, 19.6 and 19.8 RPM for the 60°, 45°, and 30° samples respectively.

Table 6.2: Electrical properties of filament wound composite tubes.

Sample #	Axial Conductivity S/m	Through Thickness Conductivity S/m
NS	0	0
IS	31.41	0
OS	16.13	0
CUC	14.37	8.04
CMC	10.99	1.95
CLC	11.76	0
4XS	83.83	0
4LS	37.35	See Below
30S	35.78	0
60S	33.00	0
	Connection Points (Left – Right)	Axial Conductivity S/m
4LS	Interior – Inside	3×10^{-6}
4LS	Interior – Interior	18.90
4LS	Inside – Inside	19.55
4LS	Inside - Interior	3×10^{-6}

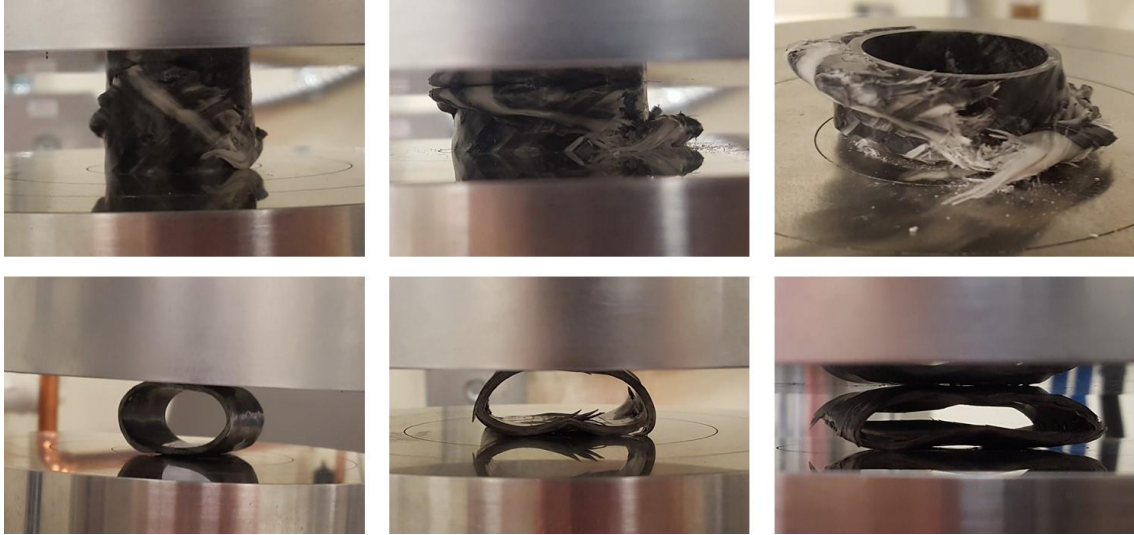


Figure 6.3: Composite tubes on the MTS between platens at various degrees of strain and failure for axial and radial compression.

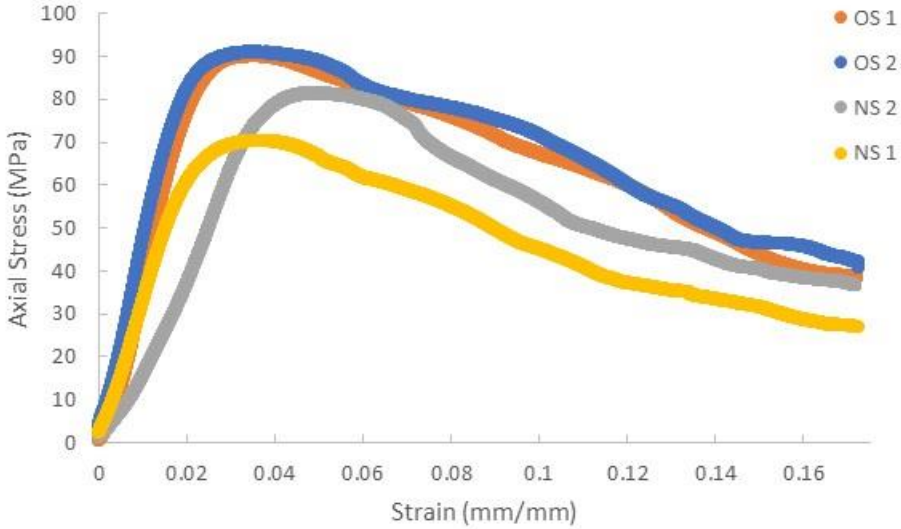


Figure 6.4: Stress strain curves for axial compression of the NS and OS samples.

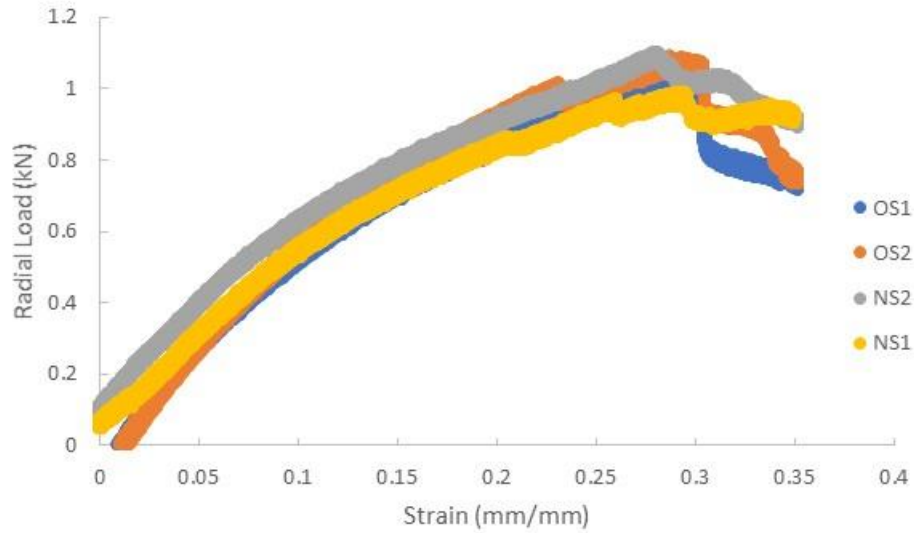


Figure 6.5: Stress strain curves for radial compression of the NS and OS samples

The axial yield strength for the composite tubes is shown in Figure 6.6. The yield strength of the material was found to vary from 75 MPa (12.25 kN load) for the neat composite without any nanotubes, NS, up to 102 MPa for the 4-layered tube 4LS. The location of the carbon nanotubes, inside vs outside vs throughout had a significant effect on the yield strength of the samples. The CNTs that were applied to the outside of the composite tube, OS, showed the greatest increase in yield strength 24.89%. Followed by the tube with the CNTs wound throughout without at 20.91% and then the inside coating which had only a marginal increase of 3.25%.

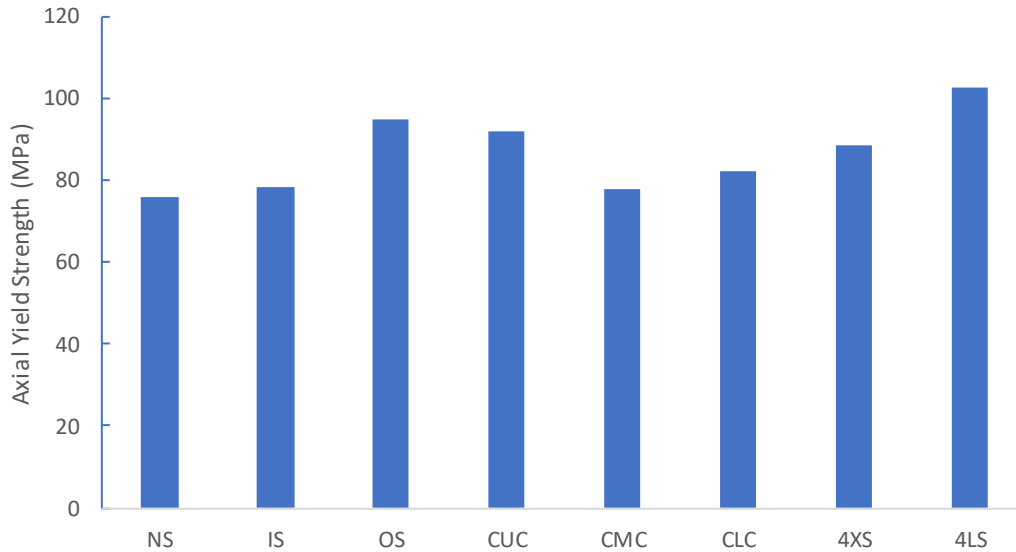


Figure 6.6: Yield strength of the composite tubes under axial compression.

The nanotubes have a high tensile strength, and any load transfer from the matrix to the nanotubes would strengthen the composite. It is likely that the composite created with the nanotubes would throughout the sample has the best encapsulation of nanotubes by the epoxy. This is because for IS the CNTs had all been added to the mandrel before the epoxy was introduced and therefore the epoxy had to diffuse through the layers of CNT. For OS the opposite was true; the none of the CNTs had been applied when the last amount of epoxy was added. Therefore, the CNTs had to soak into the epoxy and did not have the added benefit of the tension applied by the filaments as they wrapped around the CNTs as in the case of IS. However, the outer coating of CNTs showed the greatest increase in the yield strength. This is likely due to the fact that when the tubes fail under axial compression the outer walls extend outward undergoing plastic deformation. Therefore, the presence of the nanotubes at this outer layer prevents crack propagation in the epoxy matrix. Considering the strength of a material is controlled by flaws and defects mitigating crack

propagation can have a strong impact on strength. For CUC, while there are not as many CNTs on the outside of the tube and it was not quite as strong as OS there was still a significant increase of 20.91% in yield strength.

The location of the nanotubes is not the only factor that affected the yield strength. The distribution of nanotubes, unconsolidated vs medium consolidation vs high consolidation, also affected yield strength. In Samples 4 and 5 the nanotubes are located throughout the composite tube just as in CUC. However, the increase in yield strength is much lower. This is likely due to the fact that in Samples 4 and 5 while the CNTs are evenly distributed on a large scale, at the nano scale there are epoxy rich regions and CNT rich regions. While it might be expected that the medium consolidation would have a strength in between the unconsolidated sample and the high consolidation this was not what was measured.

Once the CNTs have been consolidated to the point where the mean distance between CNTs is greater than the critical crack propagation length, the strengthening mechanism will no longer function. This would explain why Samples 4 and 5 were not as strong as CUC. The amount of CNTs also plays a role on the yield strength of the samples. 4XS had 4 times as many CNTs as IS and showed a 16.54% increase in yield strength over the moderate 2.82% of IS. Interestingly, 4LS showed the greatest increase in yield strength of any sample, despite having the same ratio of CNT to number of layers of glass fiber as all the samples except 4XS.

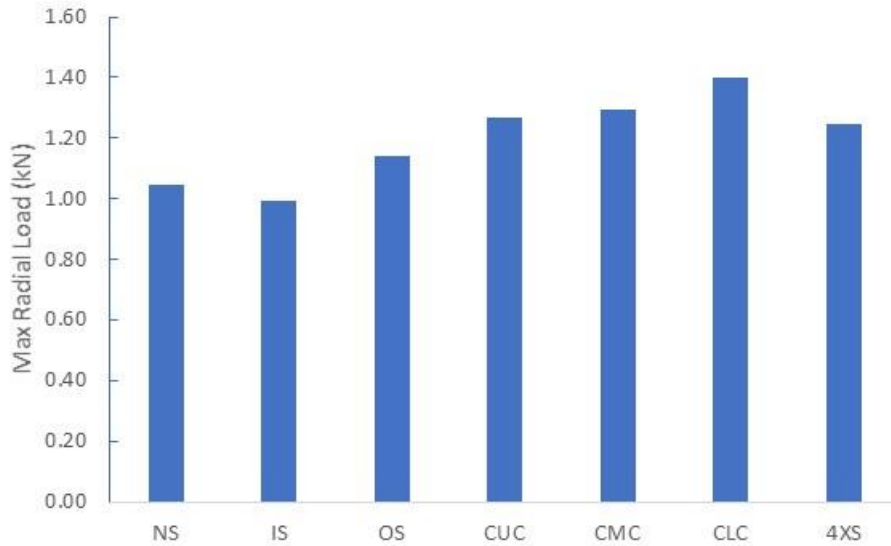


Figure 6.7: Max loads of the composite tubes under radial compression applied tangentially by flat platens.

The max radial load for each sample is shown in Figure 6.7. Interestingly, the CLC sample sustained the highest max load a summary of the max radial load and percent change to the NS is show in Table 6.3. However, these values are very sensitive to the dimensions of the sample and may not be representative of the various CNT treatments. There was also concern that the changes in the yield strength may be due to differences in the mass fraction of matrix material. To address this concern, the mass fraction of epoxy was measured in accordance with ASTM D2584 and the values can be found in Table 6.3. This concern arose from the fact that while the number of glass fiber filaments in the cross section of the sample is constant for each sample, the resin limiting mechanism is not as precise. While the load values are normalized relative to the cross sectional area into stresses, the strength of composite materials is known to have an affect on the materials strength. Unfortunately, the mass fractions did not come out exactly the same as the NS and were all below the NS. However, they were all within +/- 3% of each other and the biggest deviation from the NS was only approximately 6%. Additionally, the strongest tubes OS and CUC had fiber

glass mass fractions that varied only by -2.9% and -2.47% respectively. The affect of the epoxy mass fraction cannot be completely ruled out as having an affect on the strength. However, because sample with the smallest increase in mechanical properties, CMC, also corresponded to the largest deviation in the fiber glass mass fraction it seems unlikely that the strongest tubes gained the additional strength solely from the additional matrix material. It is much more likely that the CNT tubes are playing a role on the mechanical properties.

Also, composite tubes were created with the CNTs offset from the glass fiber so that half of the tube had CNTs incorporated into the resin half of it did not. These samples allowed for a direct comparison of the effect of CNT incorporation independent of matrix mass fraction. This sample was created with an unconsolidated CNT sheet wound through the tube’s wall thickness. In the axial and radial directions, the CNT part of this sample showed a 9.5% increase in axial strength and 19.7 % increase in radial load over the neat part of the composite tube respectively.

Table 6.3: Summary of axial yield strength and radial max load of the composite tubes and the percent change compared to the neat sample without CNTs.

Sample #	Axial Yield Strength (MPa)	Percent Change Compared to Neat Tube	Max Radial Load (kN)	Percent Change Compared to Neat Tube	FiberGlass Mass Fraction
NS	75.98	0%	1.05	0.00%	63.94%
IS	78.44	3.25%	0.99	-4.84%	61.83%
OS	94.89	24.89%	1.14	9.24%	61.04%
CUC	91.87	20.91%	1.27	21.07%	61.47%
CMC	78.12	2.82%	1.29	23.85%	55.98%
CLC	82.48	8.56%	1.40	33.88%	57.56%
4XS	88.54	16.54%	1.24	19.01%	---
4LS	102.83	35.35%	3.13	199.70%	---

To determine the ability of these CNT layers to function as structural health monitoring sensors electrical resistance measurements were made during compression tests on 4LS. The real time resistance changes measured for 4LS are plotted on top of the axial stress-strain curves shown in Figure 6.8 in Figure 6.9 these same values are plotted for the hoop-stress. While electrodes were attached to measure the inside and interior CNT layers, during the compression the displacements caused the electrodes to lose contact with the inside CNT pathway around 3% strain. These measurements were not included in the plots as they only represent a small portion of the experiment and there is no guarantee the data is representative of the sample or an artifact of the electrodes losing contact. Both the axial compression and radial compression showed net increases in the resistance at the high values of strain. For the axial direction the change was about 1200% of the initial value and for the radial direction there was approximately a 200% increase. While there were overall positive changes in the resistance, there were also some oscillatory changes at high strain values. This is particularly true for the radial compression sample. In the radial sample there are a couple of locations where there is a drastic decrease in the stress in the sample. These locations correspond to fibers breaking in the sample which was accompanied by an audible cracking noise. It is interesting that there was not a corresponding drastic change in the resistance values. One possibility is that the sampling rate for the strain data was 10 times as high as the resistance data and could just have been overlooked due to the frequency. However, these changes did occur in the regime where the resistance values are largely constant. Also, if there were a large change in resistance associated with these filaments cracking, it would be reasonable to assume that the resistance change would be present after the multimeters next measurement. As this was not witnessed it suggests that the changes in resistance are not associated with changes in the filaments but rather with the matrix epoxy.

While these trends are interesting, the strain values are well beyond the yield point and do not really provide useful information for structural health monitoring. In Figures C b.) and D b.) we see the stress-strain relationship and the resistance values plotted to strains just past the strains corresponding to the yield strengths. Examining these plots, we see that the resistance initially decreases with compressive strain and then begins to level out as the strains approach the yield point. The decreases in resistance are likely due to the compressive forces increasing the number of contact points between the CNT nanotubes and simply changing the gauge length and cross-sectional area between the electrodes. The point at which it begins to level out can be explained by the formation of microcracks which disrupt the electrical pathways. These disruptions to the electrical pathway happen to be occurring at a rate that is in equilibrium with the increases witnessed in the initial strains.

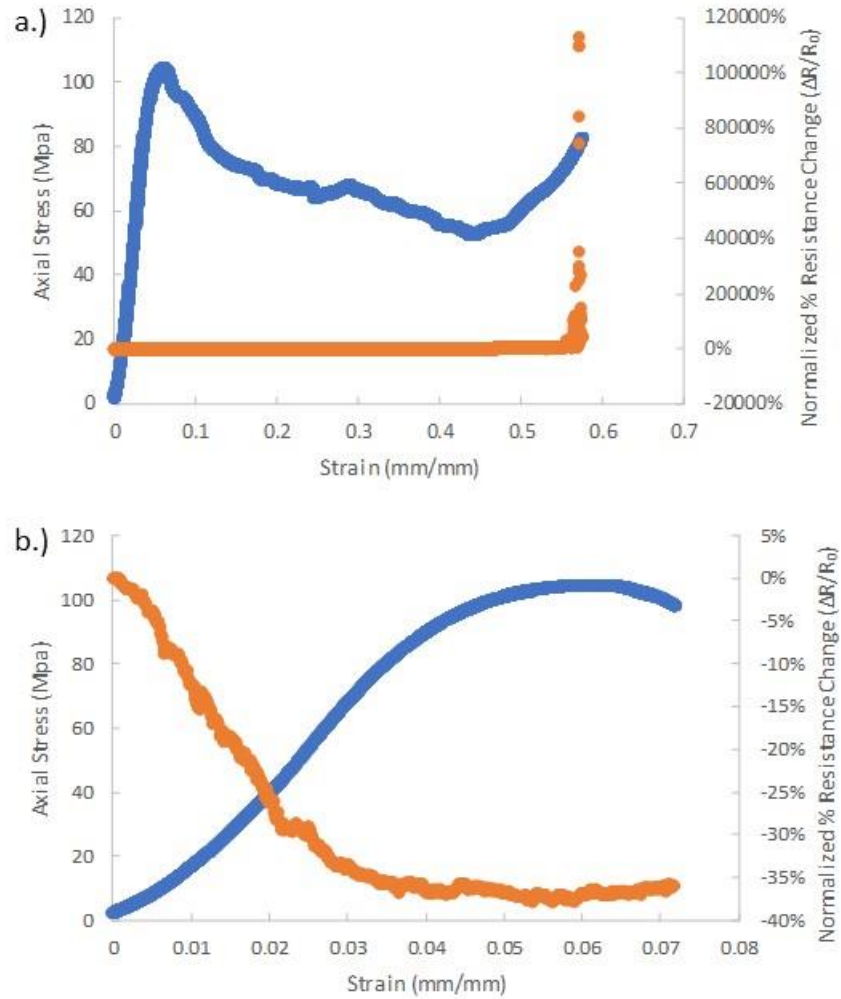


Figure 6.8: Stress-strain curves with real time resistance measurements for axial compression of the four layered composite structure. Resistance measurements represent the interior CNT pathway a.) the full strain measured b.) strain values just past strains that correspond to the yield stress.

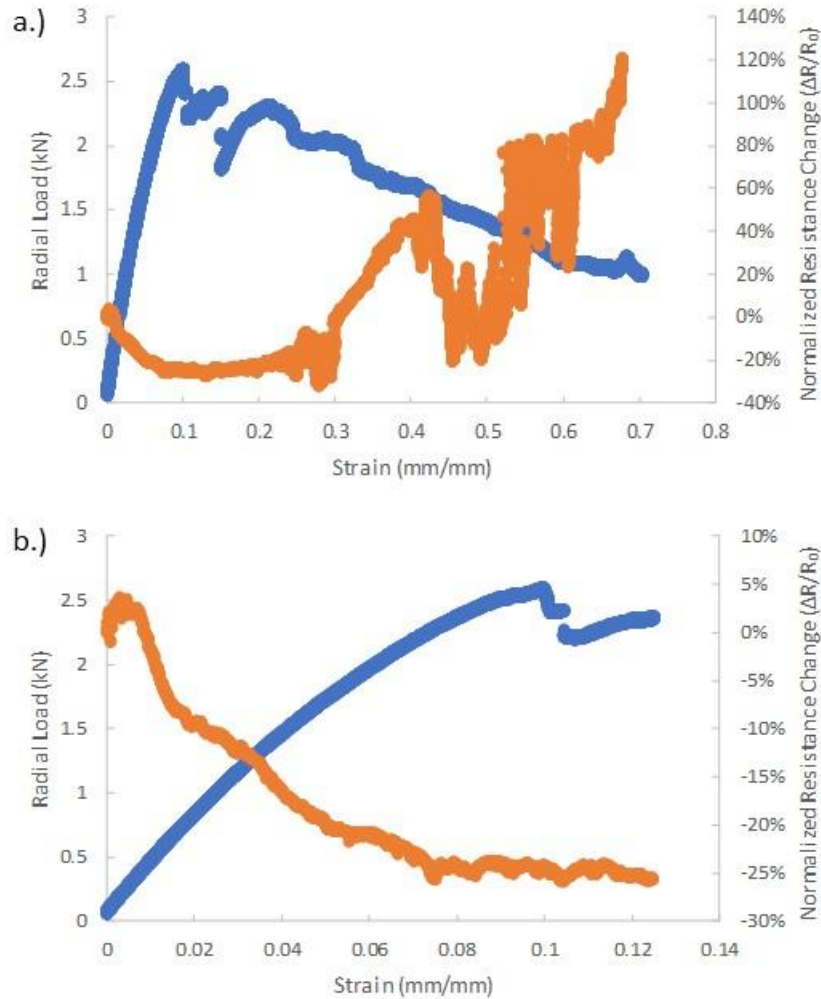


Figure 6.9: Stress-strain curves with real time resistance measurements for radial compression of the four layered composite structure. Resistance measurements represent the interior CNT pathway.

This filament winding technique was also used to create high volume fraction CNT composites that did not have any fiberglass reinforcement. However, these tubes had very small wall thicknesses and were very fragile. Some of these samples fractured as they were removed from the mandrel. Optical images of these tubes shown in Figure 6.10 show that the fractures occurred approximately along 45° angles with the respect to the tube's axis. This is interesting as it is the same angle at which the CNTs are aligned.

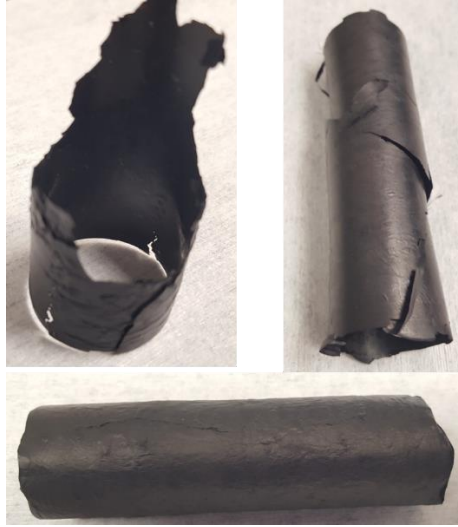


Figure 6.10: CNT epoxy tubes creating using filament winding techniques. Fracture occurred during the removal from the mandrels along 45 degrees

Due to the extreme fragility of these samples, they were not tested for mechanical or electrical properties. Creating thicker walled samples would have required tremendous amounts of nanotubes, even for short, small diameter tubes.

6.5 Conclusion

Merging filament winding and spinnable carbon nanotubes has created a technique that can create hybrid nano-composites with controlled CNT orientation, distribution and volume fraction. The addition of carbon nanotubes incorporates electrical conductivity into traditionally electrically insulating glass fiber composites. It was demonstrated that these electrical pathways can be used for structural health monitoring and sensing applications. Additionally, the incorporation of CNTs was shown to increase the axial yield strength and max radial load. The distribution of these nanotubes plays an important role on yield strength. Incorporating nanotubes into the outer surface of the composite tubes causes the greatest increase in yield strength compared to the inside surface

and distributed throughout the wall thickness. These hybrid nano composites have the potential to become the standard in the aerospace industry as a conductive, structural composite.

7. Summary and Future Work

7.1 Summary

Merging filament winding technology with VASCNTs has proven to create structures of various dimensionality with properties that are highly dependent upon the winding angle. The objective of this research was to develop the techniques to create these structures and to then characterize the properties as a function of the processing parameters and the structure property relationships. There was a heavy focus on the electrical properties and this was the constant theme throughout the research. The mechanical properties of 2 dimensional adhesive films and 3-dimensional hybrid composites were also analyzed as well as the thermal properties as the 2 dimensional adhesives films. The results and conclusions from this research are as follows:

- Conductive conformal coatings were created by the direct winding of carbon nanotubes onto small diameter filaments. The resistivity of the samples was manipulated over approximately an order of magnitude from 4.3×10^{-4} to $3.7 \times 10^{-3} \Omega\text{m}$. The resistivity decreased as the thickness of the coating increased for a given winding angle this was assumed to be a processing relationship. It was also possible to manipulate the resistivity by changing the angle between the axis of the carbon nanotubes and the axis of the filament. The structure property relationships were shown to be affected by tube-tube contacts and decreases when CNTs are consolidated and the number of tube to tube contacts increases.
- The electrical properties of CNT adhesive films were determined to be highly anisotropic as a function of the angle between current direction and CNT axis. These electrical

properties included the temperature dependence of resistivity in both the magnitude and percent change. However, both of these Both directions show evidence have a negative temperature dependence and both show hopping conduction with a linear $\ln(\sigma T^{1/2})$ versus $T^{-1/4}$ dependence. Aharonov-Bohm oscillations in the magnetoresistance indicating topological conduction when the current flows along the CNT axis are not present in the perpendicular direction and indicate a fundamentally different mechanism. Also the magnetoresistance itself is anisotropic with a maximum value of approximately 15% AMR with positive and negative MR values. However, when the current flows perpendicular to the nanotubes the AMR is about 3% given the CNT films and a change in AMR value of about 12%.

- The addition of carbon nanotubes to epoxy adhesives via filament winding has produced electrically conductive samples with specific conductivity on the same range or greater than commercial silver filled epoxies. The addition of CNTs can be used to increase the lap shear strength of the adhesive and change the failure mechanism from cohesive to a mixture of cohesive and adhesive. The through thickness thermal conductivity as estimated to be greater than that of neat epoxy, but still much lower than metallic filled commercial options. It is assumed that better consolidation would result in an epoxy with higher through thickness conductivity. Also, the in plane thermal conductivity should be much higher when aligned with the CNT axis. The electrical and mechanical properties are sensitive to the volume fraction of nanotubes present and reached their respective maximums at different values. This technique allows users to create adhesives with properties that vary over a wide a range and can be engineered to match the application.

Additionally, the technique can create adhesives with electrical properties and lap shear strengths with a varying degree of directionally dependence.

- Merging filament winding and spinnable carbon nanotubes has created a technique that can create hybrid nano-composites with controlled CNT orientation, distribution and volume fraction. The addition of carbon nanotubes incorporates electrical conductivity into traditionally electrically insulating glass fiber composites. It was demonstrated that these electrical pathways can be used for structural health monitoring and sensing applications. Additionally, the incorporation of CNTs was shown to increase the axial yield strength and hoop yield strength. The distribution of these nanotubes plays an important role on yield strength. Incorporating nanotubes into the outer surface of the composite tubes causes the greatest increase in yield strength compared to the inside surface and distributed throughout the wall thickness. These hybrid nano composites have the potential to become the standard in the aerospace industry as a conductive, structural composite.

7.2 Future Work

The variation from growth to growth is the biggest difficulty I've encounter in comparing the samples I've created. The level of precision and control required to create arrays with identical properties is something that is not currently possible and may never be attainable. Even the properties from one end of the array can vary in comparison to the other end. This is particularly true with regard to the spinnability of the edges of the CNT substrate that first encounter the gas particles and the edge that is contacted last. I think all of the work would benefit from increasing the number of samples tested over a range of CNT growths. This would provide data that is more

statistically significant in nature regarding the process used to create the samples, however the work in this dissertation serves well to act as a proof of concept and the data is representative of the samples that were created. The follow are ideas and projects that I think show promise to make an impact on the scientific community and also for engineering applications and are categorized by the chapter in this dissertation they are most related to.

7.2.1 Chapter 3 Future Work

The filament coating process could create uniform conformal coatings and has the potential to function as an effective light weight coating for EMI shielding. This capability is not something that our lab had the capability to test. I think it would be beneficial to coat copper wires with CNTs and the measure the EMI shielding. Another project that I think would benefit the research is to determine a way that can isolate all the factors that affect the tension of the system. This study examined the effect of rotational velocity on the electrical properties, but there remain other factors that were not isolated. The distance between the between the contact point with the array and the filament. Developing a stage delivery arm that can maintain this distance would isolate the tension in the ribbon due to variable lengths of ribbon.

7.2.2 Chapter 4 Future Work

I would like to demonstrate the ability to use these devices as magnetic field sensors. This sensor would essentially function by monitoring the resistance as it is expose to a magnetic field of unknown strength and then calculating the field strength based on the calibrated response previously determined. The sample's magnetic field strength would then also be measured using a standard measurement device. Potential benefits of this structure over other measurement

devices is that it can measure magnetic fields without being magnetic itself, the sample can likely be scaled down to nanoscale dimensions, is a light weight/low density structure.

The computer industry is approaching the limit of silicon based transistors. CNTs have the theoretical capability to function as field effect transistors with properties greater than silicon based counter parts. I would like to test the feasibility and capability of the structure as a high-speed field effect transistor.

A large component of the resistance of CNT based structures is the resistance associated with the hopping conduction as charge carriers transition from one material to another. It is likely that the resistance of these structures would be decrease significantly if this factor was removed. A potential way to accomplish this is to use high frequency alternating current. If the displacement caused by the electric field is significantly smaller than the length of the CNT, the charge carriers would not have to transition from one tube to another. Additionally, if the charge carrier displacement is below the ballistic conduction length of the CNTs the resistance could decrease further. Therefore, I would like to determine the effect of AC frequency upon the resistance values.

Finally, I think this structure has the potential to make an impact upon the field of thermo-electrics. The anisotropic nature of the structure can optimize the electrical conduction in one direction while minimizing thermal phonon conduction in the other direction. Additionally, the ability of CNTs to be functionalized means this structure can be created with both hole and electron charge carriers. Measuring the Seebeck coefficient of this material compared to the neat epoxy would provide insight into the use of the aligned CNTs with traditional thermoelectric materials.

7.2.3 Chapter 5 Future Work

The through thickness thermal properties were measured and found to be slightly higher than the epoxy but still much lower than metal filled counterparts. I would like to characterize the thermal properties in the in-plane directions as they are likely to be much higher than the through thickness directions because of the alignment with the CNT axis. I would also like to repeat the process with a thermoplastic polyurethane (TPU) for use in textile applications for smart textiles. These TPU composites will be more flexible than rigid epoxies but still have good adhesion and transference to textile structures. Based on these thermal properties, I would also like to incorporate traditional thermoelectric materials into the adhesive solution and drop this onto the structure. Thermoelectric materials have the potential to replace mechanical based heating and cooling air conditioning components and resistive heaters providing a more efficient option. For this to occur the figure of merit needs to be increased. I would like to determine the figure of merit for the structure compared to the traditional material and the material in the epoxy.

7.2.4 Chapter 6 Future Work

The effect of matrix mass fraction was never fully isolated in this experiment and redesigning the machine to apply resin at a controlled rate at the contact point between the filament and the mandrel. This type of application may not wet the glass fiber with the epoxy as well and could introduce different problems but could be optimized. While high volume fraction CNT composite were created without using any glass fiber these structures were incredible brittle and not able to be tested. I would like to create hybrid composite materials with higher CNT fractions on the outer coating surface and throughout the glass fiber structure as these were the most promising locations. This can be done by simply winding additional layers on the outer

surface. For the throughout winding, high CNT fractions is more difficult to accomplish but can be done by using wider arrays or creating a specialized holder that will allow multiple arrays to be applied to the mandrel all at once. This could also be done by adding the CNTs from a static stage rather than the carriage. However, this means that the CNTs would have a different alignment from the fiber glass. Therefore, I would also like to test the properties of samples with CNTs aligned at different winding angles in comparison to the neat glass fiber composite tubes. I would also like to study the effect of CNT location and distribution on composite tubes with multiple layers to compliment the four-layered sample which only had CNTs on the inside and interior interfaces. I would also like to demonstrate the functionality of the structural health monitoring during cyclic loading. Fatigue based failure is a major problem and if these CNTs can provide insight into the internal structure after loading and unloading cycles they could prevent failure and decrease costs associated with ex-situ testing techniques to measure the structural health of materials. Finally, I would like to create samples on a larger mandrel that can partially cured, removed, and the flattened into a pre-preg like structure. This would demonstrate the capability of the production technique to manufacture additional structures rather than just tube structures.

8. References

- [1] W. Callister and D. Rethwisch, *Materials Science and Engineering An Introduction*, 8th ed. 2008.
- [2] P. D. Soden, D. Leadbetter, P. R. Griggs, and G. C. Eckold, “The strength of a filament wound composite under biaxial loading,” *Composites*, vol. 9, no. 4, pp. 247–250, 1978.
- [3] P. D. Soden, R. Kitching, P. C. Tse, Y. Tsavalas, and M. J. Hinton, “Influence of winding angle on the strength and deformation of filament-wound composite tubes subjected to uniaxial and biaxial loads,” *Compos. Sci. Technol.*, vol. 46, no. 4, pp. 363–378, 1993.
- [4] N. M. Barkoula, B. Alcock, N. O. Cabrera, and T. Peijs, “Fatigue properties of highly oriented polypropylene tapes and all-polypropylene composites,” *Polym. Polym. Compos.*, vol. 16, no. 2, pp. 101–113, 2008.
- [5] M. A. Will, T. Franz, and G. N. Nurick, “The effect of laminate stacking sequence of CFRP filament wound tubes subjected to projectile impact,” *Compos. Struct.*, vol. 58, no. 2, pp. 259–270, 2002.
- [6] S. Iijima and T. Ichihashi, “Single-shell carbon nanotubes of 1-nm diameter,” *Nature*, vol. 363, pp. 603–605, 1993.
- [7] E. Flahaut, R. Bacsa, A. Peigney, and C. Laurent, “Gram-scale CCVD synthesis of double-walled carbon nanotubes To cite this version :,” *Chem. Commun.*, vol. 12, pp. 1442–1443, 2003.
- [8] S. Iijima, “Helical microtubules of graphitic carbon,” *Nature*, vol. 354, pp. 56–58, 1991.
- [9] K. Hata, D. N. Futaba, K. Mizuno, T. Namai, M. Yumura, and S. Iijima, “Water-assisted

- highly efficient synthesis of impurity-free single-walled carbon nanotubes - SOM,” *Science* (80-.), vol. 306, no. 5700, pp. 1362–1364, 2004.
- [10] Q. Zhang *et al.*, “Dry spinning yarns from vertically aligned carbon nanotube arrays produced by an improved floating catalyst chemical vapor deposition method,” *Carbon N. Y.*, vol. 48, no. 10, pp. 2855–2861, 2010.
- [11] “Multifunctional Carbon Nanotube Yarns by Downsizing an Ancient Technology Author (s): Mei Zhang , Ken R . Atkinson and Ray H . Baughman Published by : American Association for the Advancement of Science Stable URL : <http://www.jstor.org/stable/3839596> .,” vol. 306, no. 5700, pp. 1358–1361, 2013.
- [12] C.-M. Seah, S.-P. Chai, and A. R. Mohamed, “Synthesis of aligned carbon nanotubes,” *Carbon N. Y.*, vol. 49, no. 14, pp. 4613–4635, 2011.
- [13] Y. Cui, B. Wang, and M. Zhang, “Optimizing reaction condition for synthesizing spinnable carbon nanotube arrays by chemical vapor deposition,” *J. Mater. Sci.*, vol. 48, no. 21, pp. 7749–7756, 2013.
- [14] X. Lepró, M. D. Lima, and R. H. Baughman, “Spinnable carbon nanotube forests grown on thin, flexible metallic substrates,” *Carbon N. Y.*, vol. 48, no. 12, pp. 3621–3627, 2010.
- [15] C. Ghemes and A. Ghemes, “Study of Growth Enhancement of Multiwalled Carbon Nanotubes by Chlorine-Assisted Chemical Vapor Deposition,” *Jpn. J. Appl. Phys.*, vol. 52, pp. 35202-1–6, 2013.
- [16] A. M. Yu *et al.*, “Linked references are available on JSTOR for this article : Strength and Breaking Mechanism of Multiwalled Carbon Nanotubes Under Tensile Load,” vol. 287,

- no. 5453, pp. 637–640, 2016.
- [17] Y. H. Yang and W. Z. Li, “Radial elasticity of single-walled carbon nanotube measured by atomic force microscopy,” *Appl. Phys. Lett.*, vol. 98, no. 4, pp. 96–99, 2011.
- [18] I. Palaci, S. Fedrigo, H. Brune, C. Klinke, M. Chen, and E. Riedo, “Radial elasticity of multiwalled carbon nanotubes,” *Phys. Rev. Lett.*, vol. 94, no. 17, pp. 1–4, 2005.
- [19] R. S. R. Ruoff, J. Tersoff, D. C. Lorents, S. Subramoney, and B. Chan, “Radial deformation of carbon nanotubes by van der Waals forces,” *Nature*, vol. 364, no. 6437, pp. 514–516, 1993.
- [20] M. Minary-Jolandan and M. F. Yu, “Reversible radial deformation up to the complete flattening of carbon nanotubes in nanoindentation,” *J. Appl. Phys.*, vol. 103, no. 7, 2008.
- [21] M. R. Falvo *et al.*, “Bending and buckling of carbon nanotubes under large strain,” *Nature*, vol. 389, no. 6651, pp. 582–584, 1997.
- [22] M. Buongiorno Nardelli, B. I. Yakobson, and J. Bernholc, “Mechanism of strain release in carbon nanotubes,” *Phys. Rev. B*, vol. 57, no. 8, pp. R4277–R4280, 1998.
- [23] S. Hong and S. Myung, “Nanotube Electronics: A flexible approach to mobility,” *Nat. Nanotechnol.*, vol. 2, no. 4, pp. 207–208, 2007.
- [24] H. Dai, A. Javey, E. Pop, D. Mann, W. Kim, and Y. Lu, “Electrical Transport Properties and Field Effect Transistors of Carbon Nanotubes,” *Nano*, vol. 1, no. 1, pp. 1–13, 2006.
- [25] X. Zhou, J. Park, S. Huang, J. Liu, and P. L. McEuen, “Band structure, phonon scattering, and the performance limit of single-walled carbon nanotube transistors,” *Phys. Rev. Lett.*, vol. 95, no. 14, p. 146805, 2005.

- [26] Z. K. Tang *et al.*, “Superconductivity in 4 Angstrom Single-Walled Carbon Nanotubes,” *Science* (80-.), vol. 292, no. 5526, pp. 2462–2465, 2001.
- [27] W. Shi *et al.*, “Superconductivity in bundles of double-wall carbon nanotubes.,” *Sci. Rep.*, vol. 2, no. Cvd, p. 625, 2012.
- [28] A. Y. Kasumov *et al.*, “Superconductivity in ropes of single-walled carbon nanotubes,” *Phys. B Condens. Matter*, vol. 329–333, no. II, pp. 1321–1322, 2003.
- [29] P. Poncharal *et al.*, “Electrostatic Deflections and Electromechanical Resonances of Carbon Nanotubes Published by : American Association for the Advancement of Science Stable URL : <http://www.jstor.org/stable/2896911> Linked references are available on JSTOR for this article :,” *Science* (80-.), vol. 283, no. 5407, pp. 1513–1516, 1999.
- [30] C. T. White and T. N. Todorov, “Carbon nanotubes as long ballistic conductors,” *Nature*, vol. 393, no. 6682, pp. 240–242, 1998.
- [31] A. Javey, J. Guo, Q. Wang, M. Lundstrom, and H. Dai, “Ballistic carbon nanotube field-effect transistors,” *Nature*, vol. 424, no. 6949, pp. 654–657, 2003.
- [32] H. J. Li, W. G. Lu, J. J. Li, X. D. Bai, and C. Z. Gu, “Multichannel ballistic transport in multiwall carbon nanotubes,” *Phys. Rev. Lett.*, vol. 95, no. 8, pp. 1–4, 2005.
- [33] A. Javey *et al.*, “High-Field Quasiballistic Transport in Short Carbon Nanotubes,” *Phys. Rev. Lett.*, vol. 92, no. 10, pp. 106804–1, 2004.
- [34] X. Lu and Z. Chen, “Curved Pi-conjugation, aromaticity, and the related chemistry of small fullerenes (<C60) and single-walled carbon nanotubes,” *Chem. Rev.*, vol. 105, no. 10, pp. 3643–3696, 2005.

- [35] T. W. Odom, J.-L. Huang, P. Kim, and C. M. Lieber, "Structure and Electronic Properties of Carbon Nanotubes," *J. Phys. Chem. B*, vol. 104, no. 13, pp. 2794–2809, 2000.
- [36] J. C. Charlier, X. Blase, and S. Roche, "Electronic and transport properties of nanotubes," *Rev. Mod. Phys.*, vol. 79, no. 2, pp. 677–732, 2007.
- [37] E. A. Laird *et al.*, "Quantum transport in carbon nanotubes," *Rev. Mod. Phys.*, vol. 87, no. 3, pp. 703–764, 2015.
- [38] E. Pop, D. Mann, Q. Wang, K. Goodson, and H. J. Dai, "Thermal conductance of an individual single-wall carbon nanotube above room temperature," *Nano Lett.*, vol. 6, no. 1, pp. 96–100, 2006.
- [39] P. Kim, L. Shi, A. Majumdar, and P. L. McEuen, "Thermal Transport Measurements of Individual Multiwalled Nanotubes," *Phys. Rev. Lett.*, vol. 87, no. 21, p. 215502, 2001.
- [40] Y. M. Xiao *et al.*, "Enhanced thermoelectric properties of CNT/PANI composite nanofibers by highly orienting the arrangement of polymer chains," *J. Mater. Chem.*, vol. 22, no. 34, pp. 5125–5132, 2012.
- [41] D. D. L. Chung, "Carbon materials for structural self-sensing, electromagnetic shielding and thermal interfacing," *Carbon N. Y.*, vol. 50, no. 9, pp. 3342–3353, 2012.
- [42] R. F. Gibson, "A review of recent research on mechanics of multifunctional composite materials and structures," *Composite Structures*. 2010.
- [43] L. Kurzepa, A. Lekawa-Raus, J. Patmore, and K. Koziol, "Replacing copper wires with carbon nanotube wires in electrical transformers," *Adv. Funct. Mater.*, vol. 24, no. 5, pp. 619–624, 2014.

- [44] X. H. Zhong *et al.*, “Continuous multilayered carbon nanotube yarns,” *Adv. Mater.*, vol. 22, no. 6, pp. 692–696, 2010.
- [45] A. Y. Li, I. A. Kinloch, A. H. Windle, Y. Li, A. Kinloch, and A. H. Windle, “Direct Spinning of Carbon Nanotube Fibers from Chemical Vapor Deposition Synthesis
Published by : American Association for the Advancement of Science Stable URL :
<http://www.jstor.org/stable/3836770> Direct Spinning of Carbon Nanotube Fibers from
Chemicat,” vol. 304, no. 5668, pp. 276–278, 2004.
- [46] K. Liu *et al.*, “Carbon nanotube yarns with high tensile strength made by a twisting and shrinking method.,” *Nanotechnology*, vol. 21, no. 4, p. 45708, 2010.
- [47] M. Miao, “Electrical conductivity of pure carbon nanotube yarns,” *Carbon N. Y.*, vol. 49, no. 12, pp. 3755–3761, 2011.
- [48] X. Zhang *et al.*, “Spinning and processing continuous yarns from 4-inch wafer scale super-aligned carbon nanotube arrays,” *Advanced Materials*, vol. 18, no. 12. pp. 1505–1510, 2006.
- [49] K. Jiang, Q. Li, and S. Fan, “Nanotechnology: spinning continuous carbon nanotube yarns.,” *Nature*, vol. 419, no. 6909, p. 801, 2002.
- [50] X. Zhang *et al.*, “Strong carbon-nanotube fibers spun from long carbon-nanotube arrays,” *Small*, vol. 3, no. 2, pp. 244–248, 2007.
- [51] Q. Li *et al.*, “Structure-dependent electrical properties of carbon nanotube fibers,” *Adv. Mater.*, vol. 19, no. 20, pp. 3358–3363, 2007.
- [52] A. E. Bogdanovich and P. D. Bradford, “Carbon nanotube yarn and 3-D braid composites.

- Part I: Tensile testing and mechanical properties analysis,” *Compos. Part A Appl. Sci. Manuf.*, vol. 41, no. 2, pp. 230–237, 2010.
- [53] P. D. Bradford and A. E. Bogdanovich, “Carbon nanotube yarn and 3-D braid composites. Part II: Dynamic mechanical analysis,” *Compos. Part A Appl. Sci. Manuf.*, vol. 41, no. 2, pp. 238–246, 2010.
- [54] P. D. Bradford and A. E. Bogdanovich, “Electrical Conductivity Study of Carbon Nanotube Yarns, 3-D Hybrid Braids and their Composites,” *J. Compos. Mater.*, vol. 42, no. 15, pp. 1533–1545, 2008.
- [55] Y. Jia *et al.*, “Strong, conductive carbon nanotube fibers as efficient hole collectors,” *Nanoscale Res. Lett.*, vol. 7, no. 1, p. 137, 2012.
- [56] B. R. Kim, H. K. Lee, S. H. Park, and H. K. Kim, “Electromagnetic interference shielding characteristics and shielding effectiveness of polyaniline-coated films,” *Thin Solid Films*, vol. 519, no. 11, pp. 3492–3496, 2011.
- [57] I. W. Nam, H. K. Lee, and J. H. Jang, “Electromagnetic interference shielding/absorbing characteristics of CNT-embedded epoxy composites,” *Compos. Part A Appl. Sci. Manuf.*, vol. 42, no. 9, pp. 1110–1118, 2011.
- [58] S.-L. Shi and J. Liang, “The effect of multi-wall carbon nanotubes on electromagnetic interference shielding of ceramic composites,” *Nanotechnology*, vol. 19, no. 25, p. 255707, 2008.
- [59] Z. P. Wu *et al.*, “Electromagnetic interference shielding of carbon nanotube macrofilms,” *Scr. Mater.*, vol. 64, no. 9, pp. 809–812, 2011.

- [60] I. Mazov *et al.*, “Electromagnetic shielding properties of MWCNT/PMMA composites in Ka-band,” *Phys. Status Solidi Basic Res.*, vol. 246, no. 11–12, pp. 2662–2666, 2009.
- [61] W.-S. Jou, H.-Z. Cheng, and C.-F. Hsu, “The electromagnetic shielding effectiveness of carbon nanotubes polymer composites,” *J. Alloys Compd.*, vol. 434–435, pp. 641–645, 2007.
- [62] C. C. M. Ma, Y. L. Huang, H. C. Kuan, and Y. S. Chiu, “Preparation and electromagnetic interference shielding characteristics of novel carbon-nanotube/siloxane/poly-(urea urethane) nanocomposites,” *J. Polym. Sci. Part B Polym. Phys.*, vol. 43, no. 4, pp. 345–358, 2005.
- [63] C. L. Kane and E. J. Mele, “Size, Shape, and Low Energy Electronic Structure of Carbon Nanotubes,” *Phys. Rev. Lett.*, vol. 78, no. 10, pp. 1932–1935, 1997.
- [64] M. Ouyang, J. Huang, C. L. Cheung, and C. M. Lieber, “Energy Gaps in ‘ Metallic ’ Single-Walled Carbon Nanotubes Published by : American Association for the Advancement of Science Stable URL : <http://www.jstor.org/stable/3083542> Single-Walled Carbon Nanotubes,” vol. 292, no. 5517, pp. 702–705, 2017.
- [65] F. Sorbetti-guerri, S. K. Holmgren, K. M. Taylor, L. E. Bretscher, and R. T. Raines, “Scientific Correspondence,” *Nature*, vol. 379, no. 6561, pp. 126–126, 1996.
- [66] R. Saito, G. Dresselhaus, and M. Dresselhaus, “Trigonal warping effect of carbon nanotubes,” *Phys. Rev. B*, vol. 61, no. 4, pp. 2981–2990, 2000.
- [67] Y. Aharonov and D. Bohm, “Further considerations on electromagnetic potentials in the quantum theory,” *Phys. Rev.*, vol. 123, no. 4, pp. 1511–1524, 1961.

- [68] “Electronic states of carbon nanotubes.pdf.” .
- [69] H. Ajiki and T. Ando, “Aharonov-Bohm effect in carbon nanotubes,” *Phys. B Condens. Matter*, vol. 201, pp. 349–352, 1994.
- [70] “Energy Bands of Carbon Nanotubes in Magnetic Fields.pdf.” .
- [71] P. Delaney, H. Joon Choi, J. Ihm, S. Louie, and M. Cohen, “Broken symmetry and pseudogaps in ropes of carbon nanotubes,” *Phys. Rev. B*, vol. 60, no. 11, pp. 7899–7904, 1999.
- [72] H. Search, C. Journals, A. Contact, M. Iopscience, and I. P. Address, “First-Principles Study of Carbon Nanotube,” vol. 43, no. January, pp. 43–48, 1995.
- [73] S. Reich, C. Thomsen, and P. Ordejón, “Electronic band structure of isolated and bundled carbon nanotubes,” *Phys. Rev. B - Condens. Matter Mater. Phys.*, vol. 65, no. 15, pp. 1554111–15541111, 2002.
- [74] Y.-K. Kwon and D. Tománek, “Electronic and structural properties of multiwall carbon nanotubes,” *Phys. Rev. B - Condens. Matter Mater. Phys.*, vol. 58, no. 24, pp. R16001–R16004, 1998.
- [75] P. Lambin, L. Philippe, J. C. Charlier, and J. P. Michenaud, “Electronic band structure of multilayered carbon tubules,” *Comput. Mater. Sci.*, vol. 2, no. 2, pp. 350–356, 1994.
- [76] F. Triozon, P. Lambin, and S. Roche, “Electronic transport properties of carbon nanotube based metal/semiconductor/metal intramolecular junctions.,” *Nanotechnology*, vol. 16, no. 2, pp. 230–3, 2005.
- [77] T. W. Odom, J. Huang, and C. M. Lieber, “STM studies of single-walled carbon

nanotubes.”

- [78] N. F. Mott, “Conduction and switching in non-crystalline materials,” *Philos. Mag.*, vol. 19, no. 160, pp. 835–852, 1969.
- [79] N. Apsley and H. P. Hughes, “Temperature-and field-dependence of hopping conduction in disordered systems,” *Philos. Mag.*, vol. 30, no. 5, pp. 963–972, 1974.
- [80] P. C. Ma, N. A. Siddiqui, G. Marom, and J. K. Kim, “Dispersion and functionalization of carbon nanotubes for polymer-based nanocomposites: A review,” *Compos. Part A Appl. Sci. Manuf.*, vol. 41, no. 10, pp. 1345–1367, 2010.
- [81] C. A. Martin *et al.*, “Formation of percolating networks in multi-wall carbon-nanotube-epoxy composites,” *Compos. Sci. Technol.*, vol. 64, no. 15 SPEC. ISS., pp. 2309–2316, 2004.
- [82] M. J. Biercuk, M. C. Llaguno, M. Radosavljevic, J. K. Hyun, A. T. Johnson, and J. E. Fischer, “Carbon nanotube composites for thermal management,” *Appl. Phys. Lett.*, vol. 80, no. 15, pp. 2767–2769, 2002.
- [83] B. E. Kilbride *et al.*, “Experimental observation of scaling laws for alternating current and direct current conductivity in polymer-carbon nanotube composite thin films,” *J. Appl. Phys.*, vol. 92, no. 7, pp. 4024–4030, 2002.
- [84] C. Stéphan, T. P. Nguyen, B. Lahr, W. Blau, S. Lefrant, and O. Chauvet, “Raman spectroscopy and conductivity measurements on polymer-multiwalled carbon nanotubes composites,” *J. Mater. Res.*, vol. 17, no. 2, 2002.
- [85] S. Gong, Z. H. Zhu, and S. A. Meguid, “Anisotropic electrical conductivity of polymer

- composites with aligned carbon nanotubes,” *Polymer (Guildf)*., vol. 56, pp. 498–506, 2015.
- [86] H. Li and C. P. Wong, “A reworkable epoxy resin for isotropically conductive adhesive,” *IEEE Trans. Adv. Packag.*, vol. 27, no. 1, pp. 165–172, 2004.
- [87] J. T. Di *et al.*, “Ultrastrong, Foldable, and Highly Conductive Carbon Nanotube Film,” *ACS Nano*, vol. 6, no. 6, pp. 5457–5464, 2012.
- [88] L. Zhang *et al.*, “Strong and Conductive Dry Carbon Nanotube Films by Microcombing,” *Small*, vol. 11, no. 31, pp. 3830–3836, 2015.
- [89] L. Zhang, X. Wang, R. Li, Q. Li, P. D. Bradford, and Y. Zhu, “Microcombing enables high-performance carbon nanotube composites,” *Compos. Sci. Technol.*, vol. 123, pp. 92–98, 2016.
- [90] J. Hone *et al.*, “Electrical and thermal transport properties of magnetically aligned single wall carbon nanotube films,” *Appl. Phys. Lett.*, vol. 77, no. 5, pp. 666–668, 2000.
- [91] Q. Jiang and L. Wu, “Property enhancement of aligned carbon nanotube/polyimide composite by strategic prestraining,” *J. Reinf. Plast. Compos.*, vol. 35, no. 4, pp. 287–294, 2016.
- [92] D. Lu and C. P. Wong, “Effects of shrinkage on conductivity of isotropic conductive adhesives,” *Int. J. Adhes. Adhes.*, vol. 20, no. 3, pp. 189–193, 2000.
- [93] F. Tan, X. Qiao, J. Chen, and H. Wang, “Effects of coupling agents on the properties of epoxy-based electrically conductive adhesives,” *Int. J. Adhes. Adhes.*, vol. 26, no. 6, pp. 406–413, 2006.

- [94] B. Meschi Amoli, J. Trinidad, A. Hu, Y. N. Zhou, and B. Zhao, “Highly electrically conductive adhesives using silver nanoparticle (Ag NP)-decorated graphene: the effect of NPs sintering on the electrical conductivity improvement,” *J. Mater. Sci. Mater. Electron.*, vol. 26, no. 1, pp. 590–600, 2014.
- [95] I. A. Ventura, A. Rahaman, and G. Lubineau, “The thermal properties of a carbon nanotube-enriched epoxy: Thermal conductivity, curing, and degradation kinetics,” *J. Appl. Polym. Sci.*, vol. 130, no. 4, pp. 2722–2733, 2013.
- [96] H. Huang, C. Liu, Y. Wu, and S. Fan, “Aligned carbon nanotube composite films for thermal management,” *Adv. Mater.*, vol. 17, no. 13, pp. 1652–1656, 2005.
- [97] X. Fernández-Francos *et al.*, “Modification of epoxy-anhydride thermosets with a hyperbranched poly(ester amide). II. Thermal, dynamic mechanical, and dielectric properties and thermal reworkability,” *J. Appl. Polym. Sci.*, vol. 128, no. 6, pp. 4001–4013, 2013.
- [98] P. B. Kaul, M. F. P. Bifano, and V. Prakash, “Multifunctional carbon nanotube–epoxy composites for thermal energy management,” *J. Compos. Mater.*, vol. 47, no. 1, pp. 77–95, 2013.
- [99] U. Lafont, C. Moreno-Belle, H. van Zeijl, and S. van der Zwaag, “Self-healing thermally conductive adhesives,” *J. Intell. Mater. Syst. Struct.*, vol. 25, no. 1, pp. 67–74, 2014.
- [100] E. Amendola, A. M. Scamardella, C. Petrarca, and D. Acierno, “Epoxy-Nanocomposite with Ceramic Reinforcement for Electrical Insulation,” 2011.
- [101] F. H. Gojny, M. H. G. Wichmann, U. Köpke, B. Fiedler, and K. Schulte, “Carbon

- nanotube-reinforced epoxy-composites: Enhanced stiffness and fracture toughness at low nanotube content,” *Compos. Sci. Technol.*, vol. 64, no. 15 SPEC. ISS., pp. 2363–2371, 2004.
- [102] E. T. Thostenson, W. Z. Li, D. Z. Wang, Z. F. Ren, and T. W. Chou, “Carbon nanotube/carbon fiber hybrid multiscale composites,” *J. Appl. Phys.*, vol. 91, no. 9, pp. 6034–6037, 2002.
- [103] R. B. Mathur, S. Chatterjee, and B. P. Singh, “Growth of carbon nanotubes on carbon fibre substrates to produce hybrid/phenolic composites with improved mechanical properties,” *Compos. Sci. Technol.*, vol. 68, no. 7–8, pp. 1608–1615, 2008.
- [104] S. S. Wicks, R. G. de Villoria, and B. L. Wardle, “Interlaminar and intralaminar reinforcement of composite laminates with aligned carbon nanotubes,” *Compos. Sci. Technol.*, vol. 70, no. 1, pp. 20–28, 2010.
- [105] S. Storck, H. Malecki, T. Shah, and M. Zupan, “Improvements in interlaminar strength: A carbon nanotube approach,” *Compos. Part B Eng.*, vol. 42, no. 6, pp. 1508–1516, 2011.
- [106] E. Moaseri, M. Karimi, M. Baniadam, and M. Maghrebi, “Enhancement in mechanical properties of multi-walled carbon nanotube/carbon fiber hybrid epoxy composite: effect of electrostatic repulsion,” *Appl. Phys. A Mater. Sci. Process.*, vol. 122, no. 2, pp. 1–8, 2016.
- [107] Z. Fan, M. H. Santare, and S. G. Advani, “Interlaminar shear strength of glass fiber reinforced epoxy composites enhanced with multi-walled carbon nanotubes,” *Compos. Part A Appl. Sci. Manuf.*, vol. 39, no. 3, pp. 540–554, 2008.

- [108] E. J. Garcia, B. L. Wardle, and A. John Hart, "Joining prepreg composite interfaces with aligned carbon nanotubes," *Compos. Part A Appl. Sci. Manuf.*, vol. 39, no. 6, pp. 1065–1070, 2008.
- [109] S. U. Khan, A. Munir, R. Hussain, and J. K. Kim, "Fatigue damage behaviors of carbon fiber-reinforced epoxy composites containing nanoclay," *Compos. Sci. Technol.*, vol. 70, no. 14, pp. 2077–2085, 2010.
- [110] M. F. Uddin and C. T. Sun, "Strength of unidirectional glass/epoxy composite with silica nanoparticle-enhanced matrix," *Compos. Sci. Technol.*, vol. 68, no. 7–8, pp. 1637–1643, 2008.
- [111] S. Z. Shen *et al.*, "The effects of Clay on fire performance and thermal mechanical properties of woven glass fibre reinforced polyamide 6 nanocomposites," *Compos. Sci. Technol.*, vol. 70, no. 14, pp. 2063–2067, 2010.
- [112] C. M. Manjunatha, N. Jagannathan, K. Padmalatha, A. J. Kinloch, and A. C. Taylor, "Improved variable-amplitude fatigue behavior of a glass-fiber-reinforced hybrid-toughened epoxy composite," *J. Reinf. Plast. Compos.*, vol. 30, no. 21, pp. 1783–1793, 2011.
- [113] S. Sprenger, "Fiber-reinforced composites based on epoxy resins modified with elastomers and surface-modified silica nanoparticles," *J. Mater. Sci.*, vol. 49, no. 6, pp. 2391–2402, 2014.
- [114] C. M. Manjunatha, S. Sprenger, a. C. Taylor, and a. J. Kinloch, "The Tensile Fatigue Behavior of a Glass-fiber Reinforced Plastic Composite Using a Hybrid-toughened Epoxy Matrix," *J. Compos. Mater.*, vol. 44, no. 17, pp. 2095–2109, 2010.

- [115] J. Qiu, C. Zhang, B. Wang, and R. Liang, “Carbon nanotube integrated multifunctional multiscale composites,” *Nanotechnology*, vol. 18, no. 27, pp. 275708–275719, 2007.
- [116] H. Bhanushali and P. D. Bradford, “Woven Glass Fiber Composites with Aligned Carbon Nanotube Sheet Interlayers,” *J. Nanomater.*, vol. 2016, 2016.
- [117] E. J. Garcia, B. L. Wardle, A. John Hart, and N. Yamamoto, “Fabrication and multifunctional properties of a hybrid laminate with aligned carbon nanotubes grown In Situ,” *Compos. Sci. Technol.*, vol. 68, no. 9, pp. 2034–2041, 2008.
- [118] E. Bekyarova *et al.*, “Multiscale carbon nanotube-carbon fiber reinforcement for advanced epoxy composites,” *Langmuir : the ACS journal of surfaces and colloids*, vol. 23, no. 7, pp. 3970–4, 2007.
- [119] M. H. G. Wichmann, J. Sumfleth, F. H. Gojny, M. Quaresimin, B. Fiedler, and K. Schulte, “Glass-fibre-reinforced composites with enhanced mechanical and electrical properties - Benefits and limitations of a nanoparticle modified matrix,” *Eng. Fract. Mech.*, vol. 73, no. 16, pp. 2346–2359, 2006.
- [120] K. J. Kim *et al.*, “Damage characterization of 3D braided composites using carbon nanotube-based in situ sensing,” *Compos. Part A Appl. Sci. Manuf.*, vol. 41, no. 10, pp. 1531–1537, 2010.
- [121] L. Böger, M. H. G. Wichmann, L. O. Meyer, and K. Schulte, “Load and health monitoring in glass fibre reinforced composites with an electrically conductive nanocomposite epoxy matrix,” *Compos. Sci. Technol.*, vol. 68, no. 7–8, pp. 1886–1894, 2008.
- [122] V. P. Veedu *et al.*, “Multifunctional composites using reinforced laminae with carbon-

- nanotube forests.,” *Nat. Mater.*, vol. 5, no. 6, pp. 457–462, 2006.
- [123] S. Faraji, K. L. Stano, O. Yildiz, A. Li, Y. T. Zhu, and P. D. Bradford, “Ultralight anisotropic foams from layered aligned carbon nanotube sheets,” *Nanoscale*, vol. 7, no. 40, pp. 17038–17047, 2015.
- [124] M. A. Worsley, S. O. Kucheyev, J. H. Satcher, A. V. Hamza, and T. F. Baumann, “Mechanically robust and electrically conductive carbon nanotube foams,” *Appl. Phys. Lett.*, vol. 94, no. 7, pp. 2007–2010, 2009.
- [125] M. Kaempgen, G. S. Duesberg, and S. Roth, “Transparent Carbon Nanotube Coatings,” *Appl. Surf. Sci.*, vol. 252, no. 2, pp. 425–429, 2005.
- [126] B. Safadi, R. Andrews, and E. A. Grulke, “Multiwalled carbon nanotube polymer composites: Synthesis and characterization of thin films,” *J. Appl. Polym. Sci.*, vol. 84, no. 14, pp. 2660–2669, 2002.
- [127] S. W. Lee, B.-S. S. Kim, S. Chen, Y. Shao-Horn, and P. T. Hammond, “Layer-by-Layer Assembly of All Carbon Nanotube Ultrathin Films for Electrochemical Applications,” *J. Am. Chem. Soc.*, vol. 131, no. 2, pp. 671–679, 2008.
- [128] M. E. Spotnitz *et al.*, “Dip coating for the alignment of carbon nanotubes on curved surfaces,” *J. Mater. Chem.*, vol. 14, no. 8, p. 1299, 2004.
- [129] M. S. P. Shaffer, X. Fan, and A. H. Windle, “Dispersion and packing of carbon nanotubes,” *Carbon N. Y.*, vol. 36, no. 11, pp. 1603–1612, 1998.
- [130] V. Thiagarajan, X. Wang, P. D. Bradford, Y. T. Zhu, and F. G. Yuan, “Stabilizing carbon nanotube yarns using chemical vapor infiltration,” *Compos. Sci. Technol.*, vol. 90, pp. 82–

87, 2014.

- [131] O. Yildiz and P. D. Bradford, “Aligned carbon nanotube sheet high efficiency particulate air filters,” *Carbon N. Y.*, vol. 64, pp. 295–304, 2013.
- [132] O. Yildiz *et al.*, “High performance carbon nanotube--polymer nanofiber hybrid fabrics.,” *Nanoscale*, vol. 7, no. 40, pp. 16744–54, 2015.
- [133] Y. Wang, M. Li, Y. Gu, S. Wang, Q. Li, and Z. Zhang, “Structural modification for carbon nanotube film and the composite film by processing optimization,” *Appl. Surf. Sci.*, vol. 349, pp. 156–162, 2015.
- [134] A. Kaiser, G. Düsberg, and S. Roth, “Heterogeneous model for conduction in carbon nanotubes,” *Phys. Rev. B*, vol. 57, no. 3, pp. 1418–1421, 1998.
- [135] D. J. Perello *et al.*, “Analysis of hopping conduction in semiconducting and metallic carbon nanotube devices,” *J. Appl. Phys.*, vol. 105, no. 12, pp. 10–15, 2009.
- [136] C. Berger, P. Poncharal, Y. Yi, and W. de Heer, “Ballistic Conduction in Multiwalled Carbon Nanotubes,” *Journal of Nanoscience and Nanotechnology*, vol. 3, no. 1, pp. 171–177, 2003.
- [137] a. Y. Kasumov, I. I. Khodos, P. M. Ajayan, and C. Colliex, “Electrical resistance of a single carbon nanotube,” *Europhys. Lett.*, vol. 34, no. 6, pp. 429–434, 2007.
- [138] G. J. Brady, A. J. Way, N. S. Safron, H. T. Evensen, P. Gopalan, and M. S. Arnold, “Quasi-ballistic carbon nanotube array transistors with current density exceeding Si and GaAs,” *Sci. Adv.*, vol. 2, no. 9, pp. 1–9, 2016.
- [139] C. T. Xuan, N. T. Thuy, T. T. Luyen, T. T. T. Huyen, and M. A. Tuan, “Carbon Nanotube

- Field-Effect Transistor for DNA Sensing,” *J. Electron. Mater.*, vol. 46, no. 6, pp. 3507–3511, 2017.
- [140] T. Hayashi *et al.*, “Smallest freestanding single-walled carbon nanotube,” *Nano Lett.*, vol. 3, no. 7, pp. 887–889, 2003.
- [141] X. Zhao, Y. Liu, S. Inoue, T. Suzuki, R. O. Jones, and Y. Ando, “Smallest carbon nanotube is 3 angstrom in diameter,” *Phys. Rev. Lett.*, vol. 92, no. 12, pp. 125502–1, 2004.
- [142] W. A. De Heer, W. S. Bacsá, A. Chatelain, and T. Gerfin, “Aligned Carbon Nanotube Films : Production and Optical and Electronic Properties Author (s): Walt A . de Heer , W . S . Bacsá , A . Châtelain , T . Gerfin , R . Humphrey-Baker , L . Forro and D . Ugarte Published by : American Association for the Advanc,” *Science (80-.)*, vol. 268, no. 5212, pp. 845–847, 1995.
- [143] B. W. Alphenaar, K. Tsukagoshi, and M. Wagner, “Magnetoresistance of ferromagnetically contacted carbon nanotubes,” *Phys. E Low-Dimensional Syst. Nanostructures*, vol. 10, no. 1–3, pp. 499–504, 2001.
- [144] G. Baumgartner, M. Carrard, and L. Zuppiroli, “Hall effect and magnetoresistance of carbon nanotube films,” *Phys. Rev. B*, vol. 55, no. 11, pp. 6704–6707, 1997.
- [145] H. Aurich, A. Baumgartner, F. Freitag, A. Eichler, J. Trbovic, and C. Schöenberger, “Permalloy-based carbon nanotube spin-valve,” *Appl. Phys. Lett.*, vol. 97, no. 15, pp. 1–4, 2010.
- [146] W. Thomson, “On the Electro-Dynamic Qualities of Metals:--Effects of Magnetization on the Electric Conductivity of Nickel and of Iron,” *Proc. R. Soc. London*, vol. 8, pp. 546–

550, 1856.

- [147] E. Perfetto, J. González, F. Guinea, S. Bellucci, and P. Onorato, “Quantum Hall effect in carbon nanotubes and curved graphene strips,” *Phys. Rev. B*, vol. 76, no. 12, p. 125430, 2007.
- [148] T. Ando, “Crossover between quantum and classical transport: Quantum Hall effect and carbon nanotubes,” *Phys. E Low-Dimensional Syst. Nanostructures*, vol. 20, no. 1–2, pp. 24–32, 2003.
- [149] A. Bachtold, C. Strunk, J. Salvetat, Â. Forro, T. Nussbaumer, and J. Bonard, “letters to nature Aharonov \pm Bohm oscillations in carbon nanotubes,” *Nature*, pp. 673–675, 1999.
- [150] H. Peng *et al.*, “Aharonov-Bohm interference in topological insulator nanoribbons,” *Nat. Mater.*, vol. 9, no. 3, pp. 225–9, 2010.
- [151] E. Cimpoiasu, V. Sandu, G. A. Levin, A. Simpson, and D. Lashmore, “Angular magnetoresistance of stretched carbon nanotube sheets,” *J. Appl. Phys.*, vol. 111, no. 12, 2012.
- [152] J. Z. Cai *et al.*, “Pressure-induced transition in magnetoresistance of single-walled carbon nanotubes,” *Phys. Rev. Lett.*, vol. 97, no. 2, pp. 1–4, 2006.
- [153] G. Kim *et al.*, “Magnetoresistance of an entangled single-wall carbon-nanotube network,” *Phys. Rev. B*, vol. 58, no. 24, pp. 16064–16069, 1998.
- [154] P. K. Choudhury, M. Jaiswal, and R. Menon, “Magnetoconductance in single-wall carbon nanotubes: Electron-electron interaction and weak localization contributions,” *Phys. Rev. B - Condens. Matter Mater. Phys.*, vol. 76, no. 23, pp. 1–5, 2007.

- [155] K. Yanagi *et al.*, “Transport mechanisms in metallic and semiconducting single-wall carbon nanotube networks,” *ACS Nano*, vol. 4, no. 7, pp. 4027–4032, 2010.
- [156] S. H. Jhang and Y. W. Park, “Positive longitudinal magnetoresistance in carbon nanotube thin films,” *Synth. Met.*, vol. 216, pp. 72–74, 2016.
- [157] S. Hikami, A. I. Larkin, and Y. Nagaoka, “Spin-Orbit Interaction and Magnetoresistance in the Two Dimensional Random System,” *Prog. Theor. Phys.*, vol. 63, no. 2, pp. 707–710, 1980.
- [158] B. Lassagne *et al.*, “Aharonov-Bohm conductance modulation in ballistic carbon nanotubes,” *Phys. Rev. Lett.*, vol. 98, no. 17, pp. 1–4, 2007.
- [159] Q. P. Feng, J. P. Yang, S. Y. Fu, and Y. W. Mai, “Synthesis of carbon nanotube/epoxy composite films with a high nanotube loading by a mixed-curing-agent assisted layer-by-layer method and their electrical conductivity,” *Carbon N. Y.*, vol. 48, no. 7, pp. 2057–2062, 2010.
- [160] P. C. Ma, B. Z. Tang, and J. K. Kim, “Effect of CNT decoration with silver nanoparticles on electrical conductivity of CNT-polymer composites,” *Carbon N. Y.*, vol. 46, no. 11, pp. 1497–1505, 2008.
- [161] H. P. Wu, X. J. Wu, M. Y. Ge, G. Q. Zhang, Y. W. Wang, and J. Jiang, “Properties investigation on isotropical conductive adhesives filled with silver coated carbon nanotubes,” *Compos. Sci. Technol.*, vol. 67, no. 6, pp. 1182–1186, 2007.
- [162] M. Heimann, M. Wirts-Ruetters, B. Boehme, and K. J. Wolter, “Investigations of carbon nanotubes epoxy composites for electronics packaging,” *Proc. - Electron. Components*

- Technol. Conf.*, pp. 1731–1736, 2008.
- [163] Y. Kwon, B. S. Yim, J. M. Kim, and J. Kim, “Dispersion, hybrid interconnection and heat dissipation properties of functionalized carbon nanotubes in epoxy composites for electrically conductive adhesives (ECAs),” *Microelectron. Reliab.*, vol. 51, no. 4, pp. 812–818, 2011.
- [164] W. A. G. Iii, J. Che, and T. Ca, “Thermal conductivity of carbon nanotubes,” *Nanotechnology*, vol. 65, pp. 65–69, 2000.
- [165] S.-Y. Yang *et al.*, “Effect of functionalized carbon nanotubes on the thermal conductivity of epoxy composites,” *Carbon N. Y.*, vol. 48, no. 3, pp. 592–603, 2010.
- [166] S. Sihn, S. Ganguli, A. K. Roy, L. Qu, and L. Dai, “Enhancement of through-thickness thermal conductivity in adhesively bonded joints using aligned carbon nanotubes,” *Compos. Sci. Technol.*, vol. 68, no. 3–4, pp. 658–665, 2008.
- [167] F. H. Gojny *et al.*, “Evaluation and identification of electrical and thermal conduction mechanisms in carbon nanotube/epoxy composites,” *Polymer (Guildf.)*, vol. 47, no. 6, pp. 2036–2045, 2006.
- [168] M. R. Gude, S. G. Prolongo, T. Gómez-Del Río, and A. Ureña, “Mode-I adhesive fracture energy of carbon fibre composite joints with nanoreinforced epoxy adhesives,” *Int. J. Adhes. Adhes.*, vol. 31, no. 7, pp. 695–703, 2011.
- [169] A. H. Korayem, C. Y. Li, Q. H. Zhang, X. L. Zhao, and W. H. Duan, “Effect of carbon nanotube modified epoxy adhesive on CFRP-to-steel interface,” *Compos. Part B Eng.*, vol. 79, pp. 95–104, 2015.

- [170] M. B. Jakubinek *et al.*, “Single-walled carbon nanotube-epoxy composites for structural and conductive aerospace adhesives,” *Compos. Part B Eng.*, vol. 69, pp. 87–93, 2015.
- [171] E. Soliman, U. F. Kandil, and M. Reda Taha, “Limiting shear creep of epoxy adhesive at the FRPconcrete interface using multi-walled carbon nanotubes,” *Int. J. Adhes. Adhes.*, vol. 33, pp. 36–44, 2012.
- [172] S. A. Sydlik, J. H. Lee, J. J. Walish, E. L. Thomas, and T. M. Swager, “Epoxy functionalized multi-walled carbon nanotubes for improved adhesives,” *Carbon N. Y.*, vol. 59, pp. 109–120, 2013.
- [173] S. Sinha, S. Barjami, G. Iannacchione, A. Schwab, and G. Muench, “Off-axis thermal properties of carbon nanotube films,” *J. Nanoparticle Res.*, vol. 7, no. 6, pp. 651–657, 2005.
- [174] M. De Volder, S. Tawfick, R. Baughman, and A. J. Hart, “Carbon nanotubes: Present and future commercial applications,” *Science (80-.)*, vol. 339, no. 6119, pp. 535–539, 2013.
- [175] E. J. Siochi *et al.*, “High Volume Fraction Carbon Nanotube Composites for Aerospace Applications,” *Compos. Adv. Mater. Expo*, p. 10, 2015.
- [176] J. N. Coleman, U. Khan, W. J. Blau, and Y. K. Gun’ko, “Small but strong: A review of the mechanical properties of carbon nanotube-polymer composites,” *Carbon N. Y.*, vol. 44, no. 9, pp. 1624–1652, 2006.
- [177] B. Arash, Q. Wang, and V. K. Varadan, “Mechanical properties of carbon nanotube/polymer composites,” *Sci. Rep.*, vol. 4, no. 1, p. 6479, 2015.
- [178] O. Gohardani, M. C. Elola, and C. Elizetxea, “Potential and prospective implementation

- of carbon nanotubes on next generation aircraft and space vehicles: A review of current and expected applications in aerospace sciences,” *Prog. Aerosp. Sci.*, vol. 70, pp. 42–68, 2014.
- [179] L. Guadagno *et al.*, “Development of epoxy mixtures for application in aeronautics and aerospace,” *RSC Adv.*, vol. 4, no. 30, p. 15474, 2014.
- [180] A. Mehdipour, I. D. Rosca, C. W. Trueman, A. R. Sebak, and S. Van Hoa, “Multiwall carbon nanotube-epoxy composites with high shielding effectiveness for aeronautic applications,” *IEEE Trans. Electromagn. Compat.*, vol. 54, no. 1, pp. 28–36, 2012.
- [181] R. Kumar, S. R. Dhakate, T. Gupta, P. Saini, B. P. Singh, and R. B. Mathur, “Effective improvement of the properties of light weight carbon foam by decoration with multi-wall carbon nanotubes,” *J. Mater. Chem. A*, vol. 1, no. 18, pp. 5727–5735, 2013.
- [182] X. Jia, J. Zhu, W. Li, X. Chen, and X. Yang, “Compressive and tensile response of CFRP cylinders induced by multi-walled carbon nanotubes,” *Compos. Sci. Technol.*, vol. 110, pp. 35–44, 2015.
- [183] Q. Zhang *et al.*, “Influence of a liquid-like MWCNT reinforcement on interfacial and mechanical properties of carbon fiber filament winding composites,” *Polym. (United Kingdom)*, vol. 90, pp. 193–203, 2016.
- [184] M. Tasurek and N. Tarakcioglu, “Enhancing fatigue life of filament winding laminar and curved pipes containing carbon nanotubes, and their fatigue failure,” *Polym. Polym. Compos.*, vol. 25, no. 2, pp. 167–176, 2017.
- [185] M. Nemat-Alla, “Reproducing hoop stress-strain behavior for tubular material using

lateral compression test,” *Int. J. Mech. Sci.*, vol. 45, no. 4, pp. 605–621, 2003.

- [186] T. Yella Reddy and S. R. Reid, “On obtaining material properties from the ring compression test,” *Nucl. Eng. Des.*, vol. 52, no. 2, pp. 257–263, 1979.